Approaching Inner Ear Hair Cell Regeneration Through Non-Viral Gene Delivery

By

Adam J. Mellott

B.S., Biology, The University of Kansas, 2008

Submitted to the Bioengineering program and the
Graduate Faculty of the University of Kansas
in partial fulfillment of the requirements for the degree of
Doctor of Philosophy

Committee members

Dr. Michael S. Detamore, Committee Chair

Dr. Cory J. Berkland

Dr. Jennifer S. Laurence

Dr. M. Laird Forrest

Dr. Paulette Spencer

Dr. Vincent H. Key

Dr. Hinrich Staecker

April 3, 2014
Date defended

The Dissertation Committee for Adam Joseph Mellott certifies that this is the approved version of the following dissertation:

Approaching Inner Ear Hair Cell Regeneration Through Non-Viral Gene Delivery

Committee chair

Dr. Michael S. Detamore, Committee Chair

Date approved

ABSTRACT

Tissue engineering traditionally has taken an "outside-in" approach to address deformities, injuries, and wear-and-tear of tissues. The current thesis examines an opposite approach through an "inside-out" strategy using non-viral gene delivery with mesenchymal stem cells to regenerate mechanosensory hair cells and supporting cells of the inner ear responsible for hearing and balance. Primary cells, stem cells, and progenitor cells are often difficult to transfect unless using a viral vector, which may have systemic safety concerns. However, non-viral vectors circumvent the safety issues associated with viral vectors, but commonly exhibit low transfection efficiencies. The work of the current thesis identified and enhanced an effective non-viral gene delivery approach that reprogramed human mesenchymal stromal cells, isolated from Wharton's jelly of human umbilical cords to produce characteristics similar to the hair cell and supporting cell phenotype found in the cochlea and vestibular organs of the inner ear. Studies from the literature highlighted electroporative methods as effective non-viral strategies for difficult-to-transfect cells. *In vitro* studies demonstrated that human Wharton's jelly cells (hWJCs) that underwent electroporation and were treated with Y-27632 ROCK Inhibitor outperformed untreated cells in transfection efficiency and cell viability by factors of four and three, respectively. The identification and tracking of positively transfected cells was tremendously improved by use of a photo-converting reporter, which greatly increased signal to noise ratios. The up-regulation of *atoh1*, and down-regulation of *hes1* and *hes5*, in hWJCs produced a complex phenotype that exhibited over an 11-fold increase in gene expression of the critical hair cell marker, *myosin VIIa*, with visual morphological changes compared to untreated cells. The current thesis has demonstrated that hWJCs are susceptible to non-viral gene delivery methods, and for the first time non-viral genetic reprogramming of hWJCs induced phenotypic

changes characteristic of hair cells and neural epithelium. The current thesis has bridged the gap between non-viral gene delivery, stem cell therapy, and tissue engineering, which now presents new opportunities for further investigation utilizing non-viral gene delivery in concert with stem cell therapies for regenerative medicine applications.

ACKNOWLEDGMENTS

I gratefully acknowledge funding from the National Institutes of Health (NIH R01 AR056347), National Science Foundation (NSF EAPSI Fellowship, NSF CAREER Award), the Arthritis Foundation, The State of Kansas, and the KU School of Engineering. I would like to acknowledge Drs. Michael Detamore, Cory Berkland, Laird Forrest, Jennifer Laurence, Paulette Spencer, Vincent Key, and Hinrich Staecker for serving on my dissertation committee and providing me with continual support and guidance to develop my thesis and guide me in my growth as a scientist. Additionally, I would like to acknowledge those who were active in shaping my research methods: Dr. Mark Weiss for his guidance and training regarding electroporative techniques and stem cells, Dr. James Hong and Yelica Lopez for their assistance and insightful suggestions regarding fluorescent microscopy and cell staining, Dr. David Moore for his technical advice and providing access to microscopy and analytical equipment, namely, the epifluorescent/confocal inverted microscope and the fluorescent activated cell sorter, Dr. Eiji Tanaka and all of his lab members for welcoming me into his lab and allowing me to conduct research in Japan, Dr. Sumihare Noji and all of his lab members for welcoming me to Japan and kindly teaching me about RNAi methods as well as giving me the opportunity to construct a tissue engineering lab, Talia Martin for providing training on how to transform bacteria and clone DNA, Dr. Mary Krause for her technical assistance and helpful scientific advice, Dr. Amir Fakhari for providing training on how to conjugate peptides to biomaterials, Drs. Abdul Baoum and Supang Khondee for providing training on using cell-penetrating peptides for non-viral gene delivery and how to identify positively transfected cells, Jenny Nelson-Brantley and Keerthana Devarajan for providing training on how to harvest mouse cochlear organs and utricles as well as kind encouragement and scientific advice, and Dr. Taryn Bagby for her instruction on viral gene

delivery. I would like to thank Dr. Xinkun Wang at the KU Genomics Facility for his guidance on gene expression techniques and analysis, and Alan Walker for his assistance in repairing and fixing equipment in our lab so I could conduct research.

I would like to thank the many undergraduates in the lab who stuck with me and helped me to develop and refine multiple lab protocols across many projects: Anthony Frei, Megan Godsey, Austin Smith, and Mackenzie Bloom. I would like to especially thank Dr. Neethu Mohan for her incredible kindness and inspiration over the years and making the lab a wonderful place to work. I am grateful to post-docs from the Detamore group, Drs. Stefan Lohfeld, Ganesh Ingavle, Ju Hyeong Jeon, and Liang "Ryan" Zhao, for their aid and technical advice on interesting research problems. I acknowledge my fellow graduate students for their support and assistance with continual lab maintenance. Dr. Nathan Dormer has been an incredible inspiration and confidant; I am thankful for his advice and patience over the years in helping me "learn the ropes" of the lab. I am indebted to Heather Shinogle for her help, advice, time, and effort in helping me execute all the work presented in the current thesis. A very special thank you goes out to Peggy Keefe, for all of her emotional support, being a confidant, and always helping out. I am grateful for her friendship and assistance.

Special recognition goes out to Dr. Stephanie Studenski for first exposing me to medicine and research, and for starting me on the path that led me to where I am today. Thank you to Ken Bingmann for helping me to find a love for Biology and encouraging me to pursue a career in science. Many thanks to Dr. Victoria Corbin for providing me with the opportunity to study gene sequences, and sort a lifetime's worth of fruit flies. My gratitude goes out to Drs. Vincent Key and Joseph Noland for exposing me to the medical world and providing me with great memories, encouragement, and opportunities to meet and help patients.

My mentor and my friend, Dr. Michael Detamore, I am eternally grateful for his daily guidance, encouragement, and support on all things professional and personal. His contribution is immeasurable, and I would be lucky if I could help even a fraction of the people he has forever positively impacted in science, teaching, and everyday life. He has been an extraordinary human being, and the world will be a better place because of the people he has inspired.

Most Importantly, I want to thank my parents, Joe and Stephanie, my younger sister, Brianna, and my friends, Tyler Davis, Russell Davies, Chris Bell, Morgan Bell, and Alanna Terpening for your unconditional love and support. I could not have done any of this without all you. Thank you for always being there and offering encouragement and help to enable me to overcome the challenges in my life so that I could pursue my dreams.

TABLE OF CONTENTS

LIST OF FIGURES

CHAPTER 1
No Figures

CHAPTER 2

CHAPTER 3

CHAPTER 4

CHAPTER 5

CHAPTER 6

LIST OF TABLES

CHAPTER 1
No Tables

CHAPTER 2

CHAPTER 3

CHAPTER 4

CHAPTER 5

CHAPTER 6
No Tables

CHAPTER 1: Introduction

The overall objective of this thesis was to combine non-viral gene therapy with stem cell therapy to produce a tissue engineering strategy that could be applied to a variety of different tissues. Mechanosensory hair cells responsible for hearing and balance, found in the cochlea and vestibular organs, respectively, of the inner ear were targeted for the current thesis, because hair cells do not regenerate, thus sensorineural hearing loss is a disease with few treatment options. The overall progression was to preliminarily develop and evaluate a method to reprogram the intercellular gene expression of stem cells to induce a terminal phenotype not otherwise reachable by the stem cells. Nucleofection™ is an electroporative method, that was determined to be highly effective at transfecting primary cells; however, Nucleofection™ led to poor cell viabilities, which limited the use of Nucleofection™ for tissue engineering studies. Hence, development and evaluation of transfected stem cells for inner ear hair cell regeneration included three corresponding specific aims: (1) improvement of human Wharton's jelly cell (hWJC) transfection through ROCK Inhibitor treatment, (2) enhancement of identifying positively transfected cells, and (3) differentiation of hWJCs toward an inner ear hair cell phenotype.

The first aim evaluated different cell medium formulations to identify a formulation that rescued cell viability and improved transfection efficiency in hWJCs after undergoing Nucleofection™. The second aim evaluated the use of a photo-convertible reporter gene to identify positively transfected hWJCs in the presence of high auto-fluorescence or high background noise, and evaluated the use of a photo-converting reporter gene to track cell movement. The third aim investigated the effect of over-expressing *atonal homolog 1* (*atoh1*) by separately delivering the human homolog of *atoh1*, *hath1*, and the mouse homolog of *atoh1*, *math1*, to hWJCs. Additionally, key negative regulators of *atoh1*, *hes1* and *hes5*, were knocked

down simultaneously to evaluate whether the *atonal* effect would be enhanced and produce more morphological characteristics consistent with the inner ear hair cell phenotype. The progression of the chapters is chronological with respect to the development of the genetic program to alter the intercellular gene expression of hWJCs, as each aim built on one-another and culminated in the final design of the thesis. The organization of the chapters is as follows:

Chapter 2 provides a background on the field of gene delivery as it pertains to tissue engineering, differentiating between viral and non-viral vectors, and focusing on non-viral gene delivery strategies with an emphasis in physical non-viral gene delivery strategies. Chapter 2 highlights the barriers that must be overcome for non-viral vectors to successfully deliver genetic material to a target cell that results in the expression of a desired protein. The primary physical non-viral methodologies are identified and the advantages and disadvantages of each methodology are outlined with respect to tissue engineering. Chapter 2 concludes with suggestions on how to effectively apply the identified methodologies to tissue engineering, and improve the integration between tissue engineering and physical non-viral gene delivery. Chapter 2 serves as a central literature review for this thesis, and frames the approach to the work presented in the experimental chapters (3 through 5).

Chapter 3 addresses the first aim, i.e., improvement of hWJC cell transfection through treatment with a ROCK Inhibitor. The RhoA guanosine tri-phosphate (GTP) signaling pathway is associated with apoptosis when adherent cells are lifted from a surface or are flash frozen. Several studies have reported inhibition of ROCK (Rho-associated coiled-coil kinase) has improved cell viability of stem cells after lifting cells from a surface or thawing frozen cells. Y-27632 ROCK Inhibitor was used to treat hWJCs before and after Nucleofection. The results

enabled the development of a reliable protocol to transfect hWJCs through Nucleofection for all subsequent studies.

Chapter 4 introduces a strategy to differentiate between low signal expression in positively transfected cells and high background noise or auto-fluorescence. hWJCs were transfected with a photo-convertible reporter gene that enable green fluorescence to be switched to red fluorescence by exposure to a low power ultra-violet (UV) light or high power blue light. The kinetics of photo-conversion were measured, as well as the sensitivity of the photo-convertible fluorophores through time-lapse epifluorescent and confocal microscopy.

Chapter 5 addresses the third and final aim by evaluating and characterizing the phenotypic changes that occur when hWJCs are transfected with different combinations of plasmid DNA and siRNA. hWJCs were transfected with *math1 p*DNA, *hath1 p*DNA*,* siRNA against *hes1* and *hes5, math1 p*DNA and siRNA against *hes1* and *hes5*, or *hath1 p*DNA and siRNA against *hes1* and *hes5*. hWJCs were evaluated at 1, 3, and 7 days post-transfection for gene expression and protein expression of hair cell markers, development of morphological features through FM 1-43 lipophilic dye infiltration, and visual changes in cell morphology through microscopy

Chapter 6 serves as a conclusion for the thesis, where the major findings are summarized and discussed from a global perspective. Limitations of the work are presented and addressed, and suggestions of how limitations may be overcome are made with respect to recommendations for future investigations on regenerating inner ear hair cells through non-viral gene delivery.

The work within the current thesis proposes an approach for treating sensorineural hearing loss through the integration of non-viral gene delivery into tissue engineering to produce inner ear hair cells outside of the body. The available treatments for sensorineural hearing loss

are limited to hearing aids and cochlear implants. Several investigators have exploited over-expression of *atoh1* in supporting cells to induce the transdifferentiation of support cells into functional hair cells, but a successful treatment is still far off. Other investigators have explored using stem cell therapy to replace damaged hair cells, but success has been limited, and requires highly difficult surgeries to administer. Thus, the potential to produce inner ear hair cells outside of the body is highly attractive to elucidate mechanisms behind the physiological development of hair cells that are still poorly understood.

CHAPTER 2: Physical Non-Viral Gene Delivery Methods for Tissue Engineering [1]

ABSTRACT

The integration of gene therapy into tissue engineering to control differentiation and direct tissue formation is not a new concept; however, successful delivery of nucleic acids into primary cells, progenitor cells, and stem cells has proven exceptionally challenging. Viral vectors are generally highly effective at delivering nucleic acids to a variety of cell populations, both dividing and non-dividing, yet these viral vectors are marred by significant safety concerns. Non-viral vectors are preferred for gene therapy, despite lower transfection efficiencies, and possess many customizable attributes that are desirable for tissue engineering applications. However, there is no single non-viral gene delivery strategy that "fits-all" cell types and tissues. Thus, there is a compelling opportunity to examine different non-viral vectors, especially physical vectors, and compare their relative degrees of success. This review examines the advantages and disadvantages of physical non-viral methods (i.e., microinjection, ballistic gene delivery, electroporation, sonoporation, laser irradiation, magnetofection, and electric field-induced molecular vibration), with particular attention given to electroporation because of its versatility, with further special emphasis on Nucleofection™. In addition, attributes of cellular character that can be used to improve differentiation strategies are examined for tissue engineering applications. Ultimately, electroporation exhibits a high transfection efficiency in many cell types, which is highly desirable for tissue engineering applications, but electroporation

[1] Published as **Mellott, A.J.**, Forrest, M.L., and Detamore, M.S. Physical Non-Viral Gene Delivery Methods for Tissue Engineering. Annals of Biomedical Engineering, 41(3):446-468, 2013.

and other physical non-viral gene delivery methods are still limited by poor cell viability. Overcoming the challenge of poor cell viability in highly efficient physical non-viral techniques is the key to using gene delivery to enhance tissue engineering applications.

INTRODUCTION

Combining tissue engineering and gene therapy for clinical applications is not a new idea; however, figuring out how to successfully integrate them has proven to be a major challenge. Both tissue engineering and gene therapy strategies endeavor to treat degenerative diseases, cancers, trauma, and tissue defects that compromise the functions of organs.[155] However, both groups of strategies seem to utilize opposing methodologies. From a broad perspective, most tissue engineering strategies attempt to manipulate cellular behavior from an "outside-in" approach by varying cellular interactions with biomaterials, growth factors, and mechanical stimuli.[132] Conversely, gene therapy strategies attempt to control cellular behavior through an "inside-out" approach by directly delivering nucleic acids (i.e., DNA, siRNA, shRNA, miRNA, and antisense oligonucleotides) into cells to trigger or stall gene expression.[214, 220] Several tissue engineering strategies utilize progenitor cells or stem cells to regenerate damaged tissues by seeding them into biomaterial scaffolds.[252] The culture conditions, type of biomaterial, and mechanical stimuli can be used to direct progenitor and stem cells toward a specific lineage. Additionally, growth factors have been added to cell culture medium or encapsulated for controlled release from biomaterial scaffolds to promote cell differentiation.[53, 141, 148, 154] However, growth factors can be costly and exhibit short half-lives.[193] Furthermore, once growth factors are deposited into cell culture or into extracellular matrices (ECM), there is no way to control how the growth factors will disperse and interact with cells, meaning that not all cells

may interact with the growth factors uniformly or at all. Hence, a strategy where cells could produce, express, and control growth factors needed for differentiation would be beneficial for tissue engineering.

Gene therapy has been investigated as a potential solution to overcome the challenges associated with using growth factors by delivering DNA to induce gene expression or delivering siRNA, shRNA, miRNA, or antisense oligonucleotides to knockdown gene expression; however, gene therapy has its own set of unique challenges.[43, 97, 112, 121, 237] Nucleic acids have proven difficult to deliver to a variety of primary cells, progenitor cells, and stem cells, and the ability to manipulate gene expression in targeted cells has proven challenging as well.[38]

The difficulty behind achieving successful transfection is due in part to the many barriers a delivery vector must overcome to gain access to the cellular membrane, cytoplasmic compartment, and interior of the nucleus before target genes can be expressed (Figure 2.1). Nucleic acids must first be stabilized in some form to survive the extracellular environment to avoid degradation from changes in pH, exposure to proteases and nucleases, and opsonization.[1] After navigating through the extracellular environment to the target cell, nucleic acids must properly associate with the cell membrane and cross the plasma membrane via penetration, electrostatic interaction, adsorption, or ligand mediated receptor binding.[51, 96, 129, 173, 209, 211, 221, 246, 260, 279] Both Mercer *et al*.[161] and Conner *et al*.[40] have extensively reviewed cell entry methods through various endocytotic pathways. Once the nucleic acids reach the cytoplasmic compartment, they must avoid degradation by endocytotic mechanisms and cytoplasmic nucleases.[127] If a nucleic acid enters the cell through an endocytotic mechanism, the complex must successfully escape the endosome before undergoing degradation by a lysosome or before the endosome is recycled back to the cell surface.[4, 268, 282] Once the nucleic acid has escaped the

endosome, it must avoid degradation while trafficking through the highly crowded cell cytoplasm, which slows the diffusion of DNA to less than 1% of its rate in water.[151] RNA complexes and antisense oligonucleotides only need to reach mRNAs located in the cell cytoplasm; however, DNA complexes must cross the nuclear envelope before transcription can occur. We refer the reader to Merdan *et al*.[162], who have provided a comprehensive review on the "barriers" that polymeric gene delivery vectors must overcome.

A variety of methods have been engineered to overcome the barriers to gene delivery, but they each have their own unique advantages and disadvantages. Viral vectors have proven to be the most efficient and effective gene delivery method, and the benefits of viral vectors have been reviewed in depth by Kay *et al*.[122] and Zhang *et al*.[285]. However, there are major concerns regarding the safety of viral vectors such as toxicity, immunogenicity, and oncogenesis from insertional mutagenesis.[29, 244] Furthermore, viral vectors possess restricted sequence sizes, and viral vectors can be laborious and costly to engineer. Viral vectors may possess innate tropisms to specific cell types or cell-selective promoters, which may limit their effectiveness in other cell populations.[249]

Non-viral methods are able to circumvent most of the concerns associated with viral gene delivery methods. However, non-viral methods exhibit lower delivery efficacies than viral gene delivery methods. Non-viral gene delivery methods can be broadly separated into chemical and physical approaches. Chemical approaches utilize cationic lipids, cationic polymers, and cell-penetrating peptides that can be engineered to target specific cells locally or systemically.[14-16, 128] Chemical vectors avoid some safety concerns associated with disease-causing viral vehicles; however, effective doses of chemical vectors can be toxic, especially to sensitive cell populations because large doses are required to overcome the poor efficiency.[259] Chemical approaches seem

to be most effective at targeting cancer cells *in vitro* and *in vivo*, and chemical vectors can be customized for specific tissue engineering applications; however, primary cells, progenitor cells, and stem cells have proven more difficult to transfect with chemical vectors. Despite the difficulty in transfecting primary cells, progenitor cells, and stem cells, there has been considerable enthusiasm for the further improvement of chemical vectors for the hope of one day achieving efficacies and efficiencies that could potentially mimic viral vectors.[74, 75, 85, 115, 162-164, 191] Chemical vectors face many challenges and obstacles because chemical vectors must overcome all of the previously stated barriers. Physical methods, on the other hand, have been shown to be effective at transfecting primary cells, progenitor cells, and stem cells through *in vitro*, *ex vivo*, and *in vivo* approaches.[158] This effectiveness may be in part due to the fact that physical approaches attempt to directly force nucleic acids into the cytoplasmic compartment or nucleus to achieve successful transfection. However, physical delivery methods face different limitations than chemical delivery methods. Depending on the physical delivery method used, the cell may sustain heavy trauma and initiate apoptotic or programmed cell death mechanisms. Thus, physical gene delivery strategies tend to exhibit lower cell viabilities and there is risk that the physical invasion may cause cells to senesce, which could negatively influence cell phenotype. Hence, a major obstacle that limits physical gene delivery in tissue engineering applications is low cell viability.

Over the last decade, significant improvements have been made in areas of microinjection, ballistic gene delivery, electroporation, sonoporation, and laser irradiation, presenting a refreshing opportunity for using non-viral vectors for tissue engineering applications. Nonetheless, different non-viral physical vectors are successful in different cell types. Thus, there is a need to examine which attributes of different non-viral physical vectors enable

successful transfection and which physical characteristics of cells enable the ability of the cell to survive the transfection. Comparing the attributes of successful transfection techniques with characteristics of difficult-to-transfect cells that survive transfection methods may provide insight into physical details between the delivery vector and cell that may lead to more efficient gene delivery strategies for tissue engineering applications.

Hence, the goal of this review is to examine the advantages and disadvantages of non-viral physical vectors (i.e., microinjection, ballistic gene delivery, electroporation, sonoporation, laser irradiation, and less well-known methods such as magnetofection and electric field-induced molecular vibration), with special attention given to electroporation because of its versatility, and to identify the physical characteristics of cells that survive and successfully express the target gene for the purpose of determining which physical features between delivery vector and cell type can be used to enhance differentiation strategies for tissue engineering applications.

PHYSICAL GENE DELIVERY STRATEGIES

While much attention has been given to viral and chemical non-viral delivery systems for transporting nucleic acids into cells, physical non-viral gene delivery methodologies have shown promise for transfecting difficult-to-transfect cells. Physical gene delivery methods attempt to deliver nucleic acids directly to the cell, and attempt to avoid complications associated with targeting, endocytotic pathways and immunogenicity.[131] However, physical gene delivery has its own set of advantages and disadvantages, which limits its use for certain applications. Microinjection is a technique that directly delivers DNA to the cell nucleus, whereas ballistic gene delivery uses a projectile to deliver DNA to the cell. Electroporation utilizes electrical potentials to induce the formation of pores in the cell membrane while sonoporation utilizes

physical disturbances in the fluid to induce pores in the cell membrane for nucleic acid delivery. Laser irradiation perforates individual cells by focusing a laser beam on a localized area of the cell membrane to enable the entry of nucleic acids. Nonetheless, physical gene delivery has been favorable for tissue engineering applications where *ex vivo* approaches can be utilized, but there is room for improvement. In the following sections, this review attempts to illuminate some of the advantages and disadvantages of the most common (and uncommon) physical gene delivery methods from a tissue engineering perspective, provide examples of how physical gene delivery has been integrated into tissue engineering, and examine challenges that still need to be addressed to further improve the integration of gene therapy and tissue engineering.

MICROINJECTION

Microinjection is perhaps the most direct nucleic acid delivery method of all of the physical delivery methods. The development of microneedles and the applications for which they can be used have expanded considerably over the past 30 years. Prausnitz *et al*.[205, 207] have published excellent reviews regarding the evolution of microneedles for drug delivery applications and developing gene vaccines. Microneedles are no longer confined to the toolbox of cell biologists, but now are widely used by pharmaceutical manufacturers and are gaining popularity among bioengineers.

In their earliest form, microneedles were made of glass and used to inject nucleic acids directly into cellular cytoplasm and nuclei.[269] Microinjection of nucleic acids became a robust method to transfect cells with specific amounts of pure nucleic acids.[137] However, the technique proved to be tedious, and no more than a few hundred cells at best could be transfected using this method. Despite the difficulties associated with microinjection, the technique persisted, and

became quite valuable among cellular biologists for studying RNA trafficking,[196] immunocytochemistry,[140] and making transgenic animals.[9, 36, 42] Specifically, the ability to create transgenic animals became a powerful tool for illuminating functions of uncharacterized genes. Today, single microneedles are used for transfecting rat and mouse ova for creating transgenic animals and for facilitating somatic nuclear transfer.

Beyond creating transgenic animals, microneedles are used for transdermal delivery of nucleic acids and drugs.[52] Microneedles can be arranged in arrays, which have proven to be advantageous for transdermal drug delivery as microneedles can penetrate the outer layer of the skin and the stratum corneum, and deliver drugs, nucleic acids, and macromolecules directly to the epidermis by creating microchannels in the stratum corneum.[195] Furthermore, microneedles can be easily fabricated and engineered to accommodate multiple delivery applications. For example, microneedles can be manufactured from silicon, metal, or biodegradable polymers.[190] As such, the size and shape of microneedles can be easily modified for drug delivery applications. Microneedles can be made hollow to be used as an injectable vehicle, or microneedles can be made solid and coated with drug or nucleic acid for direct application to tissue as illustrated in Fig. 2.2.[73, 224] In addition, Choi *et al*.[31] and Daugimont *et al*.[44] have published exciting investigations on combining electroporation techniques with microinjection techniques for the purpose of creating DNA vaccinations delivered through the skin.

However, despite the benefits of microinjection, there are still limitations to the use of microinjection for tissue engineering. The use of single microneedles is highly inefficient for most tissue engineering applications, as typically the transfection of cells is needed on a larger scale than a few hundred cells and on multiple overlapping cell layers. Additionally, rat and mouse ova are large cells that can accommodate microneedles, whereas some smaller cells such

as fibroblasts are much more difficult to target with a microneedle. The diameter of the pipette tip and timing of injection (within the cell cycle) can play a major role in the ability of the cell membrane to reseal and survive.[250] Thus, a major factor that determines the success of the technique is the technical ability of the individual injecting the cells. Furthermore, when microneedles are used in an array format, care must be taken to ensure that the stiffness of the microneedles are strong enough to endure the shear forces of the tissue so that the needles do not break and tear the tissue layer or fail to distribute drugs or nucleic acids uniformly.

In summary, microneedles are a safe way to deliver nucleic acids to a variety of cell types directly, thus avoiding many of the gene delivery barriers mentioned earlier; however, single cell transfections are inefficient for most tissue engineering applications. Microinjection requires precision and high accuracy for success, which places the majority of the success or failure of the technique on ability of the individual performing the technique. The shape, size, and location of target cells can greatly restrict the ability of the investigator to effectively transfect cells via microinjection as well. Furthermore, isolation and immobilization of cells are an additional challenge that requires specialized training for successfully transfecting cells via microinjection. Microinjection could be far more attractive for tissue engineering if the process of isolating and injecting the cell of interest could be automated to remove the "human" factor from the process.

BALLISTIC GENE DELIVERY (GENE GUN)

Interdermal powder injection, biolistics, or ballistic gene delivery are names for a needle-free gene delivery technique originally developed by Sanford *et al*.[218] to transfect plant cells using DNA-coated metal particles. Over the years, the ballistic method was refined and commercialized for use in mammalian cells using both DNA and RNA.[272] Ballistic gene delivery

is a needle-free alternative to electroporation and microinjection that allows for DNA or RNA to be precipitated onto gold or tungsten particles, ranging in size from the nanometer to micron scale. The particles are delivered directly to mammalian tissues as a projectile out of a barrel of a pressurized ballistic device, colloquially referred to as a "gene gun". Particles are projected via a helium discharge or high-voltage electric spark, and can be propelled directly into the cell cytoplasm or nucleus (Fig. 2.3). Ballistic gene delivery has gained popularity as a potential delivery method for gene vaccines, as the DNA or RNA can penetrate the stratum corneum of the skin and reach the epidermis.[245] Additionally, investigators have successfully transfected mouse skeletal muscle fibers and liver tissue *in vivo* using ballistic gene delivery.[281] Furthermore, ballistic gene delivery has become not only a method to deliver therapeutic agents, but diagnostic agents as well. Several researchers have used the gene gun to deliver fluorescent dyes to track the functions of neurons.[18, 126] Thus, ballistic gene delivery has continued to grow in popularity as an alternative to microinjection for *in vivo* applications.

However, while useful for potential gene vaccine applications, ballistic gene delivery has several limitations. Ballistic gene delivery has a limited tissue depth to which DNA microparticles can be transmitted, thus many studies have investigated gene delivery to the skin. Furthermore, the path of the projectile can cause inflammation and damage to the target tissue with improper operation of the gene gun, or if the target tissue is bombarded with a high density of microparticles.[234] Moreover, ballistic gene delivery lacks cell specificity, so non-targeted cells may be transfected with the gene of interest if the non-targeted cells fall within the dispersal area of the gene gun. In addition, microparticles can accommodate very limited quantities of DNA or RNA. Thus, several treatments are needed to transfect a large population of cells if ballistic gene delivery is to be used for tissue engineering applications. Furthermore, there is no reliable way to

ensure that multiple treatments would uniformly distribute DNA microparticles, and not produce an inflammatory response in the target tissue. Mitchell *et al*.[168] and Kendall *et al*.[125] explored the effects of temperature, distance, and pressure on the penetration of DNA microparticles on buccal mucosa and porcine skin, respectively, and both groups found that uncontrolled environmental factors can greatly influence the efficacy of using ballistic gene delivery. Thus, the physical parameters need to be tightly regulated to optimize uniform delivery to cell cultures, which may not be possible for *in vivo* applications.

Thus, in summary, ballistic gene delivery can produce transient gene expression by directly delivering DNA to the cell cytoplasm or nucleus; however the delivery of DNA via ballistic gene delivery can be quite variable. Ballistic gene delivery is able to transfect primary tissues and difficult-to-transfect cells. However, ballistic gene delivery is limited in tissue engineering applications, as it can only transfect a limited number of cells, and not always in a uniform manner. Despite the drawbacks of ballistic gene delivery, it is an excellent method for developing gene vaccines as the DNA microparticles can readily penetrate the stratum corneum. As more research is conducted on ballistic gene delivery, perhaps a high throughput design will be developed that can consistently maintain precision and accuracy for nucleic acid delivery, or use different particle delivery materials to avoid inflammation and increase nucleic acid payload.

ELECTROPORATION

One of the most effective non-viral gene delivery methods, which has been extensively used and studied is electropermeabilization, also known as DNA electrotransfer, and colloquially referred to as "electroporation." Neumann *et al*.[178] introduced electroporation almost 30 years ago by successfully transfecting mouse lyoma cells. Since then, electroporation has evolved

rapidly. *In vivo* studies have been well underway since 1996, and since then electroporation technologies have successfully transfected skin, skeletal muscle, liver, tumor tissues *in vivo*.[3, 17, 46, 99, 101] Thus, it is necessary to look at how electroporation is thought to work to better understand its potential for tissue engineering. Additionally, we will examine two commercial electroporators that have gained much attention to aid in our understanding and discussion of how electroporation could be used for tissue engineering and cell differentiation.

In the broadest sense, electroporation is the application of an electrical field to a cell population for a finite amount of time to increase cell permeability to DNA, RNA and small proteins by creating localized transient disturbances in the cell membrane.[7, 166, 256, 257] Electroporation has shown to be highly effective in a wide variety of tissues *in vivo*, and cell cultures *in vitro*. In particular, electroporation has been used to aid chemotherapy for cancer treatment.[100, 149, 210, 228, 229, 258] In cancer treatments, irreversible electroporation is employed to ablate cancer tissues by inducing permanent formation of stable, non-resealing pores.[177] In gene therapy, reversible electroporation is employed, which keeps tissues intact because membrane pores are able to reseal.

There are many excellent reviews, in particular those published by Farvard *et al*.,[63] Teissié *et al*.,[241] Cemazar *et al*.,[25] Weaver *et al*.,[257] Mir *et al*.,[165] and Zimmerman *et al*.[287] as well as work published by Golzio *et al*.,[79, 80] which collectively explain the physical mechanisms proposed to take place during electroporation. To summarize, when an electric field is applied across a set of cells, hydrophilic pores are thought to form on the sides of the cell facing the electrodes, hence the name "electroporation."[197, 208] However, the precise mechanisms by which nucleic acids cross the cell membrane are still under investigation. Electrophoresis has been implicated as a possible process for enabling nucleic acids to diffuse from the extracellular environment into the

intracellular environment during the application of the electric field when nucleic acids are tightly associated with the cell membrane.[266] However, other studies suggest internalization of nucleic acids is restricted to nucleic acids bound to the cell membrane.[81] In addition to uptake mechanisms, the subject of how nucleic acids are transported and trafficked through the cell to the nucleus is still widely debated. Wu *et al*.[264] have recently suggested that nucleic acids may be transported via an endocytotic mechanism, while Vaughan *et al*. have provided data supporting trafficking via microtubules in TC7 cells and A549 cells.[247] Zaharoff *et al*.[278] and Lukacs *et al*.[151] provided evidence that suggested that DNA does not diffuse through the cell cytoplasm after microinjection and electroporation, but in fact must traffic via another mechanism such as endocytosis or via some form of convection.

Despite the many discrepancies over how electroporation works, a few general themes have been observed. There are distinct physical and biological considerations that must be tailored for each tissue to achieve maximum transfection efficiency. The size and type of the cell, nucleic acid concentration, and orientation of the cell are important factors to consider when adjusting pulse duration, pulse shape (square wave vs. exponential decay), and electric field strength, to achieve maximum transfection efficiency. Jordan *et al*.[117] directly addressed how to tailor physical parameters of electroporators to achieve maximum transfection efficiency in a variety of cell lines that are difficult to transfect. For example, morphological characteristics between human umbilical vein endothelial cells (HUVECs) and neuroblastomas differ dramatically.[59, 117, 157] Thus, the voltage, pulse shape, pulse duration, nucleic acid quantity, and cell density must be experimentally determined for each cell type to achieve maximum transfection efficiency, cell viability, and gene expression.[104, 153, 226] Mehier-Humbert *et al*.[158] suggested that long pulses (20 – 60 ms) combined with modest field strengths (100 – 200 V/cm) produce larger pores in cell

membranes that remain open for longer durations. Tailoring electroporation parameters is especially important for improving the stability of gene expression in primary cells such as HUVECs, neurons, and Jurkat cells, which are not as robust to electroporation procedures as opposed to skeletal muscle fibers, which are very robust to electroporation.[150, 166, 175, 216, 240, 275]

Another important component to consider in electroporation is the electrodes that are used to generate the electric field. Normally, electrodes are directly applied to the tissue *in vivo* or a cell culture *in vitro*. A variety of electrodes have been developed for different applications commercially, and several investigators have built custom electrodes for specific applications. The strength, orientation, shape, and homogeneity of the electric field are directly dependent on the geometry and spacing of the individual electrodes.[158] Furthermore, the material used to coat the surface of the electrode that interacts directly with the tissue can affect the transfection efficiency. Stainless steel is commonly chosen to minimize ion stripping during electroporation, which can change the pH of the suspension buffer of cells and increase cell toxicity.[7] A variety of different electrodes have been developed for different applications, which include plate electrodes, needle electrodes, and catheter electrodes.[98] Plate electrodes are commonly used for electroporation of surface tissues and for *in vitro* electroporation of cell suspensions in cuvettes. Needle electrodes are used to electroporate deep tissues *in vivo*, and catheter electrodes have been developed to electroporate blood vessels.[158] Figure 2.4 illustrates how plate electrodes and needle electrodes can be used to transfect cells *in vitro* and *in vivo*, respectively. Plate electrodes are able to generate more uniform (defined and homogenous) electric fields, but usually require stronger voltages for electroporation. Needle electrodes allow for more flexibility and customizability in setting up electric fields, but at the expense of less homogenous electric fields.[7, 98]

Many viral and chemical vectors have limited efficiency in non-dividing cells, but electroporation has successfully transfected both dividing and non-dividing cells.[3, 275] For tissue engineering applications, transfection of non-dividing cells is a highly desirable attribute as several primary cells in cartilage, bone, and neurons have rates of division that are too slow for passive gene delivery.[132, 193, 216, 220] Furthermore, electroporation has been shown to transfect progenitor cells and stem cells, which is another highly desirable attribute for tissue engineering, as many groups focus on utilizing various stem cell sources for differentiation and tissue regeneration.[6, 65]

Despite the advantages of electroporation, there are some major limitations restricting its use. First, several physical and biological parameters must be carefully tailored for each tissue to achieve maximum transfection efficiency, which can be very tedious. Second, electroporation may be able to efficiently transport nucleic acids into cells, but the benefit usually comes at a cost of low cell viability. Low cell viability is a major disadvantage of electroporation. Low cell viability may be a result of some cells undergoing irreversible electroporation or cells may die because of an increased cytotoxicity occurring from changing pH, resulting from the use of electrodes with poor biocompatibility. Furthermore, when electroporating tissues directly *in vivo*, there is the risk of producing inflammation, as not all cells will survive the procedure, and there may be a deposition of metal ions into the tissues from the electrodes. Another disadvantage of electroporation is that the up-front cost can be expensive, depending on the model of pulse generator and the associated electrodes. Furthermore, if *in vivo* studies are being conducted, a specially trained physician or technician must be present to properly place the electrodes on the subject to prevent injury and ensure proper alignment and generation of the electric field.

In summary, electroporation has great potential in tissue engineering and for gene vaccine applications, as electroporation is able to successfully transfect a variety of cells *in vitro* and *in vivo*, including dividing and non-dividing cells. However, electroporation can be an invasive procedure depending on the target tissue, and electroporation is notorious for producing low cell viabilities. However, unlike other transfection vectors, electroporation can transfect a large number of cells. Furthermore, the electroporative technology is rapidly evolving, and new systems are being developed each year to address the issues noted above. Nucleofection™ by Amaxa and Neon™ by Invitrogen are two such leading electroporative systems that will be further discussed below for tissue engineering applications. Both systems attempt to mitigate the issue of low cell viability and increase transfection efficiency.

NUCLEOFECTION™

Nucleofection™ has had incredible wide-reaching success in tissue engineering and cancer studies, compared against other physical non-viral gene delivery methods, and is therefore highlighted with special emphasis in this review. Nucleofection™ is a patented commercial electroporation system created by Amaxa, and owned by Lonza. Nucleofection™ is an electroporator that uses a sterile disposable cuvette to facilitate electroporation, Amaxa has developed a variety of cell specific buffers that are proprietary, and are designed to enable maximum transfection while reducing cell death. In addition to the cell specific buffers, the Nucleofector™ comes pre-programmed with an assortment of programs specific to different cell lines that vary voltage, frequency, and pulse duration. However, the voltage, frequency, and pulse duration for each cell type are not revealed to the user, although Amaxa does provide suggested protocols for the user. The Nucleofection™ system has gained great popularity among

many researchers as the Nucleofector™ is able to transfect many difficult-to-transfect cells, including several progenitor cells and stem cells. For example, Aslan *et al*.[8] transfected human bone marrow-derived stem cells (hBMSCs) with human bone morphogenetic protein 2 (*hBMP2*) and human bone morphogenetic protein 9 (*hBMP9*) via Nucleofection™ and achieved a transfection efficiency of 68 ± 41%. Aslan and colleagues confirmed that the Nucleofected™ cells were able to form new bone tissue both *in vitro* and *in vivo* through RT-qPCR, micro computed tomography (μCT), and immunohistochemistry. In an additional example, Bowles *et al*.[22] used a Nucleofector-96-Shuttle™ to transfect naïve dendritic cells with retinoic acid-inducing gene 1 (*RIG-I*) small interfering RNA (siRNA) to knockdown the *RIG-I* viral recognition receptor. Bowles *et al*. determined through RT-qPCR and western blotting that Nucleofection™ enabled a 75% knockdown of the detection of *RIG-I*. In a third experiment, Gonzalez *et al.*[82] successfully generated induced pluripotent stem cells (iPSCs) by Nucleofecting™ mouse embryonic fibroblasts with a polycistronic construct containing octamer-binding transcription factor 4 (*Oct4*), (sex determining region Y)-box 2 (*Sox2*), krueppel-like factor 4 (*Klf4*), and v-myc myelocytomatosis viral oncogene homolog (avian) (*c-Myc*). The identities of the iPSCs were confirmed via RT-qPCR, Southern blotting, and western blotting. Furthermore, iPSCs were differentiated *in vitro* toward neuronal lineages, cardiomyocyte lineages, or endoderm lineages. In addition to these studies, several more have summarized the ability of Nucleofection™ to successfully transfect progenitor cells, stem cells, and connective tissues (Table 2.1) as well as blood cells and blood vessel tissues (Table 2.2), cancer cells (Table 2.3), neuronal tissues (Table 2.4), and the Nucleofection™ technique has been successfully used for gene knockdown studies in a variety of cells (Table 2.5). However, as displayed in the tables, not all cell types tolerate Nucleofection™ well. Some cells types lack desirable cell viabilities.

Thus, the cell types lacking high cell viabilities may require more customization of buffer solution, electrical parameters, or a combination of both to increase viability.

Thus, in summary, Nucleofection™ is an effective transfection method for difficult-to-transfect cells, and Nucleofection™ can facilitate high transfection in a variety of cell types, which makes Nucleofection™ an attractive technique for *in vitro* and *ex vivo* tissue engineering applications.

NEON™

Neon™ is a proprietary electroporation system produced by Invitrogen. Neon™ uses a proprietary universal buffer for all cell types that is meant to facilitate high transfection efficiencies while preserving cell viabilities. Neon™ was released in early 2010, thus few publications are available using the Neon™ system; however, human embryonic stem cells, human embryonic kidney 293 cells (KEK293), mouse myoblasts (C2C12), adenocarcinomic human alveolar basal epithelial cells (A549), primary human fibroblasts, and several other cell types have been successfully transfected by Neon™.[30, 50, 102, 156, 169, 171, 172, 222, 235, 239]

Unlike the Nucleofector™, the Neon™ system uses an open pipette that contains a cylindrical electrode. Invitrogen claims that the design creates a more uniform electric field. In contrast to the Nucleofector™ system, the Neon™ transfection system allows the end user to program electrical parameters such as voltage, frequency, and pulse duration. Additionally, Invitrogen provides recommended protocols for end-users; however, since the Neon™ system is open, end-users may customize electrical parameters to their specific cells and experiments.

Thus, in summary, Neon™ provides the flexibility to program custom electrical parameters for experiments. However, Neon™ is still a young product, and publications are still being

produced on the effectiveness of Neon™ for cellular transfection, so it may be premature to draw conclusions regarding the Neon™ system at this time.

SONOPORATION

Similar to electroporation methods, high-intensity ultrasound has demonstrated the ability to induce pore formation in cell membranes, and allow for movement of plasmid DNA into cell cytosol.[67] This method is commonly referred to as "sonoporation," and in contrast to electroporation methods, induces pore formation through physical movement of fluid rather than using an electric field. Ultrasound is used in the clinic for diagnostic imaging, kidney stone treatment, pain relief, and ablation of cancer tissues.[120, 181, 243] High-intensity focused ultrasound (HIFU) produces localized shear forces in extracellular fluids that facilitate cavitation, or the controlled collapse of active air bubbles present in the surrounding fluid, and induce pore formation in cell membranes, increasing the permeability of cells to plasmid DNA and drugs (Fig. 2.5).[183, 204, 263] Cavitation can be enhanced with the use of ultrasound contrast agents, such as Optison™, and drugs and nucleic acids can be complexed with contrast agents for systemic delivery.[276] Zhou *et al*.[286] have examined the effects of pore formation in *Xenopus* oocytes, and have found that the resealing of pores is affected by extracellular calcium concentration. Sonoporation has gained popularity in clinical settings because it is non-invasive, and already used in the clinic to enhanced transdermal absorption of drugs. Furthermore, Newman *et al*.[179] have reviewed the use of sonoporation on a variety of cell types and tissues, and noted that sonoporation seems to be a less destructive method for delivery of plasmid DNA than electroporation. Currently, sonoporation is primarily used to enhance drug delivery and gene delivery to diseased tissues *in vivo* rather than for tissue engineering applications. Interestingly,

Liang *et al*.[144] have noted that sonoporation has exhibited enhanced transfection efficiency in tissues such as the heart, blood vessels, lung, kidney, brain, muscles, and the tumors when physical parameters of sonoporation are optimized.

Sonoporation is limited by relatively poor control of the energy localization. While sonoporation can induce cavitation in tissues, there currently is no way to control the uniformity of the cavitation or the entry of DNA. Complexation of DNA and contrast agents have greatly improved targeting; however, each target tissue needs to be carefully evaluated to ensure that cavitation induces pore formation in target cells.[158] Thus, sonoporation cannot be as precisely controlled as in electroporation, where cells are placed between electrodes. Furthermore, sonoporation seems to be more effective *in vivo* for tissues that are in direct contact with blood vessels.

In summary, sonoporation is effective for transfecting cells *in vivo* as it is non-invasive, and already used in the clinical setting. However, sonoporation exhibits lower transfection efficiencies because cavitation cannot be precisely controlled within the tissue. Improving the uniformity of cavitation for membrane pore formation and improving the accuracy of cell contrast could make sonoporation highly effective for tissue engineering.

LASER IRRADIATION

Laser irradiation is an alternative strategy under investigation for gene delivery applications. Investigators have used neodymium-doped yttrium aluminum garnet (Nd:YAG), holmium-YAG, titanium sapphire, and argon powered lasers to perforate cells to enable the entry of DNA by varying the pulse frequency of the laser.[189, 215, 238, 280] Typically, a laser is focused through an objective onto a localized area of an individual cell in culture and increases the permeability of

the cell to exogenous DNA in the culture medium. Interestingly, cells seem to not undergo any lethal injury when perforated by a laser, and they are able to repair the "holes" made by perforations in less than a second.[138, 189] Furthermore, a laser can be used indirectly to induce stress waves in the medium to perforate cells temporarily to enable the entry of DNA. Yao *et al*.[274] provided a comprehensive review of the different methods to use a laser to facilitate gene delivery in cell culture. Ogura *et al*.[184] demonstrated the precision and efficiency of using laser irradiation by injecting Sprague-Dawley rats with plasmid DNA coding for enhanced green fluorescent protein (EGFP). EGFP expression was confined to the exact area of skin irradiated with the laser 24 hours after transfection. In another report, Shirahata *et al*.[232] successfully delivered EGFP to HuH-7 and NIH/3T3 cells in culture by using a pulsed 355 nm Nd:YAG laser to perforate cells, while a 1015 nm continuous-wave Nd:YAG laser was used to trap individual cells. Figure 2.6 provides an illustration of a cell undergoing perforation by a pulsed laser while being immobilized by a continuous laser.

Laser irradiation has great potential for tissue engineering as it can be used to target precise cells in tissue or in culture. Laser irradiation is less invasive than microinjection or electroporation as no needle is required and individual cells can be targeted. The brief perforation of the cell by a pulsed laser seems not to cause cell death. Furthermore, optical fibers can deliver laser light that can be controlled by computers, and may eventually provide convenient access to tissues inside the body for gene therapy that were previously inaccessible.[274]

However, despite the advantages of laser irradiation, some key limitations exist. While precise and efficient, laser irradiation is still a young technology, and more studies are needed to determine how robust the procedure is on different cell types. Laser irradiation is highly efficient

at targeting individual cells, but it is not efficient at targeting large populations of cells efficiently. In addition, optical lasers can be very large and costly. Furthermore, specialized training is required to operate an optical laser properly.

In summary, laser irradiation has great potential for gene therapy and tissue engineering applications as optical lasers can be used to precisely target individual cells in culture or in tissue. However, laser irradiation is still a young technology that needs further investigation, and is costly. Nevertheless, as laser irradiations strategies improve and the technology is further investigated, optical lasers may allow investigators to target tissues for gene therapy and tissue engineering in ways that were previously not possible.

EMERGING TECHNIQUES IN GENE DELIVERY

In contrast to the techniques described above, there are additional techniques under development that may prove advantageous for specific gene delivery and tissue engineering applications. Here we briefly describe the techniques of electric field-induced molecular vibration gene delivery, a novel technique introduced by Tuan and colleagues in 2004 [236], and magnetofection, a technique used as a tool to enhance gene delivery strategies.

Tuan *et al*.[236] developed a unique gene delivery method known as electric field-induced molecular vibrations as an alternative to electroporation to facilitate high transfection efficiencies in mesenchymal progenitor cells and a variety of cell lines. Tuan and colleagues created a unique apparatus where cells and DNA are suspended in a glass dish that undergoes vigorous vibration induced by two electrodes.[236] The electrodes do not directly contact the cells, and no current is applied across the cells; however, the vigorous shaking enables exogenous molecules to penetrate the cell membrane and reach the cytoplasm. According to Tuan *et al*.[236] electric field-

induced vibration transfection is economical and efficient because it requires no additional reagents and exhibits high transfection efficiency with low cell mortality. Furthermore, Tuan *et al*.[236] noted that electric field-induced molecular vibration transfection does not interfere with cell proliferation, and provides stable gene expression. Limited literature is available on this technique; however, if these claims and data can be verified then electric field-induced molecular vibration transfection could be a suitable transfection technique for *ex vivo* and *in vitro* tissue engineering applications.

Magnetofection is a technique that exploits the energy of a magnetic field to enhance the delivery efficiency of DNA, siRNA, or shRNA via viral or non-viral vectors.[45, 61, 72, 225] Paramagnetic particles typically made of iron oxide are coated with viral particles, liposomes, or cationic polymers and combined with nucleic acids.[103, 107, 225] Several *in vitro* studies have placed a magnetic plate underneath a cell culture vessel once the magnetic particles and gene delivery vector have been combined with the target tissue of cells to preferentially direct or "pull" the magnetic particles into cells or tissue explants.[273] Magnetofection does not necessarily improve the transfection efficiency of gene delivery methods; instead, magnetofection increases the speed at which nucleic acids traffic into the cell and nucleus while enabling smaller doses of nucleic acids to be used.[201] Plank *et al*.[200, 202] have published insightful reviews on how magnetofection works and the potential benefits of magnetofection on *in vitro* gene delivery applications. In addition, magnetofection has been used to enhance gene delivery to primary cells such as neurons and endothelial cells *in vitro*, and has been applied to enhance gene delivery to the gastrointestinal tract and blood vessels *in vivo*.[23, 136, 198, 219, 225, 227] As new technologies develop, magnetofection could prove quite valuable to enhancing tissue engineering applications.

APPLICATIONS OF GENE DELIVERY TO TISSUE ENGINEERING

The goal behind integrating gene therapy and tissue engineering together is to manipulate the behavior of cells so that cells can be used to produce proteins and associate into tissues that are capable of replacing, restoring, regenerating, or enhancing the function of tissue defects within the human body. The marriage of these two fields is not a new idea. In fact, there are a multitude of examples where gene therapy and tissue engineering have been integrated for enhancing differentiation strategies. Multiple groups have used a variety of synthetic polymers (PEI), biodegradable polymers (PLL-PA, PBAE, PLGA), and biological polymers (chitin, fibrin, collagen) to either encapsulate or anchor nucleic acids to the scaffolding material on which cells are seeded for nucleic acid uptake.[21, 39, 76, 77, 84, 86, 87, 91, 111, 143, 145, 180, 199, 223, 270] Several of the studies have shown sustained gene delivery for periods up to two to three weeks, but the overall transfection efficiency has varied. Polymers provide flexibility in designing scaffolds to accommodate stem cells for differentiation, and the incorporation of nucleic acids to direct differentiation is a natural progression. However, no one polymer has emerged as a reliable vector for primary cells, progenitor cells, and stem cells. Nor should any one polymer be expected to successfully transfer nucleic acids to all cell types. While it seems several investigators within the field of tissue engineering have placed an emphasis on trying to deliver nucleic acids via polymers, others have focused on physical methods. Cesnulevicius *et al*.[26] transfected mesencephalic neuronal progenitor cells from Sprague-Dawley rats with fibroblast growth factor 2 (*FGF-2*) linked to enhanced green fluorescent protein (EGFP) via Nucleofection™ and found that the transfected cells tested positive for *nestin*, an important protein for neuron growth. Furthermore, the cells were able to survive transplantation into lesioned rat brains, demonstrating a potential for developing a new primary transplantation

method for neuronal tissues. The significance of the work by Cesnulevicius *et al*.[26] is that they achieved a transfection efficiency of 47% in neuronal progenitor cells, which is high for a non-viral method, especially because neuronal tissues are notoriously difficult to transfect. This study shows promise for using physical non-viral gene delivery vectors, in this case Nucleofection™.

In a different experiment, Duffy *et al*.[57] transfected human mesenchymal stem cells (hMSCs) with *Ephrin-B2* via Nucleofection™ and achieved a transfection efficiency of approximately 45%. hMSCs have been known not to transfect easily. Furthermore, in this study, the hMSCs expressed *Ephrin-B2* and took on early endothelial phenotype and are thought to have contributed to the increased detection of VEGF in cell culture, which could potentially promote angiogenesis in ischemic tissues.

UNDERSTANDING CHALLENGES THAT LIMIT NON-VIRAL GENE DELIVERY

Every single vector must first cross the plasma membrane. However, before a delivery vehicle reaches the cell membrane, there are obstacles to overcome. For example, most cells in a connective tissue are located within the labyrinth of the extracellular matrix (ECM). Some investigators have suggested that the collagen in the ECM could be hindering the diffusion of large nucleic acids and other macromolecules, preventing them from reaching the target cell surface.[176, 203] Thus, one approach to overcome this limitation is to disrupt the ECM. Disrupting the ECM *in vivo* could pose difficulties for the subject; however, if the target tissue is excised, the ECM could be disrupted with trypsin to expose cell membranes. An additional consideration is that electrophoresis may be able to help move nucleic acids through the ECM, but this process, depending on the tissue, may not be able to bring the nucleic acids close enough to the cell

membrane for interaction.[101] Thus, the ECM may be an additional barrier to consider when designing delivery vectors.

Beyond the ECM, the cell membrane remains a significant barrier for all delivery vectors. Many chemical vectors attempt to associate the nucleic acid delivery vehicle with the cell membrane through electrostatic interactions, ligand mediated receptor binding, and through adsorption. Several studies suggest that association with the cell membrane is required for entry into the cytoplasmic compartment of the cell.[62, 66, 78, 92, 206] However, microinjection and ballistic gene delivery bypass the cell membrane by directly transporting nucleic acids into the cell cytoplasm of nucleus. Electroporation, sonoporation, and laser irradiation disrupt the cell membrane to facilitate infiltration of nucleic acids. However, microinjection, ballistic gene delivery, electroporation, sonoporation, and laser irradiation display one common weakness. All methods rupture the cell membrane in some fashion, and if the cell is unable to mend the membrane, then the cell dies. Thus, taking a closer look at the function of the cell membrane may provide questions and answers to finding ways to better overcome this important barrier and maximize cell viability.

What is the plasma membrane? Simply, the plasma membrane is a barrier to separate two hydrophilic compartments, namely, the intracellular space and the extracellular space. The plasma membrane is composed of a phospholipid bilayer with proteins permeating both the intracellular and extracellular sides of the plasma membrane.[5, 24] Furthermore, the composition of lipids and proteins can vary among cell types, and the plasma membrane is not a rigid structure, meaning that lipids and proteins are not static, but rather moving targets. The composition of the cell membrane can have an influence on the physical and mechanical functions of the cell membrane. For example, cells that are a part of tissues that provide structure and support (e.g.,

bone) may be more inflexible and rigid, containing fewer unsaturated lipids to maintain a less fluid structure, and hence lower membrane permeability, whereas secretory cells may contain more unsaturated lipids and fewer proteins to maintain a more fluid membrane composition that is more permeable.[5] Furthermore, depending on the target cell and the condition of the tissue (i.e., adherent cells or cells in suspension), access to the plasma membrane may be restricted. Thus, an appropriate questions is "does exposure to cell surface affect localization of nucleic acids on the surface?" Adler *et al*.[2] endeavored to address this very subject by exploring the effect of cell surface topography on transfection efficiency. Adler plated fibroblasts onto micropitted surfaces at varying densities and found a 25% increase in transfection efficiency when using Lipofectamine 2000™ to deliver GFP for cells plated on densely pitted surfaces as opposed to smooth surfaces. This increase could have been attributed to a variety of factors. The cells did spread across the pitted surfaces, but not on the smooth surfaces. So why did transfection efficiency increase? Were delivery vehicles able to associate with the cell membrane because the membrane had an increased surface area? Did the composition of the membrane change because of the cell spreading across the pitted surface? Adler suggested that a consequence of the cell spreading was a loss of integrin mediated cell adhesion, which resulted in the internalization of caveolae, and could have been responsible for a down regulation of particle uptake through competitive mechanisms. The spreading of cells on pitted surfaces did not lead to an increase in cell proliferation. Thus, the rate of cellular mitosis did not increase, which means passive diffusion of DNA into the cell nucleus was not responsible for the increase in gene expression. Adler's study was exciting because it drew attention to the consideration of surface topography, and presented questions about how nucleic acids associate with the cell membrane and how the cell membrane might be altered to accommodate molecules. Perhaps the

permeability of a cell membrane can be manipulated mechanically to alter firmness or fluidity for delivery vectors. An exciting next step would be to see how other non-viral vectors perform when a cell spreads. For example, combining cell spreading with an electroporative technique would be an exciting study to investigate how cell spreading affects the ability of the cell to permeabilize and mend under an electric field. Another question to ask is whether different cell types produce the same results when cultured on pitted surfaces.

Chalut *et al*.[27] presented an additional insight regarding the influence of changing mesenchymal stem cell (MSC) membrane topography and how deforming the MSC changes the structure of its nucleus. As the nucleus is connected via the cytoskeleton to the cell membrane, mechanical forces on the cell membrane act via the cytoskeleton on the nucleus. They offered evidence that is consistent with findings in the literature that the nucleus changed shape in response to the deformation of the cell.[27, 142, 233] If the nucleus can alter its shape in response to mechanical forces exerted on the cytoskeleton, then how does gene expression change? Does the elongation of the nucleus in response to mechanical forces acting on the cell increase transfection efficiency by shortening the distance between the cell membrane and nucleus? These questions need further investigation.

Despite the interest in the membrane topography and deformation of the nucleus as they relate to gene expression, there is an additional parameter to consider. Chemical vectors tend to use an endocytotic route of delivery once the nucleic acids have entered the cell, while physical vectors attempt to deliver nucleic acids directly to the cytoplasm or nucleus. However, chemical methods seem to have higher cell viabilities, but low transfection rates in primary cells, progenitor cells, and stem cells, whereas the opposite is true for physical methods. Thus, the questions arises, “how do nucleic acids traffic through the cytoplasm?” Nucleic acids must

escape endosomes to avoid degradation by lysosome enzymes, but then how do the nucleic acids reach the interior of the nucleus? Dividing cells provide an opportunity on a regular interval as the nuclear envelope deconstructs during mitosis, and reforms at the conclusion of mitosis. In non-dividing cells, the nucleic acids must enter through a nuclear pore. Thus, how do the nucleic acids reach the nuclear pore? Zaharoff *et al*.[278] suggested the nucleic acids do not diffuse through the cytoplasm, but move by some other mechanism such as convection. Lukacs *et al*.[151] presented work that was consistent with Zaharoff *et al*.[278] in that DNA did not seem to diffuse through the cytoplasm. Vaughan *et al*.[247] provided evidence that suggested that nucleic acids may traffic via microtubules. Unfortunately, there is still very little that is known about how nucleic acids traffic through the cytoplasm. Elucidating how nucleic acids traffic through the cytoplasm will be crucial to improving future vectors.

DISCUSSION

Improving physical non-viral gene delivery methods for tissue engineering applications requires an examination of the fundamental mechanisms utilized by each physical non-viral gene delivery method as well as the reason different cell types are more or less responsive to each gene delivery method. Elucidating the basic mechanisms by which physical non-viral gene delivery methods work and understanding why different cell types are responsive to different gene delivery methods will allow investigators to exploit the positive attributes of gene delivery methods and different cell types to enhance tissue engineering applications.

Microinjection is perhaps the most efficient and direct method for delivering nucleic acids to cells; however, the major weaknesses associated with microinjection are the restricted access to tissues, and the inability to transfect large numbers of cells. Likewise, ballistic gene delivery

lacks access to tissues and is restricted by the quantity of nucleic acids that can be delivered. However, both of these methods have significant potential if the weaknesses previously stated can be overcome, as both methods can directly control the amount of nucleic acids directly delivered to individual cells.

In addition, electroporation, sonoporation, and laser irradiation seek to transiently disrupt the cell membrane to increase permeability of nucleic acids to the cells. Sonoporation is attractive because it is already used in a clinical setting, but the tissues that are being targeted need to be extensively evaluated to produce maximum efficiency. Electroporation suffers the same weakness as sonoporation, yet electroporation has more flexibility for targeting cells, as the electric field can be controlled via a pulse generator and electrodes can be designed specifically for individual applications. However, electroporation still suffers from low cell viability. Laser irradiation can precisely target individual cells; however, laser irradiation is not efficient for targeting thousands of cells in different layers of tissues. In contrast, several non-viral chemical vectors exhibit high cell viabilities, but limited transfection efficiencies. Thus, it is necessary to look at which physical features enable the high cell viability of most non-viral chemical transfection vectors and which physical features enable moderate to high transfection in non-viral physical vectors. Perhaps it is best to consider these questions from the point of view of the cell and the environment of the cell to gain a better understanding of what affects cell viability and limits transfection.

If the cell can be physically manipulated, how else can non-viral vectors be improved? Is it possible to make cells more susceptible to electroporation or sonoporation by adjusting the osmolarity of the extracellular fluid? If the extracellular fluid is made to be hypotonic to the intracellular fluid of the cell to induce swelling of the cell, will the swelling produce similar

responses in the cell membrane as cell spreading? These questions are important to consider when designing new vectors. Furthermore, can delivery vectors be combined to achieve higher transfection efficiencies? Is there a way to design a combinational polymer scaffold to where one polymer acts as an electrode and another polymer acts as an anchor for nucleic acids and an attachment platform for cells seeded into the scaffold to permit increased transfection efficiency?

Increasing the abilities of non-viral vectors to manipulate gene expression and mitigate cell death depend on finding ways to improve the uptake of nucleic acids into cells and minimizing the trauma to the cell membrane from points of entry. The physical methods described in this review are capable of overcoming the limitation of the cell membrane entry by directly acting on the cell membrane and forcing nucleic acids into the cytoplasm or even the nucleus. However, the method of membrane disruption can directly influence the cell's ability to mend the membrane. The diameter of the "holes" created in the cell membrane and the duration for which these "holes" remain open seem to directly correlate with the cell's ability to survive. As suggested by Mehier-Humbert *et al*.,[158] larger pores that remain open for increased durations increase the uptake of nucleic acids; however, larger pores permit the exchange of additional agents that normally cannot cross the cell membrane increasing the risk that homeostatic concentration gradients will be disrupted leading to cell death. Thus, a balance needs to be struck between facilitating the entry of nucleic acids without compromising the homeostatic concentrations of ions such as Na+ and K+ inside and outside of the cell.

As investigations continue to investigate how cell membranes and gene expression can be manipulated from a chemical and mechanical perspective, new mechanisms of how the cell membrane reseals and how nucleic acids are trafficked within the cytoplasm in different cell types are bound to be proposed in the literature. Elucidating these fundamental mechanisms will

contribute to developing new delivery strategies that enhance the delivery of nucleic acids with minimal risks to compromising the cell membrane. Perhaps even combinational approaches may yield beneficial consequences for gene transfer into target tissues. Tissue engineering currently focuses on manipulating cellular behavior externally by applying mechanical stimuli and different biomaterials to simulate native environments to aid in the differentiation of progenitor cells and stem cells. Perhaps considering the external environment as part of the nucleic acid delivery system is the key to changing the behavior of the cell to better accommodate nucleic acid delivery and improve differentiation of cells into target tissues for regeneration and tissue engineering applications.

CONCLUSION

The improvements in physical gene delivery methods over the past three decades have been impressive and have greatly enabled increased gene expression in difficult-to-transfect cells; however, the fundamental challenges still remain. Non-viral physical methods still focus on deforming the cell membrane in some manner to increase transfection rates at the expense of cell viability. However, investigators are working to elucidate mechanisms of how nucleic acids can cross the cell membrane and traffic through the cytoplasm to the nucleus. These endeavors are expected to lead to the development of new vectors that can increase the gene expression in cells without compromising significant numbers of cells *in vitro* or *in vivo*. Furthermore, exploration of how cellular behavior can be manipulated externally to achieve a desired behavior is of interest in tissue engineering, which may be key in developing new strategies to better facilitate cell differentiation. Thus, it would seem that applying a tissue engineering approach to gene therapy rather than a gene therapy approach to tissue engineering may be a potential solution for

providing a fruitful integration of these two fields together to expand approaches for cell differentiation and tissue formation in tissue engineering and regenerative medicine applications.

CHAPTER 3: Improving Viability and Transfection Efficiency with Human Umbilical Cord Wharton's Jelly Cells Through use of a ROCK Inhibitor[2]

ABSTRACT

Differentiating stem cells through gene delivery is a key strategy in tissue engineering and regenerative medicine applications. Non-viral gene delivery bypasses several safety concerns associated with viral gene delivery; however, leading non-viral techniques, such as electroporation, subject cells to high stress and can result in poor cell viabilities. Inhibition of Rho-associated coiled-coil kinase (ROCK) has been shown to mitigate apoptotic mechanisms associated with detachment and freezing of induced pluripotent stem cells and embryonic stem cells; however, inhibiting ROCK in mesenchymal stromal cells (MSCs) for improving gene delivery applications has not been reported previously. In this study, we hypothesized that ROCK Inhibitor would improve cell viability and gene expression in primary human umbilical cord Wharton's jelly cells (hWJCs) when transfected via Nucleofection™. As hypothesized, the pre-treatment and post treatment of hWJCs transfected via nucleofection with Y-27632 ROCK Inhibitor significantly improved survival rates of hWJCs and gene expression as measured by green fluorescent protein intensity. This study provides the first comparative look at the effect of Y-27632 ROCK Inhibitor on hWJCs that underwent transfection via nucleofection, and shows using Y-27632 ROCK Inhibitor in concert with nucleofection could greatly enhance the utility of differentiating and reprogramming hWJCs for tissue engineering applications.

[2] Reformatted for thesis. Published as **Mellott, A.J.**, Godsey, M.E., Shinogle, H.E., Moore, D.S., Forrest, M.L., and Detamore, M.S. Improving Viability and Transfection Efficiency with Human Umbilical Cord Wharton's Jelly Cells Through Use of a ROCK Inhibitor. Cell Reprogram. 16(2):91-97, 2014.

INTRODUCTION

Many tissue engineering strategies utilize gene delivery approaches to differentiate stem cells toward terminal lineages [110, 132, 231, 285]. While viral gene delivery remains popular for many tissue engineering applications due to high efficiency, concerns regarding toxicity, immunogenicity, and oncogenesis from insertional mutagenesis still remain [29, 244]. Non-viral vectors are an alternative to viral vectors, and in many cases are able to circumvent the safety concerns associated with viral vectors. However, in primary cells and stem cells, non-viral vectors usually exhibit low transfection efficiencies compared to their viral vector counterparts [159]. Significant technological advancements have been made in the last decade regarding electroporation that have led to increased transfection efficiencies, but low cell viabilities [7, 59, 78]. Thus, a method is needed that will enable primary cells and stem cells to be transfected at a high efficiency while maintaining acceptable cell viabilities for tissue engineering applications.

Over the past five years, several observations have been made regarding stem cell apoptosis related to detachment and freezing protocols as related to RhoA GTP signaling pathways [186, 267, 283, 284]. In particular, several research groups have noted that inhibition of the Rho-associated coiled-coil kinase (ROCK) appeared to increase cell survival by mitigating negative effects associated with cell dissociation and thawing [37, 60, 70, 71, 230]. The Y-27632 ROCK Inhibitor (Y-27632-RI) appeared to be especially useful for improving stem cell viability in human induced pluripotent (iPS) cells and embryonic stem (ES) cells [116, 174]. Furthermore, the use of Y-27632-RI was shown not to affect the pluripotency of ES cells [255]. Chatterjee et al. [28] were the first group to use RI to aid in the transfection of human iPS cells via Nucleofection™, an electroporative technique developed by Lonza Group Ltd. (Basel, Switzerland).

Human umbilical cord Wharton's jelly cells (hWJCs) have a number of advantages over other cell sources and hold great potential for clinical translation, as we have reviewed extensively [10, 253]. Unfortunately, hWJCs are difficult to transfect, and few studies are available on the transfection of hWJCs. Based on its aforementioned success in other applications, we hypothesized that Y-27632-RI would improve cell viability and transfection efficiency for hWJCs that are transfected via nucleofection. In this study, transfection efficiency, gene expression, and cell viability were evaluated for hWJCs transfected via nucleofection with green fluorescent protein (GFP), with or without Y-27632-RI.

MATERIALS AND METHODS

Procurement and expansion of hWJCs

hWJCs were isolated from Wharton's jelly of human umbilical cords obtained from the KU Medical Center Hospital (IRB# 10951), Lawrence Memorial Hospital (IRB# LMH 08-2) and Stormont-Vail Hospital (IRB approved, no reference number) for a total of five umbilical cords used in the study (n = 5). Four cords were from males that were born at full term and one cord was from a female born at 38.3 weeks, all under normal delivery conditions. Maternal age was not available. We isolated hWJCs according to our previous published protocol [48]. hWJCs were cultured in traditional hWJC medium (10% fetal bovine serum (FBS-MSC Qualified) and 1% Penicillin-Streptomycin in low glucose DMEM (Life Technologies, Grand Island, NY)). hWJC media was changed three times per week, and hWJCs were maintained at 37°C with 5% CO_2 in a cell culture grade incubator. hWJCs were trypsinized with 0.05% Trypsin-EDTA (1X) (Life Technologies) at 80 to 90% confluency. All hWJCs were expanded to passage 2 (P2) for the

experiments. Five umbilical cords (*n = 5)* were used in total for this study. All experiments were performed in triplicate for each cord.

Cell Characterization

At P2, a sub-culture of cells from each cord was characterized through cell surface marker identification via flow cytometry on a MoFlo XDF fluorescent activated cell sorter (FACS) (Beckman Coulter, Brea, CA). hWJCs were characterized using the following antibodies and secondary antibodies: STRO-1 Mouse IgM (2.5:200) (1 mg/mL; R&D Systems, Minneapolis, MN); Alexa Fluor 568® Rabbit Anti-Mouse IgG (2:200) (2 mg/ mL; Life Technologies); CD105 Mouse IgG (2.5:200) (1 mg/mL; R&D Systems); Qdot® 525 donkey anti-mouse IgG (2:200) (1 μM; Life Technologies); Human CD45 pre-conjugated to Qdot® 800 (2:200) (Life Technologies); Human CD73 pre-conjugated to FITC (5:200) (BD Biosciences, San Jose, CA); Human CD34 pre-conjugated to Brilliant Violet (5:200) (BD Biosciences); Human CD90 pre-conjugated to APC (5:200) (BD Biosciences). 20,000 events were recorded for each sample. Positive identification of cell markers was defined as fluorescent emission that exceeded the fluorescent threshold of cells stained with corresponding isotype (negative) controls. The isotype controls used in these studies were Rabbit IgG Alexa Fluor 568, Donkey IgG Qdot 525, IgG_2 Qdot 800 (all from Life Technologies), and IgG_1 FITC, IgG_1 Brilliant Violet, and IgG_1 APC (all from BD Biosciences). The cell characterization experiments were repeated three times for each cord.

ROCK Inhibitor treatments and transfection

On the day of transfection, media from all wells were removed, and cells were washed with PBS twice. Afterward, cells were incubated for 1 h at 37°C in traditional hWJC medium

(10% FBS-MSC Qualified/1% Penicillin-Streptomycin/Low glucose DMEM) or traditional hWJC medium with 10 μM of Y-27632-RI (Reagents Direct, Encinitas, CA). After 1 h, hWJCs were washed twice with PBS, trypsinized, and then resuspended in 95 μL of 4D Nucleofector™ P1 Primary Solution (P1PS) (Lonza) at a density of 500,000 cells per 95 μL in a 50-mL conical tube (Phenix Research Products, Candler, NC). 5 μL of P1PS or 5 μL of pmaxGFP (1 mg/mL; Lonza) was added to each sample, depending on the group to bring the final cell suspension volume to 100 μL. hWJCs were separated into five groups consisting of three replicates per group. Groups 1 and 3 received no pmaxGFP. Groups 2, 4, and 5 each received 5 μL of pmaxGFP (1 mg/mL; Lonza). Groups 1, 2, 3, and 4 were cultured in traditional hWJC medium before and after transfection while Group 5 was cultured in traditional hWJC medium with 10 μM of Y-27632-RI (Reagents Direct) before and after transfection. Our preliminary experiments revealed a concentration of 10 μM of Y-27632-RI used both before and after transfection were preferred for effective transfection. hWJC suspensions from Groups 1 and 2 were immediately transferred to 6-well plates (BD Biosciences) containing 1.5 mL traditional hWJC medium and incubated at 37°C. hWJC suspensions from Groups 3, 4, and 5 were transferred to 100-μL 4D Nucleofection™ cuvettes. Each cuvette was gently tapped twice then placed in a 4D Nucleofector™ (Lonza) and nucleofected with the program FF-104. hWJCs were incubated at room temperature (ca. 22°C) for 10 minutes then transferred to a 6-well plate (BD Biosciences) containing 1.5 mL traditional hWJC medium (Groups 3 and 4) or traditional hWJC medium with 10 μM of Y-27632-RI (Reagents Direct) (Group 5) and incubated at 37 °C.

Fluorescent Microscopy

At 24 h and 48 h after transfection, hWJCs were collected for analysis. 0.5-µL of Hoechst 33342 dye (Life Technologies) was added to each well, and hWJCs were incubated for 10 minutes at 37°C. Afterward, hWJCs were imaged using an Olympus IX81 inverted (Olympus America, Center Valley, PA) epifluorescent microscope with an Olympus LUCPlanFL 20X 0.4 NA objective (Olympus). Images were captured using the software, SlideBook (Intelligent imaging Innovations (3i), Denver, CO). A mercury arc lamp was used with the following excitation filters (Excitation/Emission) for image collection: Hoechst (387 ± 11 nm/447 ± 60 nm) and GFP (494 ± 20 nm/531 ± 22 nm). For each sample that was imaged, a montage was generated from 25 (five by five arrangement) neighboring fields of view that were aligned together to generate one comprehensive composite image of the sample. All experiments were repeated three times for each umbilical cord at 24 h and 48 h.

FACS Analysis

Immediately after imaging, cells were washed twice, trypsinized, and transferred into 5 mL polypropylene round-bottom tubes (BD Biosciences). 0.5 µL of propidium iodide (PI) (1 mg/mL; Life Technologies) was added to each sample just before analysis. hWJCs were analyzed via flow cytometry on the Beckman Coulter MoFlo XDP FACS. 20,000 events were recorded for each sample analyzed. Flow Cytometry was used to analyze both cell viability and transfection efficiency. Live hWJCs were characterized as hWJCs expressing Hoechst at an intensity of 10^2 Relative Fluorescent Units (RFU) or above, with expression of PI at an intensity below 10^0 RFU. Dead hWJCs were characterized as hWJCs that expressed Hoechst at an intensity below 10^2 RFU and expressed PI at an intensity of above 10^0 RFU. GFP-positive hWJCs were characterized as live hWJCs that expressed GFP at an intensity of 10^0 RFU or greater.

Transfection efficiency was determined by dividing the number of live GFP positive cells in a sample by the total population of the sample. All experiments were repeated three times for each cord at 24 h and 48 h post-transfection. An example of how cell populations were gated is provided in Figure 3.1 and the statistics for all samples from an entire umbilical cord are displayed in Table 3.1.

Statistics

All values are reported as means ± standard deviations. A one-way ANOVA was performed with a Tukey's post hoc test to assess statistical significance with n = 5 cords. Statistical significance was set at $p < 0.05$.

RESULTS AND DISCUSSION

As hypothesized, hWJCs treated with RI displayed a significantly increased survival rate and transfection efficiency after nucleofection than hWJCs that were not treated with RI. Gene delivery is a powerful tool for reprogramming hWJCs as demonstrated by [13] and Devarajan et al. [48]. Until now, non-viral delivery methods have suffered from poor transfection efficiency with high cell viability, or high transfection efficiency with poor cell viability. RhoA GTP signaling pathways are critical for inducing several apoptotic mechanisms in response to unfavorable environmental changes [105, 185]. Inhibiting ROCK can reduce apoptosis associated with detachment and freezing protocols [94, 106, 134, 139, 187]. One of the key disadvantages of using non-viral physical delivery methods such as electroporation is the need to dissociate cells from adherent surfaces. However, by using Y-27632-RI to mitigate some of the apoptotic mechanisms induced by cell detachment and electric shock, it might be possible to rescue positively transfected cells from cell death, which was the primary goal of this study.

Flow cytometry analysis revealed that the cell populations were mostly non-hematopoietic as the hWJCs were 98.1 ± 0.04% negative for CD34 expression and 90.4 ± 1.1% negative for CD45 expression. The expression of CD90, a key mesenchymal stem cell marker, was detected in 98.5 ± 0.54% of cells. The expression of remaining key mesenchymal stem cell markers, CD73 (12.0 ± 7.8%), CD105 (10.2 ± 0.15%), and STRO-1 (3.4 ± 0.33%), were low and relatively variable, suggesting sub-populations may exist within each cell population that displayed surface epitopes consistent with mesenchymal stem cell markers as reviewed by [252, 253]

As was seen in the microscopy images at 24 h (Fig. 3.2A) and 48 h (Fig. 3.3A) after transfection hWJCs that were not subjected to nucleofection displayed high cell densities compared to hWJCs that were subject to nucleofection. However, hWJCs that were treated with 10 μM of Y-27632-RI before and after transfection displayed a greater cell density than hWJCs that were subject to nucleofection and not treated with Y-27632-RI as shown in microscopy images and corroborated by flow cytometry data.

There was a clear increase in both cell viability and transfection efficiency between the experimental group of hWJCs that was nucleofected and treated with Y-27632-RI and the group of hWJCs that was nucleofected and not treated with Y-27632-RI at both 24 h and 48 h after transfection (Fig. 3.4). Cell viability was 3.3 times greater in hWJCs treated with Y-27632-RI than hWJCs that were not treated with Y-27632-RI 24 h after transfection ($p < 0.05$), while cell viability was 3.2 times greater in hWJCs treated with Y-27632-RI than hWJCs not treated with Y-27632-RI 48 h after transfection ($p < 0.01$). Transfection efficiency was 4.6 times greater in hWJCs treated with Y-27632-RI than hWJCs not treated with Y-27632-RI 24 h after transfection ($p < 0.01$). At 48 h after transfection, transfection efficiency was 4.8 times greater in hWJCs treated with Y-27632-RI than hWJCs not treated with Y-27632-RI ($p < 0.05$).

The difference in GFP intensity may have been a result of an increased number of live cells present and able to re-adhere to a surface when treated with Y-27632-RI as opposed to hWJCs that were not treated with Y-27632-RI. The flow cytometry histograms were consistent with microscopy images in showing that a greater number of hWJCs treated with Y-27632-RI survived and expressed GFP at varying intensities at both 24 h (Fig. 3.2B) and 48 h (Fig. 3.3B) after transfection than hWJCs that were not treated with Y-27632-RI. Furthermore, the data from the histograms suggested that there might be a relationship between GFP expression and cell density. Further formal studies are needed to verify if an actual relationship exists.

hWJCs treated with Y-27632-RI at both 24 h and 48 h post-transfection displayed an increase in cell viability, and a far more substantial increase in transfection efficiency compared to hWJCs that were not treated with Y-27632-RI. Thus, future studies are needed to explore whether a synergistic phenomenon is occurring in which Y-27632-RI is not only rescuing dying cells, but improving cell health to facilitate expression of GFP in cells that may not have been previously able to express GFP. Further long-term studies are needed to determine whether Y-27632-RI can prolong and sustain gene expression in hWJCs. Additionally, follow-up studies are needed to determine whether Y-27632-RI can negatively affect multipotency character and downstream differentiation of hWJCs for tissue engineering applications [188, 255].

CONCLUSION

For the first time, it was demonstrated that Y-27632-RI enhanced survival and gene expression in mesenchymal stromal cells for an electroporative gene delivery strategy. Transfection efficiency significantly increased 4 fold and cell viability increased 3 fold in hWJC populations that were treated with 10 μM of Y-27632-RI before and after transfection compared

to hWJC populations not treated with Y-27632-RI. While this study focused on hWJCs and provides an example for evaluating the effect of Y-27632-RI, other cell types undergoing electroporation may benefit from Y-27632-RI treatment, although dosing levels application of treatment, and timing of treatment should be tailored for each cell type and application. The use of Y-27632-RI provides an opportunity to benefit strategies that combine both stem cell therapy and gene therapy for regenerative medicine applications.

CHAPTER 4: Converting green to red: Tracking cells for tissue engineering[3]

ABSTRACT

Identifying or tracking cells *in vitro* with fluorescent markers can sometimes be challenging when background auto-fluorescence is high, fluorophore selection is limited, and/or background noise is high. In the current study, a new method is introduced to the tissue engineering community to address these problems based on the use of the photo-convertible protein *Dendra2*. Selective photo-conversion allows for tracking of individual cells in tissue engineering applications including differentiation, cell migration, and tissue integration. Human umbilical cord mesenchymal stromal cells isolated from Wharton's jelly were successfully transfected via Nucleofection™ with *pDendra2*, and robust photo-conversion was achieved in multiple cells and individuals cells, allowing for precise cell tracking. The current study demonstrates how *Dendra2* can enhance identification of positively transfected cells and how a photo-converting reporter gene can be used for cell tracking in tissue engineering applications.

INTRODUCTION

Fluorescent proteins are often used as reporters for a variety of different biological and chemical applications, including protein tagging, cell structure identification, and cell tracking.[11, 58, 83] Green-to-red photo-convertible proteins such as *Kaede*, *KikGR*, *EosFP*, and *Dendra2* are incredibly useful for observing cell trafficking and cell tracking, and have been well characterized.[182] However, these photo-convertible proteins have been highly under-utilized in tissue engineering. Photo-convertible proteins allow for the potential to create highly specific

[3] Under review as **Mellott A.J.**, Shinogle, H.E., Moore, D.S., and Detamore, M.S., Converting green to red: Tracking cells for tissue engineering. at Cellular and Molecular Bioengineering, March 2014.

biochemical assays, and significantly increase signal-to-noise ratios in fluorescent applications. Green fluorophores, red fluorophores, and blue fluorophores are popularly used in many biological reagents, as well as in reporter genes. However, there are times when fluorophore selection is limited, and some cells undergoing transfection weakly express the reporter gene. To further complicate matters, if a transfection occurs in a highly confluent cell culture, or *in vivo*, auto-fluorescence or high background noise can be difficult to distinguish from reporter signal. In scenarios such as these, a photo-convertible protein is attractive because the reporter protein can be converted from green to red, significantly revealing cells that have been positively transfected (Fig. 4.1). Thus, selection and targeting of transfected cells becomes highly accurate and precise. Tracking of cells is important in tissue engineering applications and developmental applications to identify cell migration in tissues as well as integration into biomaterials.[95]

In addition, photo-conversion of reporter genes may provide significant insights into the turnover of proteins within an individual cell, protein kinetics and distribution within a cell, and the structural and morphological changes occurring in organelles such as the nucleus or mitochondria as cells undergo mitosis and differentiation. Gunewardene *et al*.[89] and Wu *et al*.[265] demonstrated that photo-convertible reporter genes can be used to accurately track protein distribution and kinetics in mouse fibroblasts and multiple cell types in *Arabidopsis root*, respectively. The potential to use photo-convertible proteins in tissue engineering may become a powerful tool to provide fundamental information about proteins and cells while enabling the identification of positively transfected cells in a large population.

Dendra2 has an advantage over other photo-convertible reporter genes in that *Dendra2* can be photo-converted with low intensity ultra-violet (UV) (360 – 420 nm) light or high intensity blue light (460 – 500 nm), as opposed to only UV light at varying powers, which makes

Dendra2 more versatile in tissue engineering applications, as exposure of cells to UV light can be avoided or drastically reduced.[34, 68, 242, 265]

Human Wharton's jelly cells (hWJCs) are mesenchymal stromal cells that are an alternative to bone marrow stem cells. hWJCs are an excellent source for tissue engineering applications because they are abundant in supply, cause no donor site morbidity, are highly proliferative, and not ethically controversial.[10, 47, 167, 252] However, hWJCs are primary cells, and typically are difficult gene delivery targets unless a viral vector is used. Viral vectors are highly effective at transducing primary cells, stem cells, and progenitor cells, but safety concerns regarding toxicity, immunogenesis, and oncogenesis from insertional mutagenesis still remain.[29, 244] Non-viral vectors are able to circumvent many safety concerns associated with viral gene delivery; however, non-viral vectors suffer from low transfection efficiencies, which can make identification of positively transfected cells challenging.[159] Nucleofection™ is an electroporative method that has demonstrated a reliable ability to transfect primary cells, stem cells, and progenitor cells non-virally.[6, 57, 93] Hence, it was hypothesized that a photo-convertible reporter gene would be transfected into hWJCs and used to selectively identify positively transfected cells and used to track cell movement over time.

The current study provides a brief overview of how *Dendra2* may be used for the first time to transfect hWJCs via Nucleofection™, and presents a new way in which photo-convertible fluorophores could be utilized for tissue engineering applications. The current study examined transfection efficiency, photo-conversion kinetics of *Dendra2*, and the ability to reliably track cells.

MATERIALS AND METHODS

Procurement and expansion of hWJCs

hWJCs were isolated from Wharton's jelly of three human umbilical cords (n = 3) obtained from Lawrence Memorial Hospital (LMH) (LMH IRB approval #LMH 08-2). The three umbilical cords came from males born at full term under normal conditions. hWJCs were isolated according to the previously published protocol.[48] hWJCs were cultured in traditional hWJC medium (10% fetal bovine serum (FBS-MSC Qualified) and 1% Penicillin-Streptomycin in low glucose DMEM (Life Technologies, Grand Island, NY)). hWJC medium was changed three times per week, and hWJCs were maintained at 37°C with 5% CO_2 in a cell culture grade incubator. hWJCs were trypsinized with 0.05% Trypsin-EDTA (1X) (Life Technologies) at 80 to 90% confluency. All hWJCs were expanded to passage 1 (P1), and flash-frozen until needed for experiments. Cell were thawed and expanded to P4 for all experiments. Three umbilical cords (n = 3*)* were used in total for the current study. All experiments were performed in triplicate for each cord.

Cell surface marker characterization

At P2, a sub-culture of cells from each cord was characterized through cell surface marker identification via flow cytometry on a MoFlo XDF fluorescent activated cell sorter (FACS) (Beckman Coulter, Brea, CA). hWJCs were characterized using the following antibodies and secondary antibodies: STRO-1 Mouse IgM (2.5:200) (1 mg per mL; R&D Systems, Minneapolis, MN); Alexa Fluor 568® Rabbit Anti-Mouse IgG (2:200) (2 mg per mL; Life Technologies); CD105 Mouse IgG (2.5:200) (1 mg per mL; R&D Systems); Qdot® 525 donkey anti-mouse IgG (2:200) (1 μM; Life Technologies); Human CD45 pre-conjugated to Qdot® 800

(2:200) (Life Technologies); Human CD73 pre-conjugated to FITC (5:200) (BD Biosciences, San Jose, CA); Human CD34 pre-conjugated to Brilliant Violet (5:200) (BD Biosciences); Human CD90 pre-conjugated to APC (5:200) (BD Biosciences). 20,000 events were recorded for each sample. Positive identification of cell markers was defined as fluorescent emission that exceeded the fluorescent threshold of cells stained with corresponding isotype (negative) controls. The isotype controls used in these studies were Rabbit IgG Alexa Fluor 568, Donkey IgG Qdot 525, IgG_2 Qdot 800 (all from Life Technologies), and IgG_1 FITC, IgG_1 Brilliant Violet, and IgG_1 APC (all from BD Biosciences). The cell characterization experiments were repeated three times for each cord.

Plasmid

pDendra2-C (Clonetech, Mountain View, CA) is a fluorescent fusion protein vector, in which the gene of interest can be fused to the c-terminal of the *Dendra2* photo-convertible reporter gene, upstream of a poly-A sequence. *Dendra2* is driven by a cytomegalovirus (CMV) promoter, and contains a Kanamycin resistant gene driven by Simian virus 40 (SV40) for bacterial selection. The entire empty vector backbone is 4.7 kb.

Transfection

On the day of transfection, medium from all wells was removed, and cells were washed with phosphate buffered saline (PBS) twice. Afterward, cells were incubated for 1 h at 37°C in traditional hWJC medium (10% FBS-MSC Qualified, 1% Penicillin-Streptomycin, Low glucose DMEM) with 10 μM of Y-27632-ROCK Inhibitor (Reagents Direct, Encinitas, CA). After 1 h, hWJCs were washed twice with PBS, trypsinized, and then resuspended in either 100 μL 4D

Nucleofector™ P1 Primary Solution (P1PS) (Lonza, Basel, Switzerland) (Untreated Control) or 95 µL of P1PS and 5 µL of *pDendra2* (1 µg per µL; Clonetech). Cells were resuspended at a density of $5x10^5$ cells per 100 µL. Untreated control cells were immediately transferred to 6-well plates (BD Biosciences) containing 1.5 mL traditional hWJC medium and incubated at 37°C. hWJC suspensions containing *pDendra2* were immediately transferred to 100-µL 4D Nucleofection™ cuvettes. Each cuvette was gently tapped twice then placed in a 4D Nucleofector™ (Lonza) and nucleofected with the program FF-104. hWJCs were incubated at room temperature (ca. 22°C) for 10 minutes then transferred to a 6-well plate (BD Biosciences) containing 1.5 mL traditional hWJC medium with 10 µM of Y-27632-RI (Reagents Direct) and incubated at 37 °C.

Fluorescent microscopy

Twenty-four hours after transfection, hWJCs were collected for analysis. hWJCs were imaged using a customized Olympus IX81 inverted (Olympus America, Center Valley, PA) microscope, outfitted for both epifluorescence (filters: Semrock, Inc, Rochester, NY, filter wheels: Sutter Instrument, Novato, CA) and Spinning Disk Confocal (Yokogawa, Toyko, Japan) microscopy. The microscope is equipped with a XY stage (Prior, Rockland, MA) and temperature, humidity, and CO2 control for chronic, automated live cell imaging. Images were collected using an Olympus LUCPlanFL 20X 0.4 NA objective and were captured using the acquisition and analysis software, SlideBook (Intelligent imaging Innovations (3i), Denver, CO).

Three experiments were performed in total 24 h after transfection. In the first experiment, all cells within the field of view were exposed to a 100 mW (mercury arc lamp) of UV light (387 ± 11 nm) for photo-conversion, blue light (494 ± 20 nm) for green fluorescent expression, and

green light (560 ± 25 nm) for red fluorescent expression. Cells were exposed to UV light at a frequency of 1 Hz every 10 seconds. The experiment was repeated nine times with three sets of cells from 3 different umbilical cords (n = 3).

In the second experiment, the UV light was confined to a diameter of 15 – 20 μm to limit UV exposure to a single transfected cell. The UV light output was reduced to 20 mW (mercury arc lamp), and exposure was set to 1 Hz every 20 s. To minimize photo-conversion from blue light, excitation of green and red fluorescent expression were done using 488-nm and 561-nm solid-state lasers, respectively, through a Yokogawa Spinning Disk. The experiment was repeated nine times with three sets of cells from three different umbilical cords (n = 3).

In the third experiment, a single hWJC within a population of positively transfected cells was photo-converted by exposure to UV light at 100 mW (mercury arc lamp) for a duration of 10 s at a frequency of 1 Hz. After photo-conversion, cells within the entire field of view were exposed to 488-nm and 561-nm solid-state lasers for green and red fluorescent expression respectively every 30 min at a frequency of 1 Hz over the time period of 48 h..

RESULTS

Cell surface marker characterization

hWJCs from three different umbilical cords (n = 3) were analyzed for cell surface markers found on mesenchymal stem cells via flow cytometry (Table 4.1). hWJCs from all three cords were non-hematopoietic with cells showing little to no presentation of CD34 (97.2 ± 1.6% negative) (all values are reported as means ± standard deviations), and little to no presentation of CD45 (81 ± 13% negative). Cells from each umbilical cord displayed varying degrees of

presentation of CD73 (12.8 ± 5.3% positive), CD90 (97.1 ± 4.3% positive), CD105 (21.6 ± 9.7% positive), and STRO-1 (6.2 ± 3.8% positive), which are all found on mesenchymal stem cells.

Transfection efficiency and cell density

hWJCs were transfected from three different umbilical cords (n = 3) with 5 μg of *pDendra2* per 500,000 cells, and exhibited a transfection efficiency of 31 ± 7.4% with a cell density of 3,200 ± 1,900 per randomized field of view.

Fluorescence Microscopy

Multiple cell photo-conversion

hWJCs transfected with *pDendra2* showed reliable and consistent photo-conversion of all cells within the field of view. The kinetics of photo-conversion were measured in randomized fields of view from hWJCs from three different umbilical cords (n = 3), as cells were exposed to UV light (384 nm) for a duration of 300 s (Fig. 4.2). The intensity of the green fluorescence dropped dramatically from 5,300 ± 1900 Arbitrary Units (AU) to under 1,200 ± 360 AU in 300 s, while the intensity of the red fluorescence started at 750 ± 130 AU and increased to 4,200 ± 2,400 AU in 300 s. The critical point at which the intensity of red fluorescence overtook green fluorescence occurred at 125 ± 60 s. There was a marked visual change in the overall fluorescent color of the hWJCs that underwent photo-conversion, which is displayed in a time-lapse video from one recording that is representative of all attempts (Supplementary Fig. 4.6). The experiment was repeated nine times, with three attempts from a different set of cells from each umbilical cord. Each experiment yielded reproducible results.

Individual cell photo-conversion

Individual hWJCs were photo-converted from green to red fluorescence without inducing photo-conversion in surrounding hWJCs (Fig. 4.3). A single hWJC within a population of positively transfected hWJCs was targeted for photo-conversion, and the photo-conversion kinetics of the targeted cell and an adjacent cell were measured. The procedure was repeated nine times with three different sets of cells used from each of three different umbilical cords (n =3). In each procedure, the cell targeted for photo-conversion was labeled "Target 1" while the adjacent cell was labeled "Target 2". The green fluorescent intensity of Target 1 started out at 2,655 ± 700 AU and decreased to 900 ± 260 AU over 720 s, whereas the red fluorescent intensity started at 480.5 ± 4.9 AU and increased to 1,470 ± 290 AU over 720 s. The critical point at which red fluorescent intensity overtook green fluorescent intensity occurred at 197.0 ± 4.2 s. The green fluorescent intensity in Target 2 started at 3,700 ± 2,800 AU and was recorded at 2,800 ± 1,700 AU at the end of 720 s, whereas the red fluorescent intensity of Target 2 started at 480 ± 7.8 AU and was recorded at 1,200 ± 750 AU at the end of 720 s. The starting and ending green and red fluorescent intensities varied between each set of cells; however, no photo-conversion occurred in cells not directly targeted for photo-conversion. Each experiment yielded reproducible results. A time-lapse video from one recording that is representative of all attempts clearly shows Target 1 photo-converts from green to red, while Target 2 and all surrounding cells remain green (Supplementary Fig. 4.7).

Tracking cell movement of photo-converted cells

A single hWJC was photo-converted within a population of hWJCs positively transfected with *pDendra2*. The photo-converted cell was tracked over 48 h and monitored to observe

whether long-term exposure of a photo-converted cell induced photo-conversion of surrounding cells (Fig. 4). The experimental procedure was repeated twice with two different sets of hWJCs (n = 2), yielding reproducible results. The photo-converted hWJC displayed a red fluorescence that changed to an orange fluorescence over 48 h in both experiments; while surrounding cells remained firmly green (Fig. 4.5). In both experiments the photo-converted cell moved in a circular pattern, and touched several cells over the duration of 48 h. At the end of 48 h, the photo-converted cell from one experiment appeared to be undergoing cell division, and is represented in Figure 5. None of the cells that came in contact with the photo-converted cell in each experiment showed any visual signs of photo-conversion. The entire time-lapse video shows the movement of the photo-converted cell and is representative of both experiments (Supplementary Fig. 4.8).

DISCUSSION

Dendra2 is a monomeric photo-convertible protein that was engineered by Gurskaya *et al*.[90] *Dendra2* is highly photo-stable, and matures at 37°C, which makes *Dendra2* an attractive candidate for labeling proteins or structures within cells. Chudakov *et al*.[33, 35] have conducted extensive research on using photo-convertible proteins, such as *Dendra2* for studying and tracking protein movement in cells. *Kaede* is a popular rival photo-convertible protein used in many experiments to track cells; however, *Dendra2* has not been utilized for cell tracking experiments. *Dendra2* has been extensively used for molecule identification and tracking in cells, and offers the advantage of being able to be photo-converted with blue light instead of UV, and can be precisely photo-converted.[123, 130, 261] Thus, the objective of the current study was to use *Dendra2* to identify and track stem cells in culture.

For the first time, it was demonstrated that hWJCs responded well to photo-conversion when exposed to UV light (384 nm) at 100 mW output every 10 s for 1 Hz. Individual hWJCs were photo-converted successfully multiple times without triggering photo-conversion of surrounding cells, which is consistent with studies that have precisely tracked intercellular proteins within much smaller spatial areas than cells.[33, 130, 182] Tracking of photo-converted cells in tissue culture revealed that photo-converted cells did not trigger photo-conversion events in cells that came in contact with the photo-converted cell. Interestingly, the photo-converted cell changed from red to orange over the course of 48 h. The shift from red fluorescence to orange fluorescence may have been the result of de-localization of protein or protein turnover in the cell as the cell stretched and migrated over the course of 48 h.

The current study demonstrates that *Dendra2* could be a highly effective tool for gene delivery and tissue engineering studies, and future investigation of *Dendra2* in *ex vivo* and *in vivo* transfection experiments may yield fascinating results that improve diagnostic techniques for research. The use of *Dendra2*-transfected cells seeded on tissue engineering scaffolds could provide valuable information on how cells interact with biomaterials regarding migration, tissue integration, and morphological changes over time. The use of a photo-convertible reporter gene has been highly underutilized in tissue engineering, and could be an extremely effective tool in tissue engineering experiments by allowing continuous real-time observation of cells in materials and tissues.

CONCLUSION

In summary, *Dendra2* is a robust non-toxic photo-convertible protein that expressed well in hWJCs, and allowed for precise control of photo-conversion from green to red in individual cells

or multiple cells over the time scale of 120 s. For the first time, a photo-convertible reporter gene was transfected into hWJCs, and the current study demonstrates how photo-convertible reporter genes may be used for experiments where fluorophore selection is limited and gene expression is low in contrast to high background noise. Photo-convertible reporter genes are attractive tools for increasing signal-to-noise ratios in low expression systems. Photo-convertible proteins such as Dendra2 enable strategic photo-conversion of select cells without photo-converting surrounding cells, which could be highly beneficial for *in vivo* applications. Thus, the potential to use a photo-convertible protein in tissue engineering applications could provide new insights regarding cell behavior in tissues and biomaterials, which could provide means to create new therapies in regenerative medicine.

CHAPTER 5: Non-viral reprogramming of human Wharton's jelly cells reveals differences between Atoh1 homologues[4]

ABSTRACT

The transcription factor *atonal homolog 1* (*atoh1*) has multiple homologues that are functionally conserved between species and is responsible for the generation of sensory hair cells. To evaluate potential functional differences between homologues, human and mouse atoh1 were delivered to human umbilical cord mesenchymal stromal cells from Wharton's jelly. Delivery of the human *atonal* homolog, *hath1*, to human Wharton's jelly cells demonstrated superior expression of inner ear hair cell markers and characteristics compared to delivery of the mouse homolog, *math1*. Inhibition of *hes1* and *hes5* signaling further increased the potency of the *atonal* effect. Transfection of Wharton's jelly cells with *hath1* DNA, *hes1* siRNA, and *hes5* siRNA displayed positive identification of key hair cell and support cell markers found in the organ of Corti. In the first side-by-side evaluation of *hath1* and *math1* in human cells, substantial differences were observed, suggesting that the two *atonal* homologues may not be interchangeable between species as previously thought, perhaps opening the door for evaluation of other homologues currently believed to be interchangeable.

[4] Reformatted in expanded version as **Mellott, A.J.**, Devarajan, K., Shinogle, H.E., Moore, D.S., Talata, Z., Laurence, J.S., Forrest, M.L., Noji, S., Tanaka, E., Staecker, H., and Detamore, M.S. Non-viral reprogramming of human Wharton's jelly cells reveals differences between Atoh1 homologues. To be submitted to Nature Biotechnology, April 2014.

INTRODUCTION

Hair cells located in the cochlea and vestibular organs of the inner ear are responsible for hearing and balance, respectively. Sensorineural hearing loss occurs when the hair cells are irreversibly damaged. Mammalian hair cells in the inner ear do not regenerate and are susceptible to damage from noise-induced trauma, genetic diseases, viral infections, ototoxic antibiotics, and age-related wear and tear.[49, 55] Hearing aids and cochlear implants are the only available therapies for sensorineural hearing loss. As such, considerable effort has been invested into developing ways to regenerate damaged hair cells via gene delivery or replace hair cells via transplantation through stem cell therapy.[32, 108, 114, 192] *Atonal homolog 1* (*atoh1*) is a basic helix-loop-helix (bHLH) transcription factor necessary for hair cell differentiation that is negatively regulated by *hes1* and *hes5* via the *notch*-signaling pathway.[56, 69, 118, 119, 170, 277] Several groups have demonstrated that delivery of *atoh1* or *math1* (Mouse homolog of *atoh1*) *in vivo* to neuroprogenitors and supporting cells have enabled the target cells to transdifferentiate into hair cells.[54, 124, 135, 147] However, while highly encouraging, most studies have focused on targeting inner ear epithelium in mouse and rat models that rely on treatment during embryogenesis or shortly after birth. Several research groups have focused on differentiating stem cells into neuroprogenitors or hair cells through gene delivery, co-culture, or growth factor exposure using *math1* with limited success.[20, 41, 146, 194, 212] Transdifferentiation has been demonstrated but not post-mitotic cell division and differentiation, which is a key barrier that needs to be overcome for hair cell regeneration. Transdifferentiation induces one differentiated cell type to change into another differentiated cell type without self-renewal of the original cell.[152] Thus, there is still much that is unknown about how hair cells develop and the mechanisms required for regenerating functional hair cells.

The potential to engineer terminal cell phenotypes outside of the body through cellular reprogramming may provide significant insights into the physiology of hair cells. An *ex vivo* model would be highly beneficial in understanding hair cell physiology and aiding in the development of a therapy for hearing loss. Thus, the current study endeavored to explore the possibility of producing hair cells by transfecting human Wharton's jelly cells (hWJCs) with two different homologues of *atoh1*. hWJCs are a highly desirable cell population because hWJCs are abundant in supply, not ethically controversial, exhibit no risk of injury to the donor, are highly proliferative, and have demonstrated differentiation potential similar to human bone marrow stem cells.[10, 47, 167, 251]

Devarajan *et al*.[48] were first to show that hWJCs are amenable to inner ear hair cell lineage differentiation when transduced with *math1* via adenovirus. However, while viral gene delivery is popular for high transduction efficiency and gene expression, challenges regarding toxicity, immunogenicity, and oncogenesis from insertional mutagenesis still exist for some viral delivery systems, such as lentivirus.[29, 244] To circumvent safety concerns associated with viral gene delivery, hWJCs in the current study were transfected with *hath1* (Human homolog of *atoh1*) and *math1* via Nucleofection™. Nucleofection™ is a highly effective electroporation method for transfecting primary cells and stem cells, which are known to be notoriously difficult to transfect.[6, 26, 88, 159] While, electroporation has been known to cause high cell death, cell pre-treatment and post-treatment with a Y-27632 ROCK Inhibitor can mitigate cell death and low gene expression by preventing apoptosis associated with the RhoA GTP signaling pathways.[160]

Math1 has received more attention in investigation in both mouse and human tissues, but focus on *hath1* has been limited.[133, 217, 271] The *atonal* homologues *hath1* and *math1* share 86.04% nucleotide identity and 89.17% amino acid identity.[19] More specifically, *hath1* is 1,385

base-pairs (bp) in length and located on human chromosome 4 (Entrez Gene ID: 474), whereas *math1* is 2,728 bp in length and located on mouse chromosome 6 (Entrez Gene ID: 11921), yet no side-by-side evaluation of the two *atonal* homologues in the same tissue exists. While *math1* and *hath1* show similar identity, it was hypothesized that the differences in sequences were not interchangeable as implied by Wang *et al*.[254], and that *math1* may not interact with human signaling pathways in human tissues as *math1* would interact with mouse signaling pathways in mouse tissues. Furthermore, given that *hes1* and *hes5* are known negative regulators of *atoh1*, it was hypothesized that knocking down *hes1* and *hes5* could enhance the expression of *atoh1* and promote development of hair cell characteristics.

MATERIALS AND METHODS

Procurement and expansion of human Wharton's jelly cells

Human Wharton's jelly cells (hWJCs) were isolated from Wharton's jelly of five human umbilical cords with informed consent (KU-IRB #15402) following a modification of our previous protocol.[48] Two cords were from males who were born at full term and delivered under normal delivery conditions. Two cords were from females born at 38.3 and 39 weeks under normal delivery conditions. The gender of the last cord used was not available; however, the child was born at full term under normal conditions. Within 24 h of delivery, umbilical cords were soaked in sterile 2% antibiotic-antimycotic (AA) (100X; Life Technologies, Grand Island, NY) in phosphate-buffered saline (PBS) and drained of excess cord blood. Umbilical cords were cut into approximately 3-cm segments, which were filleted open and stripped of blood vessels. The umbilical cord segments were minced finely and were suspended in a sterile digesting media composed of 0.2% type II collagenase (298 U per mg; Worthington Biochemical, Lakewood, NJ,

USA) and 1% Penicillin-Streptomycin (10,000 U per mL; Life Technologies) in low glucose Dulbecco's Modified Eagle Medium (DMEM) (Life Technologies), and then incubated at 37°C in a 5% CO_2 environment on a shaker table at 50 rpm for 6 h. After digestion, the homogenous solution was diluted in sterile 2% AA in PBS at a 1:16 ratio and centrifuged. The supernatant was discarded and cells were combined and plated at a density of $7x10^3$ cells per cm^2 in tissue culture treated T-75 flasks (MidSci, St. Louis, MO). hWJCs were cultured in traditional hWJC medium (10% fetal bovine serum (FBS-MSC Qualified) and 1% Penicillin-Streptomycin in low glucose DMEM (Life Technologies)). hWJCs medium was changed three times per week, and hWJCs were maintained at 37°C with 5% CO_2 in a cell culture grade incubator. hWJCs were trypsinized with 0.05% Trypsin-EDTA (1X) (Life Technologies) at 80 to 90% confluency. All hWJCs were expanded to passage 1 (P1). Upon reaching 90% confluency, cells were washed with PBS twice, trypsinized, and resuspended at a concentration of $1x10^6$ cells per 1 mL of Recovery™ Cell Culture Freezing Medium (Life Technologies) in 2-mL round-bottom cryogenic vials (Corning Incorporated, Acton, MA). Cryogenic vials were immediately placed in a Nalgene® Mr. Frosty container (Sigma-Aldrich, St. Louis, MO) filled with isopropanol, and stored at -80°C for 12 h. Cryogenic vials were then transferred and stored in liquid nitrogen. When ready for use, cells were thawed by transferring cryogenic vials into a 10-cm petri dish filled with PBS warmed to room temperature. Cells were diluted into 50 mL of thawing medium (Low glucose DMEM, 20% FBS-MSC Qualified, and 1% Penicillin-Streptomycin) (Life Technologies), and transferred to a T-300 flask (MidSci). Cells were expanded from P2 to P5, then used for experiments. Five umbilical cords (n = 5*)* were used in total for this study. All experiments were performed in triplicate for each cord.

Plasmid and siRNA

Two PrecisionShuttle mammalian vectors with independent turboGFP expression from OriGene (Rockville, MD) were used to deliver target genes to hWJCs. Cloning and verification services were provided by Blue Heron (Blue Heron Biotech LLC, Bothell, WA) to manufacture the vectors. In one vector, a *math1* insert (NCBI GenBank ID: NM-007500.4) was cloned in, and in the other vector a *hath1* insert (NCBI GenBank ID: U61148.1) was cloned in. The *math1* and *hath1* gene inserts were driven by a cytomegalovirus (CMV) promoter followed by a Kozak sequence, and the turboGFP gene was driven by a Simian virus 40 (SV40) promoter. The PrecisionShuttle vectors contained a Kanamycin resistance gene for bacterial selection. Upon arrival, vectors were reconstituted in 10 mM Tris and 1 mM EDTA (TE) Buffer Solution and stored at -20°C. Plasmids were verified and sequenced by Blue Heron to ensure no mutations or shifts in reading frame occurred after *math1* or *hath1* plasmid generation from a Qiagen Plasmid Plus Giga kit (Qiagen, Valencia, CA).

Based on data from pilot studies (Data not shown) custom *hes1* siRNA (Hs_*hes1*_5, Gene Accession no.: NM_005524, Gene ID: 3280) modified with 3'-Alexa Fluor 555 and custom *hes5* siRNA (Hs_*hes5*_5, Gene Accession no.: NM_001010926, Gene ID: 388585) modified with 3'-Alexa Fluor 647 (Qiagen) were selected for experiments. Upon arrival, siRNA was reconstituted with RNase-Free water and both *hes1* and *hes5* siRNA were diluted to 100 nM and stored at -20°C.

Experimental design and transfection

Twenty-four hours before transfection, hWJCs were trypsinized and plated into tissue culture treated 6-well plates (BD Biosciences, San Jose, CA) at a density of $5x10^5$ cells per well.

On the day of transfection, media from all wells were removed and cells were washed with PBS twice. Afterward, cells were incubated for 1 h in a 37°C culture grade incubator supplied with 5% CO_2 in 37°C pre-warmed traditional hWJC medium (10% FBS-MSC Qualified, 1% Penicillin-Streptomycin, Low glucose DMEM) with 10 μM of Y-27632 ROCK Inhibitor (Reagents Direct, Encinitas, CA). After 1 h, hWJCs were washed twice with PBS, trypsinized, and then resuspended in 4D Nucleofector™ P1 Primary Solution (4DNP1) (Lonza) and one of six treatment solutions. All cells were suspended at a concentration of $5x10^5$ cells per 100-μL solution at one of the five following ratios: 100 μL 4DNP1 (Untreated), 95 μL 4DNP1: 5 μL *math1* pDNA (1μg per μL) (*Math1*), 95 μL 4DNP1: 5 μL *hath1* pDNA (1μg per μL) (*Hath1*), 99 μL 4DNP1: 0.5 μL *hes1* siRNA (100 nM): 0.5 μL *hes5* siRNA (100 nM) (H1/H5), 94 μL 4DNP1: 5 μL *math1* pDNA (1 μg per μL): 0.5 μL *hes1* siRNA (100 nM): 0.5 μL *hes5* siRNA (100 nM) (*Math1*/H1/H5), 94 μL 4DNP1: 5 μL *hath1* pDNA (1 μg per μL): 0.5 μL *hes1* siRNA (100 nM): 0.5 μL *hes5* siRNA (100 nM) (*Hath1*/H1/H5). The untreated control cells were not nucleofected and were immediately pipetted into 6-well plates (BD Biosciences) or Nunc™ Lab-Tek™ 8-well chambered coverglass slides (Thermo Scientific, Waltham, MA) pre-coated with Fibronectin (BD Biosciences) containing 1.5 mL or 0.5 mL, respectively, of 37 °C pre-warmed traditional hWJC medium. Cells were placed into a cell culture grade incubator set at a temperature of 37°C and supplied with 5% CO_2. hWJC suspensions were transferred to 100-μL 4D Nucleofection™ cuvettes via separate pipettes. The cuvettes were placed in a 4D Nucleofector™ (Lonza) and nucleofected with the FF-104 program. Afterward, hWJCs were allowed to incubate at room temperature (ca. 22°C) for 10 minutes. hWJCs were transferred to a 6-well plate (BD Biosciences) or Nunc™ Lab-Tek™ 8-well chambered coverglass slides (Thermo Scientific) pre-coated with Fibronectin (BD Biosciences) containing 1.5 mL or 0.5 mL

of pre-warmed 37°C traditional hWJC medium with 10 μM of Y-27632 ROCK Inhibitor, and placed into a cell culture grade incubator at 37°C with 5% CO_2.

Gene expression

At 1, 3, and 7 d after transfection, cells were collected and harvested for gene expression analysis via real time quantitative polymerase chain reaction (RT-qPCR). At each time point, RNA was collected from each cell sample according to manufacturer's instructions of Qiagen RNeasy Plus Mini Kit (Qiagen). RNA purity and quality was assessed via NanoDrop 2000 (Thermo Scientific) and Agilent 2200 TapeStation (Agilent Technologies, Santa Clara, CA), respectively. An RNA integrity number (RIN) of 7-10 was considered acceptable for cDNA conversion.

RNA was converted to cDNA using the High Capacity cDNA conversion Kit (Life Technologies) and the Eppendorf Realplex Mastercycler (Eppendorf, Hamburg, Germany). Converted cDNA purity and quality was assessed quantitatively via the NanoDrop 2000 (Thermo Scientific) and qualitatively via the Agilent 2200 TapeStation (Agilent), respectively.

cDNA from each sample was loaded into a MicroAmp® Fast Optical 96-well Reaction plate (0.1-mL, Life Technologies). Individual wells were loaded sequentially in the following ratios: 1 μL TaqMan Assay (Life Technologies), 9 μL sample cDNA, 10 μL TaqMan Fast Universal PCR Master Mix (Life Technologies). The TaqMan Assays used are listed in Table 1.

Plates were sealed with MicroAmp® Optical Adhesive Film (Life Technologies) and centrifuged. Afterward, the samples were loaded into the Eppendorf Realplex Mastercycler and run according to the recommended TaqMan Fast Universal PCR Master Mix Protocol (Life Technologies). Cycle threshold (Ct) values were recorded and analyzed via the Delta-Delta-Ct

method. Values were normalized to day 0 untreated control samples and the endogenous controls. Three replicates from each of five umbilical cords (n = 5) were taken for gene expression analysis at 1, 3, and 7 d post transfection.

Live cell fluorescent imaging and flow cytometry

hWJCs were collected for live stain imaging 24 h after transfection. A 0.5-μL aliquot of Hoechst 33342 dye (Life Technologies) was added to each well, and hWJCs were incubated for 10 min at 37°C in 5% CO_2. Afterward, hWJCs were imaged using a custom epifluorescent and confocal microscope composed of the following components: an Olympus IX81 inverted spinning disc confocal microscope base (Olympus America, Center Valley, PA), a Prior microscope stage for automated image acquisition (Prior Scientific, Rockland, MA), an Olympus 40X Long Working Distance Air objective (Olympus), and a Hamamatsu Electron Multiplying Charge-Coupled Device (EMCCD) camera (Hamamatsu, Hamamatsu, Shizuoka Prefecture, Japan). Images were captured using the acquisition and analysis software, SlideBook (Intelligent Imaging Innovations (3i), Denver, CO). A mercury arc lamp was used with the following excitation filters (Excitation/Emission) for image collection: Hoechst (387 ± 11 nm/447 ± 60 nm), GFP (494 ± 20 nm/531 ±22 nm), Alexa Fluor 555 (575 ± 25 nm/624 ± 40 nm), and Alexa Fluor 647 (650 ± 25 nm/684 ± 25 nm). A montage was generated from 25 (five by five arrangement) neighboring fields of view that were aligned together to generate one comprehensive composite image of the sample.

So as to not bias cell viability after imaging, spent medium containing non-adhering or loose adhering cells was collected from each sample and transferred into a pre-labeled 15-mL conical tube (Phenix, Candler, NC). Remaining adherent hWJCs were washed twice with PBS

then trypsinized and added to corresponding 15-mL conical tubes containing the previous spent medium with the unattached cells so that both live cells and dead cells would be retained for analysis. Then 4 mL of fresh traditional hWJC medium was added to each conical tube, and all conical tubes were centrifuged at 1,500 rpm (~500 g) for 5 min. The supernatant was discarded, and hWJCs were resuspended in 500 µL of PBS and pipetted through a 70-µm nylon mesh cell strainer (BD Biosciences). 0.5 µL of Sytox Red (Life Technologies) was added just before analysis. hWJCs were analyzed via flow cytometry on the MoFlo XDP Fluorescent Activated Cell Sorter (FACS) (Beckman Coulter, Brea, CA). Flow Cytometry was used to analyze both cell viability and transfection efficiency. Live hWJCs were characterized as hWJCs expressing Hoechst at an intensity of 10^2 Relative Fluorescent Units (RFU) or above, with expression of Sytox Red at an intensity below 10^0 RFU. Dead hWJCs were characterized as hWJCs that expressed Hoechst at an intensity below 10^2 RFU and expressed Sytox Red at an intensity of above 10^0 RFU. GFP-positive hWJCs were characterized as live hWJCs that expressed GFP at an intensity of 10^0 RFU or greater. Transfection efficiency was determined by dividing the number of live GFP positive cells in a sample by the total population of the sample. All experiments were performed in triplicate for each umbilical cord 24 h after transfection.

FM® 1-43 staining

Cells from each cord were stained with FM 1-43 and imaged 7 d after transfection under a confocal microscope. Briefly, cells were washed twice with PBS, and 500 µL of FM 1-43 (5 µg per mL in Hanks Balanced Salt Solution (HBSS)) was added to the cells while on ice. Cells were fixed with 500 µL of 4% formaldehyde in HBSS on ice for 10 min then washed three times with HBSS. Cells were then sealed with ProLong® Gold Antifade Reagent with DAPI (Life

Technologies) and imaged on the same custom confocal microscope as stated previously. A 488 nm solid-state laser was used for excitation with a confocal emission of 625 ± 11 nm. A montage was generated from 25 (five by five arrangement) neighboring fields of view that were aligned together to generate one comprehensive composite image of the sample.

Immunocytochemistry

At 1, 3, and 7 d after transfection, cells were collected for immunocytochemistry. Primary antibodies were pre-conjugated to Quantum Dots (Qdot®) using the 525, 565, 605, 655, and 805 Qdot® Antibody Conjugation Kits (Life Technologies). Primary antibodies were conjugated to Qdots according to manufacturer's instructions, and stored at 4°C for immediate use. The following primary antibodies were conjugated to the following Qdots: Anti-human *atoh1* (Millipore, Billerica, MA) pre-conjugated to Qdot 525 (1:200; Life Technologies), Anti-human *hes1* (Millipore) pre-conjugated to Qdot 565 (1:200; Life Technologies), Anti-human *myosin VIIa* (Novus, Littleton, CO) pre-conjugated to Qdot 605 (1:500, Life Technologies), Anti-human *hes5* (Millipore) pre-conjugated to Qdot 655 (1:200, Life Technologies), and Anti-human *GFAP* (Millipore) pre-conjugated to Qdot 800 (1:100, Life Technologies). Cells were fixed by first washing cells in 37°C PBS, followed by fixation with 4% formaldehyde in PBS for 15 min. Cells were then washed and incubated for 5 min with PBS three times. Afterward, cells were permeabilized with 0.25% Triton X-100 in PBS, then washed three times in PBS. Cells were blocked with 4% bovine serum albumin (BSA) in PBS for 60 min. Afterward, cells were incubated with all primary antibodies pre-conjugated to respective Qdots as listed above for 60 min in blocking buffer. Following three PBS washes, cells were counterstained with Syto 9 (10 nM, Life Technologies) for 30 min, and then dehydrated with graded ethanol, followed by

double exposure to 100% toluene. Cells were then mounted in Qmount™ Qdot® Mounting Media (Life Technologies). Cells were imaged using confocal microscopy using a 405 nm solid-state laser for Qdot excitation, a 488 nm solid-state laser for Syto 9 excitation, and the following emission filters: Syto 9 (531 ± 22 nm), Qdot 525 (531 ± 22 nm), Qdot 565 (560 ± 25 nm), Qdot 605 (613 ± 20 nm), Qdot 655 (655 ± 15 nm), and Qdot 800 (788 ± 20 nm). Cells were collected from each umbilical cord at 1, 3, and 7 d after transfection and images were taken from individual wells on 8-well chambered glass slides.

Analysis of stem cell characteristics

A sub-culture of cells from each cord was characterized through cell surface marker identification via flow cytometry. hWJCs were trypsinized and centrifuged. The supernatant was discarded and hWJCs were suspended in 5% FBS-MSC Qualified (Life Technologies) in PBS and placed on ice and kept in the dark for 20 min. Aliquots containing $5x10^5$ hWJCs in approximately 200-µL were pipetted into 50-mL conical tubes (Phenix). Primary cell surface antibodies and secondary antibodies were added sequentially one-at-a-time per incubation-wash cycle to avoid cross-reaction; however, pre-conjugated primary antibodies with secondary antibodies were added simultaneously. A single incubation-wash cycle consisted of adding a primary antibody, secondary fluorescent antibody, or primary antibody pre-conjugated to a specific fluorescent secondary antibody to the cell suspension. After incubation, 800 µL of 5% FBS in PBS was added to the cell suspension to bring the total volume of the cell suspension up to 1 mL, and the cell suspension was then centrifuged. The supernatant was discarded, and cell pellets were suspended in 5% FBS-MSC Qualified (Life Technologies) in PBS, which concluded one incubation-wash cycle. Cell surface marker antibodies and secondary antibodies were added

in the following order at the following ratios: STRO-1 Mouse IgM (2.5:200) (1 mg per mL; R&D Systems, Minneapolis, MN); Alexa Fluor 568® Rabbit Anti-Mouse IgG (2:200) (2 mg per mL; Life Technologies); CD105 Mouse IgG (2.5:200) (1 mg per mL; R&D Systems); Qdot® 525 donkey anti-mouse IgG (2:200) (1 μM; Life Technologies); Human CD45 pre-conjugated to Qdot® 800 (2:200) (Life Technologies); Human CD73 pre-conjugated to FITC (5:200) (BD Biosciences); Human CD34 pre-conjugated to Brilliant Violet (5:200) (BD Biosciences); Human CD90 pre-conjugated to APC (5:200) (BD Biosciences). At the end of the last incubation-wash cycle, hWJCs were resuspended in PBS and pipetted through a 70-μm nylon mesh cell strainer (BD Biosciences). hWJCs were analyzed by flow cytometry on a MoFlo XDF FACS (Beckman Coulter). Positive identification of cell markers was defined as fluorescent emission that exceeded the fluorescent threshold of cells stained with corresponding isotype (negative) controls. The isotype controls used in these studies were Rabbit IgG Alexa Fluor 568, Donkey IgG Qdot 525, IgG_2 Qdot 800 (all from Life Technologies), and IgG_1 FITC, IgG_1 Brilliant Violet, and IgG_1 APC (all from BD Biosciences). The cell characterization experiments were repeated three times for each cord.

Statistical analysis

All values are reported as statistical means with standard deviations, unless otherwise noted. Cells were isolated from five (n = 5) different umbilical cords, and three technical replicates were used for each quantitative analysis. Five samples were considered adequate based on Mead's resource equation. A one-way ANOVA was performed with a Least Sum of Differences (LSD) post hoc in conjunction with a Dunnett's (multi-comparison) test to assess statistical significance with p set at ≤ 0.05, and power > 0.8. The Dunnett's test was set up as a

one-tailed assessment to examine increased values against control samples. The software SPPS (IBM) version 22 was used to compute all statistical analyses.

RESULTS

Cells transfected with hath1 showed greater cell density than cells transfected with math1

hWJCs were transfected via Nucleofection™, an electroporative technique (Lonza, Basel Switzerland), with one of five different treatments: *math1p*DNA, *hath1p*DNA, siRNA against *hes1* and *hes5*, *math1 p*DNA and siRNA against *hes1* and *hes5*, or *hath1 p*DNA and siRNA against *hes1* and *hes5*. At 24 h post-transfection, there was a noticeable visual difference in cell numbers between cells treated with *hath1* versus cells treated with *math1* (Fig. 5.1). Twenty-four hours after transfection, flow cytometry revealed that there were 1.9 times more viable cells transfected with *hath1*, and 2.2 times more viable cells transfected with *hath1* and siRNA against *hes1* and *hes5*, than viable cells transfected with *math1* (Fig. 5.2). In addition, 24 h post-transfection cells co-transfected with *hath1* and siRNA against *hes1* and *hes5* displayed 3.7 times more viable cells than cells co-transfected with *math1* and siRNA against *hes1* and *hes5*. At 24 h post-transfection, cells transfected with *hath1* displayed transfection efficiency that was 0.2 times greater than cells transfected with *math1*. Moreover, 7 d after transfection, cell counts revealed that there were 2.8 times more viable cells transfected with *hath1*, and 3.1 times more viable cells transfected with *hath1* and siRNA against *hes1* and *hes5*, than cells transfected with *math1*. At 7 d post-transfection cells co-transfected with *hath1* and siRNA against *hes1* and hes5 displayed 2.8 times more viable cells than cells co-transfected with *math1* and siRNA against *hes1* and.

Only cells transfected with hath1 revealed significant visual changes in morphology

Visual morphological differences were evident between untreated control cells and cells treated with *hath1* and siRNA against *hes1* and *hes5* starting at Day 3 (Fig. 5.3). Cells treated with *math1* displayed a fibroblastic morphology, consistent with hWJCs. However, cells treated with *hath1*, siRNA against *hes1* and *hes5*, or a combination of both showed an elongated cell body with small projections expanding away from the cell body. Cells treated with both *hath1* and siRNA against *hes1* and *hes5* displayed a bipolar phenotype with cell extensions reaching out from the nucleus and terminating with multiple slender projections, uncharacteristic of hWJCs.

Hath1- transfected cells revealed infiltration of lipophilic dye, FM® 1-43

To further evaluate the development of morphological features of hair cells, controls and treatment groups were stained 7 d after transfection with FM® 1-43, a lipophilic dye that is known to enter cells through transduction channels found in hair cells and neurons. Cells treated with *hath1* stained positive for FM® 1-43, as did cells treated with only siRNA against *hes1* and *hes5*. FM® 1-43 entered *hath1*-transfected cells more readily and robustly than *math1*–transfected cells. Across cells from all five umbilical cords, we saw positive FM® 1-43 staining in the greatest quantities in cells treated with *hath1* only or *hath1* and *hes1* siRNA and *hes5* siRNA. The amount of positive FM® 1-43 staining varied between cells treated only with *hath1* and cells treated with *hath1* and siRNA against *hes1* and *hes5* (Fig. 5.4). Limited infiltration of FM® 1-43 was observed in some of the samples co-transfected with *math1* and siRNA against *hes1* and *hes5* across cell samples from all five umbilical cords.

Hath1-transfected cells up-regulated different genes from math1-transfected cells

Gene expression was evaluated across all treated cells from all human umbilical cords at 1, 3, and 7 d after transfection. The relationship regarding how all of the analyzed genes are related to each other is illustrated in Supplementary Figure 5.7. The common trend observed across all analyzed genes was an up-regulation of gene expression 1 d after transfection, and gene expression levels returned to levels similar to untreated controls 7 d after transfection (Fig. 5.5). Gene expression in *math1-transfected cells* did not significantly differ from untreated control cells within the 7-day time period following transfection, except for *jagged2*, *hes1*, and *hes5* genes, 1 d after transfection. Cells co-transfected with *math1* and siRNA against *hes1* and *hes5* displayed no significant gene expression differences from untreated control samples within the 7-day time period following transfection. Perhaps most importantly, *math1*-transfected cells failed to show any significant increase in gene expression over the 7-day time period, whereas *hath1*-transfected cells showed significant ($p < 0.05$) increases in gene expression 1 d after transfection compared to untreated control cells in *atoh1* (4.5 $x10^5$ fold change), *hes1* (6.8 fold change), *hes5* (33.3 fold change), and *myosin VIIa* (6.5 fold change). Cells that were co-transfected with *hath1* and siRNA against *hes1* and *hes5* displayed significant ($p < 0.05$) increases in gene expression across *atoh1* (3.2 x 10^5 fold change), *hes5* (17.6 fold change), *myosin VIIa* (11.0 fold change), *gfi1* (2.9 fold change), and *jagged2* (2.4 fold change) 1 d after transfection. hWJCs co-transfected with *hath1* and siRNA against *hes1* and *hes5* displayed significant ($p < 0.05$) increases in gene expression across m*yosin VIIa* (9.1 fold change) and *jagged2* (1.2 fold change) 3 d after transfection. To further explore biochemical pathways related to hair cell morphology, a pilot trial microarray analysis was performed with a single cord (in triplicate) in collaboration with Agilent Technologies. In the cells from the umbilical cord

analyzed, *math1* had a far greater impact on gene expression than *hath1*, with twice as many genes experiencing at least a two-fold change (Supp. Fig. 5.8).

Only cells transfected with hath1 displayed prolonged protein expression of myosin VIIa

Cells were analyzed for protein expression via immunocytochemistry 1 d and 7 d after transfection (Fig. 5.6). All treated cells displayed positive identification of *myosin VIIa* and *hes5* 1 d after transfection. However, cells co-transfected with *hath1* and siRNA against *hes1* and *hes5* displayed positive identification of glial fibrillary acidic protein (*GFAP*) 1 d after transfection. *Math1*-transfected cells displayed a visual decrease in *myosin VIIa* and *hes5* expression, whereas *hath1*-transfected cells displayed a visual increase in immunostaining for m*yosin VIIa* and *hes5* 7 d after transfection. No *GFAP* expression was detected in any treated group 7 d after transfection. Untreated control cells displayed no presentation of any hair cell marker proteins at 1 d or 7 d after culture.

In a pilot study 7 d after transfection, treated cells from one cord were stained with a fluorescent probe, developed by Vytla *et al*.[248], against the α-amino-3-hydroxy-5-methyl-4-isoxazolepropionic acid (AMPA) receptor to identify active calcium permeable ion channels. *Math1*-transfected cells and cells co-transfected with *math1* and siRNA against *hes1* and *hes5* visually displayed limited presentation of the AMPA receptor, whereas *hath1*-transfected cells, and cells co-transfected with *hath1* and siRNA against *hes1* and *hes5* displayed strong presentation of active AMPA receptors (Supp. Fig. 5.9).

Only minor changes in cell surface markers observed between untreated and treated cells

We characterized hWJCs for CD markers associated with stem cells 10 d after transfection and found no significant changes between untreated and treated cells. All cell populations were strongly negative for CD34 and CD45, which indicated that cell populations were non-hematopoietic. Additionally, all cell populations displayed presentation of CD73, CD90, and CD105, which are surface markers found on mesenchymal stem cells. Supplementary Table 1.2 summarizes the flow cytometry data collected from cell characterization.

DISCUSSION

The key challenge in treating sensorineural hearing loss is that mammalian hair cells in the inner ear do not regenerate, unlike avian hair cells, which are able to renew and regenerate after damage.[64, 213] However, researchers have made numerous advances in revealing the molecular cues that enable the development of mammalian hair cells. *Atoh1* is the key transcription factor that is implicated in starting several different biochemical pathways that lead to the development of both hair cells and supporting cells.[41, 54] Hence, several groups have explored and exploited over-expression of *atoh1* as a method for producing ectopic hair cells *in vivo* and *ex vivo*, with varying success.[32, 54, 108, 135, 262] The inner ear epithelium, specifically the organ of Corti in the cochlea, and the utricle and saccule in the vestibular organs, require precise quantities, types, and spacing of both hair cells and supporting cells to enable proper reception and transmission of neurosensory signal. While several groups have succeeded at producing cells structurally similar to hair cells *in vivo* or *ex vivo*, no group has found a way to fully restore or repair inner ear sensory epithelium to its original state. While strategies rely on overexpression of *atoh1* to generate hair cells, there is currently no genetic protocol that allows for generation of

new hair cells without over-generation of hair cells. Kraft *et al.*[135] demonstrated that over-expression of *atoh1* can help improve hearing after damage; however, Yang *et al.*[271] revealed that *atoh1* overexpression in supporting cells results in direct transdifferentiation, not regeneration. Furthermore, Liu *et al.*[147] found that the ability of supporting cells, such as pillar cells or Deiter's cells, to transdifferentiate into hair cells is age-restricted to neonatal and juvenile stages in mice. Thus, there is still much left to explore and understand regarding hair cell development and regeneration. The development of a hair cell model outside the body may have a significant impact on further understanding how hair cells develop and are damaged, which may lead to new approaches for developing a therapy or a model for screening ototoxic drugs.

Very few gene delivery studies have been conducted with hWJCs.[12, 48] In the current study, we demonstrated that *hath1*- transfected hWJCs expressed critical markers associated with hair cells and neural epithelium. We compared *math1* and *hath1* gene delivery in human cells and demonstrated for the first time that *hath1* expression differed from *math1* expression in cells from human tissue.

The results of the current study have suggested that there might be a functional difference between *math1* and *hath1* in human tissues, as *math1* has been predominantly used for most studies focusing on mammalian hair cell regeneration. In hWJCs, treatment with *hath1* displayed significant immediate increases in mRNA and protein expression of key hair cell markers, as compared to cells treated with *math1*, which displayed limited increases in gene expression and protein expression 1 d after transfection. The positive identity of *GFAP* in cells co-transfected with *hath1* and siRNA against *hes1* and *hes5* suggested an initial differentiation toward a neural-like phenotype. *Myosin VIIa* expression is expected if cells are differentiating toward a hair cell lineage, but *hes5* expression is surprising, because *hes5* encourages support cell differentiation

by negatively regulating *atoh1*. The positive expression of *hes5* both at the gene and protein level suggested that hWJCs may be differentiating into both hair cells and supporting cells concurrently. The significant up-regulations *gfi1* gene expression in cells co-transfected with *hath1* and siRNA against *hes1* and *hes5* suggested that presentation of a hair cell phenotype had started within at least a sub-population of treated cells. The gene expression and protein expression findings combined with the visual morphological changes in *hath1*-transfected cells implied that some level of neuronal differentiation had taken place outside of the body, with limited stimulation by *hath1* and intercellular mediators of the *notch* pathway. Based on the findings by Wang *et al*.[254], the presumption that *atonal* homologues are interchangeable between species has been maintained for over a decade.[109, 113] While this may be the case, the current study found that hWJCs showed increased gene, protein, and morphological features as well as increased viability when transfected with *hath1*. In addition, transduction channels characteristic of hair cells and active neurons were implicated in the cell membranes of *hath1*-transfected cells and cells co-transfected with *hath1* and siRNA against *hes1* and *hes5* based on the superior infiltration of FM® 1-43 dye into hWJCs

Now that measureable and observable differences have been established in hWJCs transfected with *hath1* and hWJCs transfected with *math1*, there is motivation and a strong rationale for future investigation of functional testing such as full electrophysiological testing and full AMPA receptor staining. Mechanistic analyses such as microarray analysis will help illuminate which biochemical pathways are active after hWJCs are transfected, which may help determine the terminal lineages hWJCs are moving toward (i.e. hair cells, cerebellar neurons, goblet cells) outside the body. Culturing of treated cells in a three-dimensional environment may further enhance the atonal effect and potential display of hair cell characteristics. Conversely,

transfecting *hath1* and *math1* into mouse Wharton's jelly cells should yield interesting results that provide more evidence on whether *hath1* and *math1* are truly able to be used interchangeably between species or not. Furthermore, evaluation of gene knockdown of *hes1* and *hes5* via miRNA may increase or decrease the *atonal* effect in hWJCs.

CONCLUSION

In summary, the data revealed that hWJCs transfected with *hath1* displayed far superior expression of key hair cell markers in relation to presentation of mRNA transcripts, proteins, and morphological features in contrast to hWJCs transfected with *math1*. The development and presentation of hair cell markers were further enhanced when *hath1*-transfected hWJCs were co-transfected with siRNA against *hes1* and *hes5*. The current study demonstrated that hWJCs can be manipulated outside of a target tissue to produce a rare and complex phenotype that may aid in illuminating how hair cells develop in the human body and potentially allow for a way to screen new drugs for ototoxicity. For the first time, the *atoh1* homologues *hath1* and *math1* were compared in cells from human tissue, and human cells conclusively responded differently to *hath1* and *math1*, which suggests that the two homologues may not be interchangeable among species.

CHAPTER 6: Conclusion

Tissue engineering has traditionally focused on regenerating tissues through an "outside-in" approach examining sources of stem cells and progenitor cells, extracellular signals both chemical and mechanical, and the design of biomaterials to aid in tissue repair or regeneration. However, the relationship between tissues and organs is complex, and even more sophisticated between cells. While tissue engineering classically examines how a cell can be externally stimulated to induce a desired behavior, the underlying hypothesis driving the work presented in the current thesis is that if gene expression within a cell is reprogrammed to mimic a desired cell phenotype, the cell will modulate the gene expression and protein production accordingly to move toward the desired cell phenotype. Hence, the "inside-out" approach presented in the current thesis (Fig. 6.1).

While the inside-out approach is fascinating, there are many challenges that prevented the inside-out approach form being widely followed. Viral gene delivery strategies are effective, but researchers must continuously convince regulatory agencies that the safety concerns associated with viral gene delivery have been mitigated. Physical non-viral gene delivery approaches are effective, but invasive, especially electroporation. Thus, the work presented in the current thesis focused on improving the integration of gene delivery into tissue engineering for regenerating a target tissue, namely, inner ear hair cells.

Electroporation causes high cytotoxicity because adherent cells must be lifted from a surface, followed by a brief disruption of the cellular membrane facilitated by exposure to a current, thus a consequence in many cells is the activation of the RhoA GTP signaling pathway associated with apoptosis. Inhibiting Rho associated coiled-coil kinase (ROCK) improved transfection efficiency by over four fold, and cell viability by over three fold in cells treated with

Y-27632 ROCK Inhibitor versus untreated cells. Thus, inhibition of ROCK is an effective strategy for mitigating some of the negative effects associated with electroporation and increasing transfection efficiency.

In the photo-convertible study, hWJCs transfected with *pDendra2* robustly photo-converted in two minutes with gentle exposure to UV light. Furthermore, the sensitivity of *pDendra2* demonstrated that individual cells could be targeted for photo-conversion without inducing photo-conversion in surrounding cells within the field of view, allowing for cell tracking over an extended period of time. The utility of photo-convertible reporter genes was demonstrated for the first time *in vitro* in hWJCs, and verified the potential to use photo-convertible reporter genes in low expression systems to track cells, which presents the opportunity to monitor in real-time how cells migrate, differentiate, and integrate into tissues.

hWJCs transfected with *hath1* outperformed hWJCs transfected with *math1* as compared against untreated hWJCs. Cells transfected with *hath1* displayed clear increases gene expression of key markers found on inner ear hair cells within a seven day period. Furthermore, the development of transduction channels was implied by the infiltration of FM 1-43 lipophilic dye into *hath1*-trasnfected hWJCs, where infiltration of FM 1-43 was limited in *math1*-transfected hWJCs. *Hath1*-transfected hWJCS exhibited morphological changes compared to *math1*-trasnfected hWJCs, which was observed by microscopy. *Atonal* effects were enhanced by inhibition of *hes1* and *hes5*, especially in *hath1*-trasnfected hWJCs. Interestingly, lower cell viabilities and densities were recorded with cells transfected with *math1* as opposed to *hath1*-transfected cells, which suggest the mouse homolog of *atoh1* may not be compatible with human tissues. Thus, *atonal* homologues may not be interchangeable as previously thought.

The work presented in the current thesis serves as a starting point for a new approach to tissue engineering. hWJCs are a promising source of stem cells that are highly attractive for tissue engineering, because of their wide abundance, lack of donor site morbidity, high proliferation potential, and similarity to bone marrow stem cells (BMSCs), which are regarded as the "gold standard" of tissue engineering. For the first time, hWJCs were transfected with *atoh1* *p*DNA and siRNA against *hes1* and *hes5*. The work presented in the current thesis clearly demonstrates that hWJCs are susceptible to being guided toward a terminal cellular phenotype not within the differentiation potential of hWJCs naturally. However, while the work presented is an exciting starting point, there are many questions left unanswered that need further investigation, such as the design of a cuvette used in the electroporation technique, Nucleofection™. The current design suspends cells and genetic material randomly between two electrodes, which leads to varying transfection efficiencies and cell viabilities. However, activation of ROCK signaling pathways could be minimized if adherent cells were plated on one electrode, and the other electrode was pre-coated with genetic material or creating a mock extracellular matrix environment that could anchor cells on a material that could act as an electrode could improve transfection efficiency without requiring removal of adherent cells from a surface. Such a design could significantly reduce the negative effects of cellular membrane disruption that occur during electroporation, and allow for uniform delivery of genetic material to cells, maximizing transfection potential. Combining an updated design with ROCK Inhibitor treatment could greatly improve cell transfection efficiencies and viabilities for tissue engineering studies.

Fusing photo-convertible reporter genes with target genes will allow for clear identification of genetic material within the cell against high background. However, caution must

be exercised when *Dendra2* is photo-converted via UV lights as UV light exposure can cross-link thymine nucleotides, which may damage DNA and lead to apoptosis or oncogenesis, if not repaired. The use of photo-converting proteins may be limited to *in vitro* applications for the foreseeable future and basic cell tracking applications as photo-convertible fluorophores may interfere with detailed mechanistic analyses that rely of fluorescence, such as microarrays and mitochondria staining. The value of photo-convertible proteins may be further enhanced by follow-up studies that evaluate the fluorescence lifetime of both the green fluorescence and red fluorescence of *Dendra2*. Thus, photo-conversion of select cells that are positively transfected with a photo-convertible reporter gene will enable the tracking of cell migration and observation of real-time morphological changes in treated cells, and provide detailed insights into changes the treated cells undergo with high precision and accuracy.

While *hath1* induced a superior *atonal* effect in human tissues, the *atonal* effect requires investigation in mouse tissues to confirm that the two homologues are not interchangeable. Will *math1* outperform *hath1* in mouse tissues? Additionally, mechanistic and functional analyses are still required to further evaluate the *atonal* response in human tissues that are transfected with the *atonal* homologues. Microarray analysis will elucidate which signals are active in the *notch*-signaling pathway when cells are transfected with either *hath1* or *math1*. The electrophysiology functionality must still be confirmed, even though the development of transduction channels has been implied through FM 1-43 infiltration. Pilot studies yielded encouraging results, and further analysis is required to determine if calcium permeable ion channels are indeed developing on *hath1* treated hWJCs. Also in question is whether expression of the *atonal* effect is actually guiding cells toward a hair cell phenotype, a cerebellar neuron phenotype, or a goblet cell phenotype. Co-culture of *hath1*-transfected cells with native inner ear hair cells or support cells

may further induce hair cell characteristics in *hath1* treated cells as contact with native cells may provide intercellular signaling and expression of functional traits found in inner ear hair cells. In addition culturing *hath1*-trasnfected cells in a mock extracellular matrix environment, such as a decellularized cochlea or environment that mimics the endolymp of the inner ear may improve hair cell differentiation. Further investigation of the dosing of *hath1* and *math1* will reveal more insights to the biochemical signals being activated within the transfected cells, as well as evaluation of gene knockdown through miRNA delivery instead of siRNA delivery. Improvement and refinement of differentiating hWJCs toward inner ear hair cells could be beneficial in translational studies for inducing hair cell phenotypes outside of the body that could be used to screen ototoxic drugs and study human hair cell morphology, which could aid in the development of therapies for hair cell regeneration.

In addition, tissue engineering studies could be further enhanced by developing better ways to isolate mesenchymal stem cells from Wharton's jelly and preserve the stem cell character. hWJCs may be losing self-renewal abilities and differentiation potential once removed from the extracellular matrix of Wharton's jelly. Thus, further characterization of the extracellular matrix merits investigation to determine if the extracellular matrix influences or maintains stem cells character.

With the evidence presented in this current thesis, it is apparent that hWJCs are capable of differentiating toward neuronal lineages with artificial guidance, and that physical non-viral gene delivery can be improved and applied to difficult-to-transfect cells for tissue engineering studies. The work presented in the current thesis provides preliminary evidence that supports an inside-out approach for tissue engineering that may be combined with current outside-in approaches, which may yield more information about cellular behavior and development. There

is much left to be explored and investigated regarding cellular reprogramming within tissue engineering, but the work presented here combines a promising stem cell source with an unlikely delivery system to manipulate key biochemical signals within a cell to induce a complex phenotype outside of the body. A hypothesis that was only an idea has been translated in a short amount of time to a viable approach for tissue engineering, which has produced exciting results for treatment of sensorineural hearing loss, and challenged established paradigms regarding genetic homologues in biochemical signaling. Perhaps, most importantly, the work presented here has shown a way to bridge physical non-viral gene delivery with stem cell therapy that may generate new questions and ideas to consider to develop innovative ways to overcome exciting challenges in regenerative medicine.

REFERENCES

[1]Adler A. F. and K. W. Leong. Emerging links between surface nanotechnology and endocytosis: impact on nonviral gene delivery. *Nano Today*. 5:553-569, 2010.

[2]Adler A. F., A. T. Speidel, N. Christoforou, K. Kolind, M. Foss, and K. W. Leong. High-throughput screening of microscale pitted substrate topographies for enhanced nonviral transfection efficiency in primary human fibroblasts. *Biomaterials*. 32:3611-9, 2011.

[3]Aihara H. and J. Miyazaki. Gene transfer into muscle by electroporation in vivo. *Nat Biotechnol*. 16:867-70, 1998.

[4]Akinc A., M. Thomas, A. M. Klibanov, and R. Langer. Exploring polyethylenimine-mediated DNA transfection and the proton sponge hypothesis. *J Gene Med*. 7:657-63, 2005.

[5]Alberts B., D. Bray, A. Johnson, J. Lewis, M. Raff, K. Roberts, P. Walter, and A. Campbell. *Essential cell biology*: Garland Science New York. 2004.

[6]Aluigi M., M. Fogli, A. Curti, A. Isidori, E. Gruppioni, C. Chiodoni, M. Colombo, P. Versura, A. D'Errico Grigioni, and E. Ferri. Nucleofection Is an Efficient Nonviral Transfection Technique for Human Bone MarrowñDerived Mesenchymal Stem Cells. *Stem Cells*. 24:454-461, 2006.

[7]Andre F. M. and L. M. Mir. Nucleic acids electrotransfer in vivo: mechanisms and practical aspects. *Curr Gene Ther*. 10:267-80, 2010.

[8]Aslan H., Y. Zilberman, V. Arbeli, D. Sheyn, Y. Matan, M. Liebergall, J. Li, G. Helm, D. Gazit, and Z. Gazit. Nucleofection-based ex vivo nonviral gene delivery to human stem cells as a platform for tissue regeneration. *Tissue Engineering*. 12:877-889, 2006.

[9]Baertschi A. J. Antisense oligonucleotide strategies in physiology. *Mol Cell Endocrinol*. 101:R15-24, 1994.

[10]Bailey M., L. Wang, C. Bode, K. Mitchell, and M. Detamore. A comparison of human umbilical cord matrix stem cells and temporomandibular joint condylar chondrocytes for tissue engineering temporomandibular joint condylar cartilage. *Tissue engineering*. 13:2003-2010, 2007.

[11]Baker S. M., R. W. Buckheit, 3rd, and M. M. Falk. Green-to-red photoconvertible fluorescent proteins: tracking cell and protein dynamics on standard wide-field mercury arc-based microscopes. *BMC Cell Biol*. 11:15, 2010.

[12]Baksh D., L. Song, and R. Tuan. Adult mesenchymal stem cells: characterization, differentiation, and application in cell and gene therapy. *Journal of Cellular and Molecular Medicine*. 8:301-316, 2004.

[13]Baksh D., R. Yao, and R. S. Tuan. Comparison of proliferative and multilineage differentiation potential of human mesenchymal stem cells derived from umbilical cord and bone marrow. *Stem Cells*. 25:1384-92, 2007.

[14]Baoum A., N. Dhillon, S. Buch, and C. Berkland. Cationic surface modification of PLG nanoparticles offers sustained gene delivery to pulmonary epithelial cells. *J Pharm Sci*. 99:2413-22, 2010.

[15]Baoum A., D. Ovcharenko, and C. Berkland. Calcium condensed cell penetrating peptide complexes offer highly efficient, low toxicity gene silencing. *Int J Pharm*. 2011.

[16]Baoum A. A. and C. Berkland. Calcium condensation of DNA complexed with cell-penetrating peptides offers efficient, noncytotoxic gene delivery. *J Pharm Sci*. 100:1637-42, 2011.

[17]Bier M., S. M. Hammer, D. J. Canaday, and R. C. Lee. Kinetics of sealing for transient electropores in isolated mammalian skeletal muscle cells. *Bioelectromagnetics*. 20:194-201, 1999.

[18]Bittman K. S., J. A. Panzer, and R. J. Balice-Gordon. Patterns of cell-cell coupling in embryonic spinal cord studied via ballistic delivery of gap-junction-permeable dyes. *J Comp Neurol*. 477:273-85, 2004.

[19]Blake J. A., C. J. Bult, J. T. Eppig, J. A. Kadin, J. E. Richardson, and G. Mouse Genome Database. The Mouse Genome Database: integration of and access to knowledge about the laboratory mouse. *Nucleic Acids Res*. 42:D810-7, 2014.

[20]Boddy S. L., W. Chen, R. Romero-Guevara, L. Kottam, I. Bellantuono, and M. N. Rivolta. Inner ear progenitor cells can be generated in vitro from human bone marrow mesenchymal stem cells. *Regen Med*. 7:757-67, 2012.

[21]Bolliet C., M. C. Bohn, and M. Spector. Non-viral delivery of the gene for glial cell line-derived neurotrophic factor to mesenchymal stem cells in vitro via a collagen scaffold. *Tissue Eng Part C Methods*. 14:207-19, 2008.

[22]Bowles R., S. Patil, H. Pincas, and S. C. Sealfon. Validation of efficient high-throughput plasmid and siRNA transfection of human monocyte-derived dendritic cells without cell maturation. *J Immunol Methods*. 363:21-8, 2010.

[23]Buerli T., C. Pellegrino, K. Baer, B. Lardi-Studler, I. Chudotvorova, J. M. Fritschy, I. Medina, and C. Fuhrer. Efficient transfection of DNA or shRNA vectors into neurons using magnetofection. *Nat Protoc*. 2:3090-101, 2007.

[24]Campbell N., L. Mitchell, and J. Reece. *Biology: concepts & connections*: Benjamin Cummings New York:. 2003.

[25]Cemazar M., M. Golzio, G. Sersa, M. P. Rols, and J. Teissie. Electrically-assisted nucleic acids delivery to tissues in vivo: where do we stand? *Curr Pharm Des*. 12:3817-25, 2006.

[26]Cesnulevicius K., M. Timmer, M. Wesemann, T. Thomas, T. Barkhausen, and C. Grothe. Nucleofection is the most efficient nonviral transfection method for neuronal stem cells derived from ventral mesencephali with no changes in cell composition or dopaminergic fate. *Stem Cells*. 24:2776-91, 2006.

[27]Chalut K. J., K. Kulangara, M. G. Giacomelli, A. Wax, and K. W. Leong. Deformation of stem cell nuclei by nanotopographical cues. *Soft Matter*. 6:1675-1681, 2010.

[28]Chatterjee P., Y. Cheung, and C. Liew. Transfecting and nucleofecting human induced pluripotent stem cells. *J Vis Exp*. 2011.

[29]Check E. Gene therapy put on hold as third child develops cancer. *Nature*. 433:561, 2005.

[30]Chen Y., Y. Yao, Y. Sumi, A. Li, U. K. To, A. Elkhal, Y. Inoue, T. Woehrle, Q. Zhang, C. Hauser, and W. G. Junger. Purinergic signaling: a fundamental mechanism in neutrophil activation. *Sci Signal*. 3:ra45, 2010.

[31]Choi S. O., Y. C. Kim, J. H. Park, J. Hutcheson, H. S. Gill, Y. K. Yoon, M. R. Prausnitz, and M. G. Allen. An electrically active microneedle array for electroporation. *Biomed Microdevices*. 12:263-73, 2010.

[32]Chonko K. T., I. Jahan, J. Stone, M. C. Wright, T. Fujiyama, M. Hoshino, B. Fritzsch, and S. M. Maricich. Atoh1 directs hair cell differentiation and survival in the late embryonic mouse inner ear. *Dev Biol*. 381:401-10, 2013.

[33]Chudakov D. M., S. Lukyanov, and K. A. Lukyanov. Tracking intracellular protein movements using photoswitchable fluorescent proteins PS-CFP2 and Dendra2. *Nat Protoc*. 2:2024-32, 2007.

[34]Chudakov D. M., S. Lukyanov, and K. A. Lukyanov. Using photoactivatable fluorescent protein Dendra2 to track protein movement. *Biotechniques*. 42:553, 555, 557 passim, 2007.

[35]Chudakov D. M., V. V. Verkhusha, D. B. Staroverov, E. A. Souslova, S. Lukyanov, and K. A. Lukyanov. Photoswitchable cyan fluorescent protein for protein tracking. *Nat Biotechnol*. 22:1435-9, 2004.

[36]Cinkornpumin J. K. and R. L. Hong. RNAi mediated gene knockdown and transgenesis by microinjection in the necromenic Nematode Pristionchus pacificus. *J Vis Exp*.e3270, 2011.

[37]Claassen D. A., M. M. Desler, and A. Rizzino. ROCK inhibition enhances the recovery and growth of cryopreserved human embryonic stem cells and human induced pluripotent stem cells. *Mol Reprod Dev*. 76:722-32, 2009.

[38]Clackson T. Regulated gene expression systems. *Gene Ther*. 7:120-5, 2000.

[39]Clements B. A., V. Incani, C. Kucharski, A. Lavasanifar, B. Ritchie, and H. Uludag. A comparative evaluation of poly-L-lysine-palmitic acid and Lipofectamine 2000 for plasmid delivery to bone marrow stromal cells. *Biomaterials*. 28:4693-704, 2007.

[40]Conner S. D. and S. L. Schmid. Regulated portals of entry into the cell. *Nature*. 422:37-44, 2003.

[41]Cox B. C., R. Chai, A. Lenoir, Z. Liu, L. Zhang, D. H. Nguyen, K. Chalasani, K. A. Steigelman, J. Fang, A. G. Cheng, and J. Zuo. Spontaneous hair cell regeneration in the neonatal mouse cochlea in vivo. *Development*. 141:816-29, 2014.

[42]Dahlhoff M., M. Grzech, F. A. Habermann, E. Wolf, and M. R. Schneider. A transgenic mouse line expressing cre recombinase in pancreatic beta-cells. *Genesis*. 2011.

[43]Dang J. M. and K. W. Leong. Natural polymers for gene delivery and tissue engineering. *Adv Drug Deliv Rev*. 58:487-99, 2006.

[44]Daugimont L., N. Baron, G. Vandermeulen, N. Pavselj, D. Miklavcic, M. C. Jullien, G. Cabodevila, L. M. Mir, and V. Preat. Hollow microneedle arrays for intradermal drug delivery and DNA electroporation. *J Membr Biol*. 236:117-25, 2010.

[45]del Pino P., A. Munoz-Javier, D. Vlaskou, P. Rivera Gil, C. Plank, and W. J. Parak. Gene silencing mediated by magnetic liposphere tagged with small interfering RNA. *Nano Lett*. 10:3914-21, 2010.

[46]Denet A. R., R. Vanbever, and V. Preat. Skin electroporation for transdermal and topical delivery. *Adv Drug Deliv Rev*. 56:659-74, 2004.

[47]Detamore M. S. Human umbilical cord mesenchymal stromal cells in regenerative medicine. *Stem Cell Res Ther*. 4:142, 2013.

[48]Devarajan K., M. L. Forrest, M. S. Detamore, and H. Staecker. Adenovector-mediated gene delivery to human umbilical cord mesenchymal stromal cells induces inner ear cell phenotype. *Cell Reprogram*. 15:43-54, 2013.

[49]Devarajan K., H. Staecker, and M. S. Detamore. A review of gene delivery and stem cell based therapies for regenerating inner ear hair cells. *Journal of Functional Biomaterials*. 2:249-270, 2011.

[50]Di Lisio L., G. Gomez-Lopez, M. Sanchez-Beato, C. Gomez-Abad, M. E. Rodriguez, R. Villuendas, B. I. Ferreira, A. Carro, D. Rico, M. Mollejo, M. A. Martinez, J. Menarguez, A. Diaz-Alderete, J. Gil, J. C. Cigudosa, D. G. Pisano, M. A. Piris, and N. Martinez. Mantle cell lymphoma: transcriptional regulation by microRNAs. *Leukemia*. 24:1335-42, 2010.

[51]Doherty G. J. and H. T. McMahon. Mechanisms of endocytosis. *Annu Rev Biochem*. 78:857-902, 2009.

[52]Donnelly R. F., T. R. Raj Singh, and A. D. Woolfson. Microneedle-based drug delivery systems: microfabrication, drug delivery, and safety. *Drug Deliv*. 17:187-207, 2010.

[53]Dormer N. H., Y. Qiu, A. M. Lydick, N. D. Allen, N. Mohan, C. J. Berkland, and M. S. Detamore. Osteogenic Differentiation of Human Bone Marrow Stromal Cells in Hydroxyapatite-Loaded Microsphere-Based Scaffolds. *Tissue Eng Part A*. 2011.

[54]Driver E. C., L. Sillers, T. M. Coate, M. F. Rose, and M. W. Kelley. The Atoh1-lineage gives rise to hair cells and supporting cells within the mammalian cochlea. *Dev Biol*. 376:86-98, 2013.

[55]Dror A. A. and K. B. Avraham. Hearing loss: mechanisms revealed by genetics and cell biology. *Annu Rev Genet*. 43:411-37, 2009.

[56]Du X., W. Li, X. Gao, M. B. West, W. M. Saltzman, C. J. Cheng, C. Stewart, J. Zheng, W. Cheng, and R. D. Kopke. Regeneration of mammalian cochlear and vestibular hair cells through Hes1/Hes5 modulation with siRNA. *Hear Res*. 304:91-110, 2013.

[57]Duffy G. P., S. D'Arcy, T. Ahsan, R. M. Nerem, T. O'Brien, and F. Barry. Mesenchymal stem cells overexpressing ephrin-b2 rapidly adopt an early endothelial phenotype with simultaneous reduction of osteogenic potential. *Tissue Eng Part A*. 16:2755-68, 2010.

[58]Durisic N., L. Laparra-Cuervo, A. Sandoval-Alvarez, J. S. Borbely, and M. Lakadamyali. Single-molecule evaluation of fluorescent protein photoactivation efficiency using an in vivo nanotemplate. *Nat Methods*. 11:156-62, 2014.

[59]Ear T., P. Giguere, A. Fleury, J. Stankova, M. D. Payet, and G. Dupuis. High efficiency transient transfection of genes in human umbilical vein endothelial cells by electroporation. *J Immunol Methods*. 257:41-9, 2001.

[60]Emre N., J. G. Vidal, J. Elia, E. D. O'Connor, R. I. Paramban, M. P. Hefferan, R. Navarro, D. S. Goldberg, N. M. Varki, M. Marsala, and C. T. Carson. The ROCK inhibitor Y-27632 improves recovery of human embryonic stem cells after fluorescence-activated cell sorting with multiple cell surface markers. *PloS one*. 5:e12148, 2010.

[61]Ensenauer R., D. Hartl, J. Vockley, A. A. Roscher, and U. Fuchs. Efficient and gentle siRNA delivery by magnetofection. *Biotech Histochem*. 86:226-31, 2011.

[62]Faurie C., M. Rebersek, M. Golzio, M. Kanduser, J. M. Escoffre, M. Pavlin, J. Teissie, D. Miklavcic, and M. P. Rols. Electro-mediated gene transfer and expression are controlled by the life-time of DNA/membrane complex formation. *J Gene Med*. 12:117-25, 2010.

[63]Favard C., D. S. Dean, and M. P. Rols. Electrotransfer as a non viral method of gene delivery. *Curr Gene Ther*. 7:67-77, 2007.

[64]Fekete D., S. Muthukumar, and D. Karagogeos. Hair cells and supporting cells share a common progenitor in the avian inner ear. *Journal of Neuroscience*. 18:7811, 1998.

[65]Flanagan M. B., J. M. Gimble, G. Yu, X. Xia, B. Bunnell, and S. Li. Competitive DNA transfection formulation via electroporation for human adipose stem cells and mesenchymal stem cells. *Biol Proced Online*. 14:7, 2012.

[66]Frantescu A., S. Kakorin, K. Toensing, and E. Neumann. Adsorption of DNA and electric fields decrease the rigidity of lipid vesicle membranes. *Phys Chem Chem Phys*. 7:4126-31, 2005.

[67]Frenkel V. and K. C. Li. Potential role of pulsed-high intensity focused ultrasound in gene therapy. *Future Oncol*. 2:111-9, 2006.

[68]Fron E., M. Van der Auweraer, B. Moeyaert, J. Michiels, H. Mizuno, J. Hofkens, and V. Adam. Revealing the Excited-State Dynamics of the Fluorescent Protein Dendra2. *J Phys Chem B*. 2013.

[69]Fukui H. and Y. Raphael. Gene therapy for the inner ear. *Hear Res*. 297:99-105, 2013.

[70]Gauthaman K., C. Y. Fong, and A. Bongso. Effect of ROCK inhibitor Y-27632 on normal and variant human embryonic stem cells (hESCs) in vitro: its benefits in hESC expansion. *Stem Cell Rev*. 6:86-95, 2010.

[71]Gauthaman K., C. Y. Fong, A. Subramanian, A. Biswas, and A. Bongso. ROCK inhibitor Y-27632 increases thaw-survival rates and preserves stemness and differentiation potential of human Wharton's jelly stem cells after cryopreservation. *Stem Cell Rev*. 6:665-76, 2010.

[72]Gersting S. W., U. Schillinger, J. Lausier, P. Nicklaus, C. Rudolph, C. Plank, D. Reinhardt, and J. Rosenecker. Gene delivery to respiratory epithelial cells by magnetofection. *J Gene Med*. 6:913-22, 2004.

[73]Gill H. S. and M. R. Prausnitz. Coated microneedles for transdermal delivery. *J Control Release*. 117:227-37, 2007.

[74]Godbey W. T. and A. G. Mikos. Recent progress in gene delivery using non-viral transfer complexes. *J Control Release*. 72:115-25, 2001.

[75]Godbey W. T., K. K. Wu, and A. G. Mikos. Poly(ethylenimine) and its role in gene delivery. *J Control Release*. 60:149-60, 1999.

[76]Godbey W. T., K. K. Wu, and A. G. Mikos. Poly(ethylenimine)-mediated gene delivery affects endothelial cell function and viability. *Biomaterials*. 22:471-80, 2001.

[77]Godbey W. T., K. K. Wu, and A. G. Mikos. Tracking the intracellular path of poly(ethylenimine)/DNA complexes for gene delivery. *Proc Natl Acad Sci U S A*. 96:5177-81, 1999.

[78]Golzio M., J. M. Escoffre, T. Portet, C. Mauroy, J. Teissie, D. S. Dean, and M. P. Rols. Observations of the mechanisms of electromediated DNA uptake--from vesicles to tissues. *Curr Gene Ther*. 10:256-66, 2010.

[79]Golzio M., S. Mazeres, and J. Teissie. Electrodes for in vivo localised subcutaneous electropulsation and associated drug and nucleic acid delivery. *Expert Opin Drug Deliv*. 6:1323-31, 2009.

[80]Golzio M., M. P. Rols, B. Gabriel, and J. Teissie. Optical imaging of in vivo gene expression: a critical assessment of the methodology and associated technologies. *Gene Ther*. 11 Suppl 1:S85-91, 2004.

[81]Golzio M., J. Teissie, and M. P. Rols. Direct visualization at the single-cell level of electrically mediated gene delivery. *Proc Natl Acad Sci U S A*. 99:1292-7, 2002.

[82]Gonzalez F., M. Barragan Monasterio, G. Tiscornia, N. Montserrat Pulido, R. Vassena, L. Batlle Morera, I. Rodriguez Piza, and J. C. Izpisua Belmonte. Generation of mouse-induced pluripotent stem cells by transient expression of a single nonviral polycistronic vector. *Proc Natl Acad Sci U S A*. 106:8918-22, 2009.

[83]Gould T. J., M. S. Gunewardene, M. V. Gudheti, V. V. Verkhusha, S. R. Yin, J. A. Gosse, and S. T. Hess. Nanoscale imaging of molecular positions and anisotropies. *Nat Methods*. 5:1027-30, 2008.

[84]Green J. J., E. Chiu, E. S. Leshchiner, J. Shi, R. Langer, and D. G. Anderson. Electrostatic ligand coatings of nanoparticles enable ligand-specific gene delivery to human primary cells. *Nano Lett*. 7:874-9, 2007.

[85]Green J. J., R. Langer, and D. G. Anderson. A Combinatorial Polymer Library Approach Yields Insight into Nonviral Gene Delivery. *Acc Chem Res*. 2008.

[86]Green J. J., J. Shi, E. Chiu, E. S. Leshchiner, R. Langer, and D. G. Anderson. Biodegradable polymeric vectors for gene delivery to human endothelial cells. *Bioconjug Chem*. 17:1162-9, 2006.

[87]Green J. J., B. Y. Zhou, M. M. Mitalipova, C. Beard, R. Langer, R. Jaenisch, and D. G. Anderson. Nanoparticles for gene transfer to human embryonic stem cell colonies. *Nano Lett*. 8:3126-30, 2008.

[88]Gresch O. and L. Altrogge. Transfection of Difficult-to-Transfect Primary Mammalian Cells. *Methods Mol Biol*. 801:65-74, 2012.

[89]Gunewardene M. S., F. V. Subach, T. J. Gould, G. P. Penoncello, M. V. Gudheti, V. V. Verkhusha, and S. T. Hess. Superresolution imaging of multiple fluorescent proteins with highly overlapping emission spectra in living cells. *Biophys J*. 101:1522-8, 2011.

[90]Gurskaya N. G., V. V. Verkhusha, A. S. Shcheglov, D. B. Staroverov, T. V. Chepurnykh, A. F. Fradkov, S. Lukyanov, and K. A. Lukyanov. Engineering of a monomeric green-to-red photoactivatable fluorescent protein induced by blue light. *Nat Biotechnol*. 24:461-5, 2006.

[91]Gwak S. J. and B. S. Kim. Poly(lactic-co-glycolic acid) nanosphere as a vehicle for gene delivery to human cord blood-derived mesenchymal stem cells: comparison with polyethylenimine. *Biotechnol Lett*. 30:1177-82, 2008.

[92]Haberl S., D. Miklavcic, and M. Pavlin. Effect of Mg ions on efficiency of gene electrotransfer and on cell electropermeabilization. *Bioelectrochemistry*. 79:265-71, 2010.

[93]Hamm A., N. Krott, I. Breibach, R. Blindt, and A. Bosserhoff. Efficient transfection method for primary cells. *Tissue Engineering*. 8:235-245, 2002.

[94]Harb N., T. Archer, and N. Sato. The Rho-Rock-Myosin signaling axis determines cell-cell integrity of self-renewing pluripotent stem cells. *PloS one*. 3, 2008.

[95]Hatta K., H. Tsujii, and T. Omura. Cell tracking using a photoconvertible fluorescent protein. *Nat Protoc*. 1:960-7, 2006.

[96]Hay J. C. Calcium: a fundamental regulator of intracellular membrane fusion? *EMBO Rep*. 8:236-40, 2007.

[97]He C. X., Y. Tabata, and J. Q. Gao. Non-viral gene delivery carrier and its three-dimensional transfection system. *Int J Pharm*. 386:232-42, 2010.

[98]Heller L. C. and R. Heller. In vivo electroporation for gene therapy. *Hum Gene Ther*. 17:890-7, 2006.

[99]Heller R., M. Jaroszeski, A. Atkin, D. Moradpour, R. Gilbert, J. Wands, and C. Nicolau. In vivo gene electroinjection and expression in rat liver. *FEBS Lett*. 389:225-8, 1996.

[100]Henshaw J., B. Mossop, and F. Yuan. Enhancement of electric field-mediated gene delivery through pretreatment of tumors with a hyperosmotic mannitol solution. *Cancer Gene Ther*. 18:26-33, 2011.

[101]Henshaw J. W. and F. Yuan. Field distribution and DNA transport in solid tumors during electric field-mediated gene delivery. *J Pharm Sci*. 97:691-711, 2008.

[102]Hsu M. F. and T. C. Meng. Enhancement of insulin responsiveness by nitric oxide-mediated inactivation of protein-tyrosine phosphatases. *J Biol Chem*. 285:7919-28, 2010.

[103]Huth S., J. Lausier, S. W. Gersting, C. Rudolph, C. Plank, U. Welsch, and J. Rosenecker. Insights into the mechanism of magnetofection using PEI-based magnetofectins for gene transfer. *J Gene Med*. 6:923-36, 2004.

[104]Hutson T. H., W. J. Buchser, J. L. Bixby, V. P. Lemmon, and L. D. Moon. Optimization of a 96-Well Electroporation Assay for Postnatal Rat CNS Neurons Suitable for Cost-

Effective Medium-Throughput Screening of Genes that Promote Neurite Outgrowth. *Front Mol Neurosci*. 4:55, 2011.

[105]Ichikawa H., Y. Kanoh, S. Shirasawa, T. Yokoyama, F. Yue, D. Tomotsune, and K. Sasaki. Unique kinetics of Oct3/4 microlocalization following dissociation of human embryonic stem cell colonies. *Ann Anat*. 195:50-6, 2013.

[106]Ichikawa H., N. Nakata, Y. Abo, S. Shirasawa, T. Yokoyama, S. Yoshie, F. Yue, D. Tomotsune, and K. Sasaki. Gene pathway analysis of the mechanism by which the Rho-associated kinase inhibitor Y-27632 inhibits apoptosis in isolated thawed human embryonic stem cells. *Cryobiology*. 64:12-22, 2012.

[107]Ino K., T. Kawasumi, A. Ito, and H. Honda. Plasmid DNA transfection using magnetite cationic liposomes for construction of multilayered gene-engineered cell sheet. *Biotechnol Bioeng*. 100:168-76, 2008.

[108]Izumikawa M., R. Minoda, K. Kawamoto, K. A. Abrashkin, D. L. Swiderski, D. F. Dolan, D. E. Brough, and Y. Raphael. Auditory hair cell replacement and hearing improvement by Atoh1 gene therapy in deaf mammals. *Nat Med*. 11:271-6, 2005.

[109]Jahan I., N. Pan, J. Kersigo, and B. Fritzsch. Beyond generalized hair cells: molecular cues for hair cell types. *Hear Res*. 297:30-41, 2013.

[110]Jang J. H., T. L. Houchin, and L. D. Shea. Gene delivery from polymer scaffolds for tissue engineering. *Expert Rev Med Devices*. 1:127-38, 2004.

[111]Jang J. H., T. L. Houchin, and L. D. Shea. Gene delivery from polymer scaffolds for tissue engineering. *Expert Review of Medical Devices*. 1:127-138, 2004.

[112]Jang J. H. and L. D. Shea. Controllable delivery of non-viral DNA from porous scaffolds. *J Control Release*. 86:157-68, 2003.

[113]Jarman A. P. and A. K. Groves. The role of Atonal transcription factors in the development of mechanosensitive cells. *Semin Cell Dev Biol*. 24:438-47, 2013.

[114]Jeon S. J., K. Oshima, S. Heller, and A. S. Edge. Bone marrow mesenchymal stem cells are progenitors in vitro for inner ear hair cells. *Mol Cell Neurosci*. 34:59-68, 2007.

[115]Jo J. and Y. Tabata. Non-viral gene transfection technologies for genetic engineering of stem cells. *Eur J Pharm Biopharm*. 68:90-104, 2008.

[116]Joo H., D.-K. Choi, J. Lim, J.-S. Park, S.-H. Lee, S. Song, J. Shin, D.-S. Lim, I. Kim, K.-C. Hwang, and G. Koh. ROCK suppression promotes differentiation and expansion of endothelial cells from embryonic stem cell-derived Flk1(+) mesodermal precursor cells. *Blood*. 120:2733-2744, 2012.

[117]Jordan E. T., M. Collins, J. Terefe, L. Ugozzoli, and T. Rubio. Optimizing electroporation conditions in primary and other difficult-to-transfect cells. *J Biomol Tech*. 19:328-34, 2008.

[118]Jung J. Y., M. R. Avenarius, S. Adamsky, E. Alpert, E. Feinstein, and Y. Raphael. siRNA targeting Hes5 augments hair cell regeneration in aminoglycoside-damaged mouse utricle. *Mol Ther*. 21:834-41, 2013.

[119]Kageyama R. and T. Ohtsuka. The Notch-Hes pathway in mammalian neural development. *Cell Res*. 9:179-88, 1999.

[120]Kaneda Y. Update on non-viral delivery methods for cancer therapy: possibilities of a drug delivery system with anticancer activities beyond delivery as a new therapeutic tool. *Expert Opin Drug Deliv*. 7:1079-93, 2010.

[121]Kasper F. K., S. K. Seidlits, A. Tang, R. S. Crowther, D. H. Carney, M. A. Barry, and A. G. Mikos. In vitro release of plasmid DNA from oligo(poly(ethylene glycol) fumarate) hydrogels. *J Control Release*. 104:521-39, 2005.

[122]Kay M. A., J. C. Glorioso, and L. Naldini. Viral vectors for gene therapy: the art of turning infectious agents into vehicles of therapeutics. *Nat Med*. 7:33-40, 2001.

[123]Kaya A. I., O. Ugur, O. Altuntas, K. Sayar, and H. O. Onaran. Long and short distance movements of beta(2)-adrenoceptor in cell membrane assessed by photoconvertible fluorescent protein dendra2-beta(2)-adrenoceptor fusion. *Biochim Biophys Acta*. 1813:1511-24, 2011.

[124]Kelly M. C., Q. Chang, A. Pan, X. Lin, and P. Chen. Atoh1 directs the formation of sensory mosaics and induces cell proliferation in the postnatal mammalian cochlea in vivo. *J Neurosci*. 32:6699-710, 2012.

[125]Kendall M., S. Rishworth, F. Carter, and T. Mitchell. Effects of relative humidity and ambient temperature on the ballistic delivery of micro-particles to excised porcine skin. *J Invest Dermatol*. 122:739-46, 2004.

[126]Kettunen P., J. Demas, C. Lohmann, N. Kasthuri, Y. Gong, R. O. Wong, and W. B. Gan. Imaging calcium dynamics in the nervous system by means of ballistic delivery of indicators. *J Neurosci Methods*. 119:37-43, 2002.

[127]Khalil I. A., K. Kogure, H. Akita, and H. Harashima. Uptake pathways and subsequent intracellular trafficking in nonviral gene delivery. *Pharmacol Rev*. 58:32-45, 2006.

[128]Khondee S., A. Baoum, T. J. Siahaan, and C. Berkland. Calcium condensed LABL-TAT complexes effectively target gene delivery to ICAM-1 expressing cells. *Mol Pharm*. 8:788-98, 2011.

[129]Kirkham M. and R. G. Parton. Clathrin-independent endocytosis: new insights into caveolae and non-caveolar lipid raft carriers. *Biochim Biophys Acta*. 1746:349-63, 2005.

[130]Kitagawa M. and T. Fujita. Quantitative imaging of directional transport through plasmodesmata in moss protonemata via single-cell photoconversion of Dendra2. *J Plant Res*. 2013.

[131]Kobayashi N., J. D. Rivas-Carrillo, A. Soto-Gutierrez, T. Fukazawa, Y. Chen, N. Navarro-Alvarez, and N. Tanaka. Gene delivery to embryonic stem cells. *Birth Defects Res C Embryo Today*. 75:10-8, 2005.

[132]Kofron M. D. and C. T. Laurencin. Bone tissue engineering by gene delivery. *Adv Drug Deliv Rev*. 58:555-76, 2006.

[133]Kong J., M. A. Crissey, A. R. Sepulveda, and J. P. Lynch. Math1/Atoh1 contributes to intestinalization of esophageal keratinocytes by inducing the expression of Muc2 and Keratin-20. *Dig Dis Sci*. 57:845-57, 2012.

[134]Koyanagi M., J. Takahashi, Y. Arakawa, D. Doi, H. Fukuda, H. Hayashi, S. Narumiya, and N. Hashimoto. Inhibition of the Rho/ROCK pathway reduces apoptosis during transplantation of embryonic stem cell-derived neural precursors. *J Neurosci Res*. 86:270-80, 2008.

[135]Kraft S., C. Hsu, D. E. Brough, and H. Staecker. Atoh1 induces auditory hair cell recovery in mice after ototoxic injury. *Laryngoscope*. 123:992-9, 2013.

[136]Krotz F., H. Y. Sohn, T. Gloe, C. Plank, and U. Pohl. Magnetofection potentiates gene delivery to cultured endothelial cells. *J Vasc Res*. 40:425-34, 2003.

[137]Kucherlapati R. and A. I. Skoultchi. Introduction of purified genes into mammalian cells. *CRC Crit Rev Biochem*. 16:349-79, 1984.

[138]Kurata S., M. Tsukakoshi, T. Kasuya, and Y. Ikawa. The laser method for efficient introduction of foreign DNA into cultured cells. *Exp Cell Res*. 162:372-8, 1986.

[139]Kurosawa H. Application of Rho-associated protein kinase (ROCK) inhibitor to human pluripotent stem cells. *J Biosci Bioeng*. 114:577-581, 2012.

[140]Lamb N. J., C. Gauthier-Rouviere, and A. Fernandez. Microinjection strategies for the study of mitogenic signaling in mammalian cells. *Front Biosci*. 1:d19-29, 1996.

[141]Langer R. and M. Moses. Biocompatible controlled release polymers for delivery of polypeptides and growth factors. *J Cell Biochem*. 45:340-5, 1991.

[142]Leipzig N. D. and K. A. Athanasiou. Static compression of single chondrocytes catabolically modifies single-cell gene expression. *Biophys J*. 94:2412-22, 2008.

[143]Liang D., Y. K. Luu, K. Kim, B. S. Hsiao, M. Hadjiargyrou, and B. Chu. In vitro non-viral gene delivery with nanofibrous scaffolds. *Nucleic Acids Res*. 33:e170, 2005.

[144]Liang H. D., J. Tang, and M. Halliwell. Sonoporation, drug delivery, and gene therapy. *Proc Inst Mech Eng H*. 224:343-61, 2010.

[145]Lim S. H., I. C. Liao, and K. W. Leong. Nonviral gene delivery from nonwoven fibrous scaffolds fabricated by interfacial complexation of polyelectrolytes. *Mol Ther*. 13:1163-72, 2006.

[146]Lin Z., P. Perez, Z. Sun, J. J. Liu, J. H. Shin, K. L. Hyrc, D. Samways, T. Egan, M. C. Holley, and J. Bao. Reprogramming of single-cell-derived mesenchymal stem cells into hair cell-like cells. *Otol Neurotol*. 33:1648-55, 2012.

[147]Liu Z., J. A. Dearman, B. C. Cox, B. J. Walters, L. Zhang, O. Ayrault, F. Zindy, L. Gan, M. F. Roussel, and J. Zuo. Age-dependent in vivo conversion of mouse cochlear pillar and Deiters' cells to immature hair cells by Atoh1 ectopic expression. *J Neurosci*. 32:6600-10, 2012.

[148]Lo H., S. Kadiyala, S. E. Guggino, and K. W. Leong. Poly(L-lactic acid) foams with cell seeding and controlled-release capacity. *J Biomed Mater Res*. 30:475-84, 1996.

[149]Lohr F., D. Y. Lo, D. A. Zaharoff, K. Hu, X. Zhang, Y. Li, Y. Zhao, M. W. Dewhirst, F. Yuan, and C. Y. Li. Effective tumor therapy with plasmid-encoded cytokines combined with in vivo electroporation. *Cancer Res*. 61:3281-4, 2001.

[150]Long X., S. D. Xiong, W. N. Xiong, and Y. J. Xu. Effect of intramuscular injection of hepatocyte growth factor plasmid DNA with electroporation on bleomycin-induced lung fibrosis in rats. *Chin Med J (Engl)*. 120:1432-7, 2007.

[151]Lukacs G. L., P. Haggie, O. Seksek, D. Lechardeur, N. Freedman, and A. S. Verkman. Size-dependent DNA mobility in cytoplasm and nucleus. *J Biol Chem*. 275:1625-9, 2000.

[152]Manohar R. and E. Lagasse. Transdetermination: a new trend in cellular reprogramming. *Mol Ther*. 17:936-8, 2009.

[153]Marine S., J. Freeman, A. Riccio, M. L. Axenborg, J. Pihl, R. Ketteler, and S. Aspengren. High-throughput transfection of differentiated primary neurons from rat forebrain. *J Biomol Screen*. 17:692-6, 2012.

[154]Mark Saltzman W. and S. P. Baldwin. Materials for protein delivery in tissue engineering. *Adv Drug Deliv Rev*. 33:71-86, 1998.

[155]Martinek V., F. H. Fu, and J. Huard. Gene therapy and tissue engineering in sports medicine. *Phys Sportsmed*. 28:34-51, 2000.

[156]Masuda K., Y. Ishikawa, I. Onoyama, M. Unno, I. M. de Alboran, K. I. Nakayama, and K. Nakayama. Complex regulation of cell-cycle inhibitors by Fbxw7 in mouse embryonic fibroblasts. *Oncogene*. 29:1798-809, 2010.

[157]McCall J., L. Nicholson, N. Weidner, and A. Blesch. Optimization of adult sensory neuron electroporation to study mechanisms of neurite growth. *Front Mol Neurosci*. 5:11, 2012.

[158]Mehier-Humbert S. and R. H. Guy. Physical methods for gene transfer: improving the kinetics of gene delivery into cells. *Adv Drug Deliv Rev*. 57:733-53, 2005.

[159]Mellott A. J., M. L. Forrest, and M. S. Detamore. Physical Non-Viral Gene Delivery Methods for Tissue Engineering. *Annals of Biomedical Engineering*.1-23, 2013.

[160]Mellott A. J., M. E. Godsey, H. E. Shinogle, D. S. Moore, M. L. Forrest, and M. S. Detamore. Improving Viability and Transfection Efficiency with Human Umbilical Cord Wharton's Jelly Cells Through Use of a ROCK Inhibitor. *Cell Reprogram*. 2014.

[161]Mercer J., M. Schelhaas, and A. Helenius. Virus entry by endocytosis. *Annu Rev Biochem*. 79:803-33, 2010.

[162]Merdan T., J. Kopecek, and T. Kissel. Prospects for cationic polymers in gene and oligonucleotide therapy against cancer. *Adv Drug Deliv Rev*. 54:715-58, 2002.

[163]Middaugh C. R. and J. D. Ramsey. Analysis of cationic-lipid-plasmid-DNA complexes. *Anal Chem*. 79:7240-8, 2007.

[164]Midoux P., C. Pichon, J. J. Yaouanc, and P. A. Jaffres. Chemical vectors for gene delivery: a current review on polymers, peptides and lipids containing histidine or imidazole as nucleic acids carriers. *Br J Pharmacol*. 157:166-78, 2009.

[165]Mir L. M. Nucleic acids electrotransfer-based gene therapy (electrogenetherapy): past, current, and future. *Mol Biotechnol*. 43:167-76, 2009.

[166]Mir L. M., M. F. Bureau, J. Gehl, R. Rangara, D. Rouy, J. M. Caillaud, P. Delaere, D. Branellec, B. Schwartz, and D. Scherman. High-efficiency gene transfer into skeletal muscle mediated by electric pulses. *Proc Natl Acad Sci U S A*. 96:4262-7, 1999.

[167]Mitchell K., M. Weiss, B. Mitchell, P. Martin, D. Davis, L. Morales, B. Helwig, M. Beerenstrauch, K. Abou Easa, and T. Hildreth. Matrix cells from Wharton's jelly form neurons and glia. *Stem cells*. 21:50-60, 2003.

[168]Mitchell T. J., M. A. F. Kendall, and B. J. Bellhouse. A ballistic study of micro-particle penetration to the oral mucosa. *International journal of impact engineering*. 28:581-599, 2003.

[169]Miyake M., S. Hayashi, S. Iwasaki, G. Chao, H. Takahashi, K. Watanabe, S. Ohwada, H. Aso, and T. Yamaguchi. Possible role of TIEG1 as a feedback regulator of myostatin and TGF-beta in myoblasts. *Biochem Biophys Res Commun*. 393:762-6, 2010.

[170]Mizutari K., M. Fujioka, M. Hosoya, N. Bramhall, H. J. Okano, H. Okano, and A. S. Edge. Notch inhibition induces cochlear hair cell regeneration and recovery of hearing after acoustic trauma. *Neuron*. 77:58-69, 2013.

[171]Moore J. C., K. Atze, P. L. Yeung, A. J. Toro-Ramos, C. Camarillo, K. Thompson, C. L. Ricupero, M. A. Brenneman, R. I. Cohen, and R. P. Hart. Efficient, high-throughput transfection of human embryonic stem cells. *Stem Cell Res Ther*. 1:23, 2010.

[172]Motani K., K. Kawase, R. Imamura, T. Kinoshita, H. Kushiyama, and T. Suda. Activation of ASC induces apoptosis or necrosis, depending on the cell type, and causes tumor eradication. *Cancer Sci*. 101:1822-7, 2010.

[173]Nabi I. R. and P. U. Le. Caveolae/raft-dependent endocytosis. *J Cell Biol*. 161:673-7, 2003.

[174]Narumiya S., T. Ishizaki, and M. Uehata. Use and properties of ROCK-specific inhibitor Y-27632. *Methods Enzymol*. 325:273-84, 2000.

[175]Nathwani A. C., K. M. Gale, K. D. Pemberton, D. C. Crossman, E. G. Tuddenham, and J. H. McVey. Efficient gene transfer into human umbilical vein endothelial cells allows functional analysis of the human tissue factor gene promoter. *Br J Haematol*. 88:122-8, 1994.

[176]Netti P. A., D. A. Berk, M. A. Swartz, A. J. Grodzinsky, and R. K. Jain. Role of extracellular matrix assembly in interstitial transport in solid tumors. *Cancer Res*. 60:2497-503, 2000.

[177]Neu W. K. and J. C. Neu. Mechanism of Irreversible Electroporation in Cells: Insight from the Models. *Irreversible Electroporation*.85-122, 2010.

[178]Neumann E., M. Schaefer-Ridder, Y. Wang, and P. H. Hofschneider. Gene transfer into mouse lyoma cells by electroporation in high electric fields. *EMBO J*. 1:841-5, 1982.

[179]Newman C. M. and T. Bettinger. Gene therapy progress and prospects: ultrasound for gene transfer. *Gene Ther*. 14:465-75, 2007.

[180]Nie H. and C. H. Wang. Fabrication and characterization of PLGA/HAp composite scaffolds for delivery of BMP-2 plasmid DNA. *J Control Release*. 120:111-21, 2007.

[181]Nomikou N. and A. P. McHale. Exploiting ultrasound-mediated effects in delivering targeted, site-specific cancer therapy. *Cancer Lett*. 296:133-43, 2010.

[182]Nowotschin S. and A. K. Hadjantonakis. Photomodulatable fluorescent proteins for imaging cell dynamics and cell fate. *Organogenesis*. 5:217-26, 2009.

[183]O'Neill B. E. and K. C. Li. Augmentation of targeted delivery with pulsed high intensity focused ultrasound. *Int J Hyperthermia*. 24:506-20, 2008.

[184]Ogura M., S. Sato, K. Nakanishi, M. Uenoyama, T. Kiyozumi, D. Saitoh, T. Ikeda, H. Ashida, and M. Obara. In vivo targeted gene transfer in skin by the use of laser-induced stress waves. *Lasers Surg Med*. 34:242-8, 2004.

[185]Ohgushi M., M. Matsumura, M. Eiraku, K. Murakami, T. Aramaki, A. Nishiyama, K. Muguruma, T. Nakano, H. Suga, M. Ueno, T. Ishizaki, H. Suemori, S. Narumiya, H. Niwa, and Y. Sasai. Molecular pathway and cell state responsible for dissociation-induced apoptosis in human pluripotent stem cells. *Cell Stem Cell*. 7:225-239, 2010.

[186]Ohgushi M. and Y. Sasai. Lonely death dance of human pluripotent stem cells: ROCKing between metastable cell states. *Trends Cell Biol*. 21:274-82, 2011.

[187]Olson M. F. Applications for ROCK kinase inhibition. *Curr Opin Cell Biol*. 20:242-8, 2008.

[188]Pakzad M., M. Totonchi, A. Taei, A. Seifinejad, S. N. Hassani, and H. Baharvand. Presence of a ROCK inhibitor in extracellular matrix supports more undifferentiated growth of feeder-free human embryonic and induced pluripotent stem cells upon passaging. *Stem Cell Rev*. 6:96-107, 2010.

[189]Palumbo G., M. Caruso, E. Crescenzi, M. F. Tecce, G. Roberti, and A. Colasanti. Targeted gene transfer in eucaryotic cells by dye-assisted laser optoporation. *J Photochem Photobiol B*. 36:41-6, 1996.

[190]Park J. H., M. G. Allen, and M. R. Prausnitz. Biodegradable polymer microneedles: fabrication, mechanics and transdermal drug delivery. *J Control Release*. 104:51-66, 2005.

[191]Park T. G., J. H. Jeong, and S. W. Kim. Current status of polymeric gene delivery systems. *Adv Drug Deliv Rev*. 58:467-86, 2006.

[192]Park Y. H., K. F. Wilson, Y. Ueda, H. Tung Wong, L. A. Beyer, D. L. Swiderski, D. F. Dolan, and Y. Raphael. Conditioning the Cochlea to Facilitate Survival and Integration of Exogenous Cells into the Auditory Epithelium. *Mol Ther*. 2014.

[193]Partridge K. A. and R. O. Oreffo. Gene delivery in bone tissue engineering: progress and prospects using viral and nonviral strategies. *Tissue Eng*. 10:295-307, 2004.

[194]Pauley S., B. Kopecky, K. Beisel, G. Soukup, and B. Fritzsch. Stem cells and molecular strategies to restore hearing. *Panminerva Med*. 50:41-53, 2008.

[195]Pearton M., C. Allender, K. Brain, A. Anstey, C. Gateley, N. Wilke, A. Morrissey, and J. Birchall. Gene delivery to the epidermal cells of human skin explants using microfabricated microneedles and hydrogel formulations. *Pharm Res*. 25:407-16, 2008.

[196]Pederson T. Movement and localization of RNA in the cell nucleus. *FASEB J*. 13 Suppl 2:S238-42, 1999.

[197]Phez E., C. Faurie, M. Golzio, J. Teissie, and M. P. Rols. New insights in the visualization of membrane permeabilization and DNA/membrane interaction of cells submitted to electric pulses. *Biochim Biophys Acta*. 1724:248-54, 2005.

[198]Pickard M. R., P. Barraud, and D. M. Chari. The transfection of multipotent neural precursor/stem cell transplant populations with magnetic nanoparticles. *Biomaterials*. 32:2274-84, 2011.

[199]Pimpha N., P. Sunintaboon, S. Inphonlek, and Y. Tabata. Gene delivery efficacy of polyethyleneimine-introduced chitosan shell/poly(methyl methacrylate) core nanoparticles for rat mesenchymal stem cells. *J Biomater Sci Polym Ed*. 21:205-23, 2010.

[200]Plank C., M. Anton, C. Rudolph, J. Rosenecker, and F. Krotz. Enhancing and targeting nucleic acid delivery by magnetic force. *Expert Opin Biol Ther*. 3:745-58, 2003.

[201]Plank C., U. Schillinger, F. Scherer, C. Bergemann, J. S. Remy, F. Krotz, M. Anton, J. Lausier, and J. Rosenecker. The magnetofection method: using magnetic force to enhance gene delivery. *Biol Chem*. 384:737-47, 2003.

[202]Plank C., O. Zelphati, and O. Mykhaylyk. Magnetically enhanced nucleic acid delivery. Ten years of magnetofection-progress and prospects. *Adv Drug Deliv Rev*. 63:1300-31, 2011.

[203]Pluen A., Y. Boucher, S. Ramanujan, T. D. McKee, T. Gohongi, E. di Tomaso, E. B. Brown, Y. Izumi, R. B. Campbell, D. A. Berk, and R. K. Jain. Role of tumor-host interactions in interstitial diffusion of macromolecules: cranial vs. subcutaneous tumors. *Proc Natl Acad Sci U S A*. 98:4628-33, 2001.

[204]Postema M. and O. H. Gilja. Ultrasound-directed drug delivery. *Curr Pharm Biotechnol*. 8:355-61, 2007.

[205]Prausnitz M. R. Microneedles for transdermal drug delivery. *Adv Drug Deliv Rev*. 56:581-7, 2004.

[206]Prausnitz M. R., J. D. Corbett, J. A. Gimm, D. E. Golan, R. Langer, and J. C. Weaver. Millisecond measurement of transport during and after an electroporation pulse. *Biophys J*. 68:1864-70, 1995.

[207]Prausnitz M. R. and R. Langer. Transdermal drug delivery. *Nat Biotechnol*. 26:1261-8, 2008.

[208]Ramos C. and J. Teissie. Electrofusion: a biophysical modification of cell membrane and a mechanism in exocytosis. *Biochimie*. 82:511-8, 2000.

[209]Rejman J., A. Bragonzi, and M. Conese. Role of clathrin- and caveolae-mediated endocytosis in gene transfer mediated by lipo- and polyplexes. *Mol Ther*. 12:468-74, 2005.

[210]Rols M. P., C. Delteil, M. Golzio, P. Dumond, S. Cros, and J. Teissie. In vivo electrically mediated protein and gene transfer in murine melanoma. *Nat Biotechnol*. 16:168-71, 1998.

[211]Rols M. P., P. Femenia, and J. Teissie. Long-lived macropinocytosis takes place in electropermeabilized mammalian cells. *Biochem Biophys Res Commun*. 208:26-35, 1995.

[212]Ronaghi M., M. Nasr, M. Ealy, R. Durruthy-Durruthy, J. Waldhaus, G. H. Diaz, L. M. Joubert, K. Oshima, and S. Heller. Inner ear hair cell-like cells from human embryonic stem cells. *Stem Cells Dev*. 2014.

[213]Rubel E., E. Oesterle, and P. Weisleder. *Hair cell regeneration in the avian inner ear*. 1991.

[214]Russell S. J. Science, medicine, and the future. Gene therapy. *BMJ*. 315:1289-92, 1997.

[215]Sagi S., T. Knoll, L. Trojan, A. Schaaf, P. Alken, and M. S. Michel. Gene delivery into prostate cancer cells by holmium laser application. *Prostate Cancer Prostatic Dis*. 6:127-30, 2003.

[216]Saijilafu, E. M. Hur, and F. Q. Zhou. Genetic dissection of axon regeneration via in vivo electroporation of adult mouse sensory neurons. *Nat Commun*. 2:543, 2011.

[217]Salsano E., B. Pollo, M. Eoli, M. T. Giordana, and G. Finocchiaro. Expression of MATH1, a marker of cerebellar granule cell progenitors, identifies different medulloblastoma sub-types. *Neurosci Lett*. 370:180-5, 2004.

[218]Sanford J. C., M. K. THEODORE, D. EDWARD, and N. Allen. Delivery of substances into cells and tissues using a particle bombardment process. *Particulate Science and Technology*. 5:27-37, 1987.

[219]Sapet C., N. Laurent, A. de Chevigny, L. Le Gourrierec, E. Bertosio, O. Zelphati, and C. Beclin. High transfection efficiency of neural stem cells with magnetofection. *Biotechniques*. 50:187-9, 2011.

[220]Saraf A. and A. G. Mikos. Gene delivery strategies for cartilage tissue engineering. *Adv Drug Deliv Rev*. 58:592-603, 2006.

[221]Satkauskas S., M. F. Bureau, A. Mahfoudi, and L. M. Mir. Slow accumulation of plasmid in muscle cells: supporting evidence for a mechanism of DNA uptake by receptor-mediated endocytosis. *Mol Ther*. 4:317-23, 2001.

[222]Sato S., M. Nishizuka, M. Asano, T. Ohtake, M. Imagawa, and E. Kobayashi. RNA interference-mediated knockdown of the mouse gene encoding potassium channel subfamily K member 10 inhibits hormone-induced differentiation of 3T3-L1 preadipocytes. *Comp Biochem Physiol B Biochem Mol Biol*. 157:46-53, 2010.

[223]Saul J. M., M. P. Linnes, B. D. Ratner, C. M. Giachelli, and S. H. Pun. Delivery of non-viral gene carriers from sphere-templated fibrin scaffolds for sustained transgene expression. *Biomaterials*. 28:4705-16, 2007.

[224]Saurer E. M., R. M. Flessner, S. P. Sullivan, M. R. Prausnitz, and D. M. Lynn. Layer-by-Layer Assembly of DNA- and Protein-Containing Films on Microneedles for Drug Delivery to the Skin. *Biomacromolecules*. 2010.

[225]Scherer F., M. Anton, U. Schillinger, J. Henke, C. Bergemann, A. Kruger, B. Gansbacher, and C. Plank. Magnetofection: enhancing and targeting gene delivery by magnetic force in vitro and in vivo. *Gene Ther*. 9:102-9, 2002.

[226]Schwachtgen J. L., V. Ferreira, D. Meyer, and D. Kerbiriou-Nabias. Optimization of the transfection of human endothelial cells by electroporation. *Biotechniques*. 17:882-7, 1994.

[227]Schwerdt J. I., G. F. Goya, M. P. Calatayud, C. B. Herenu, P. C. Reggiani, and R. G. Goya. Magnetic field-assisted gene delivery: achievements and therapeutic potential. *Curr Gene Ther*. 12:116-26, 2012.

[228]Sersa G., M. Cemazar, C. S. Parkins, and D. J. Chaplin. Tumour blood flow changes induced by application of electric pulses. *Eur J Cancer*. 35:672-7, 1999.

[229]Sersa G., T. Jarm, T. Kotnik, A. Coer, M. Podkrajsek, M. Sentjurc, D. Miklavcic, M. Kadivec, S. Kranjc, A. Secerov, and M. Cemazar. Vascular disrupting action of electroporation and electrochemotherapy with bleomycin in murine sarcoma. *Br J Cancer*. 98:388-98, 2008.

[230]Shi J., X. Wu, M. Surma, S. Vemula, L. Zhang, Y. Yang, R. Kapur, and L. Wei. Distinct roles for ROCK1 and ROCK2 in the regulation of cell detachment. *Cell Death Dis*. 4:e483, 2013.

[231]Shin S., D. M. Salvay, and L. D. Shea. Lentivirus delivery by adsorption to tissue engineering scaffolds. *Journal of biomedical materials research. Part A*. 2009.

[232]Shirahata Y., N. Ohkohchi, H. Itagak, and S. Satomi. New technique for gene transfection using laser irradiation. *J Investig Med*. 49:184-90, 2001.

[233]Smith R. L., J. Lin, M. C. Trindade, J. Shida, G. Kajiyama, T. Vu, A. R. Hoffman, M. C. van der Meulen, S. B. Goodman, D. J. Schurman, and D. R. Carter. Time-dependent effects of intermittent hydrostatic pressure on articular chondrocyte type II collagen and aggrecan mRNA expression. *J Rehabil Res Dev*. 37:153-61, 2000.

[234]Sohn R. L., M. T. Murray, K. Schwarz, J. Nyitray, P. Purray, A. P. Franko, K. C. Palmer, L. N. Diebel, and S. A. Dulchavsky. In-vivo particle mediated delivery of mRNA to mammalian tissues: ballistic and biologic effects. *Wound Repair Regen*. 9:287-96, 2001.

[235]Song J. Y., H. S. Han, K. Sabapathy, B. M. Lee, E. Yu, and J. Choi. Expression of a homeostatic regulator, Wip1 (wild-type p53-induced phosphatase), is temporally induced by c-Jun and p53 in response to UV irradiation. *J Biol Chem*. 285:9067-76, 2010.

[236]Song L., L. Chau, Y. Sakamoto, J. Nakashima, M. Koide, and R. S. Tuan. Electric field-induced molecular vibration for noninvasive, high-efficiency DNA transfection. *Mol Ther*. 9:607-16, 2004.

[237]Storrie H. and D. J. Mooney. Sustained delivery of plasmid DNA from polymeric scaffolds for tissue engineering. *Adv Drug Deliv Rev*. 58:500-14, 2006.

[238]Tao W., J. Wilkinson, E. J. Stanbridge, and M. W. Berns. Direct gene transfer into human cultured cells facilitated by laser micropuncture of the cell membrane. *Proc Natl Acad Sci U S A*. 84:4180-4, 1987.

[239]Tatsumi K., Y. S. Sou, N. Tada, E. Nakamura, S. Iemura, T. Natsume, S. H. Kang, C. H. Chung, M. Kasahara, E. Kominami, M. Yamamoto, K. Tanaka, and M. Komatsu. A novel type of E3 ligase for the Ufm1 conjugation system. *J Biol Chem*. 285:5417-27, 2010.

[240]Teifel M., L. T. Heine, S. Milbredt, and P. Friedl. Optimization of transfection of human endothelial cells. *Endothelium*. 5:21-35, 1997.

[241]Teissie J., M. Golzio, and M. P. Rols. Mechanisms of cell membrane electropermeabilization: a minireview of our present (lack of ?) knowledge. *Biochim Biophys Acta*. 1724:270-80, 2005.

[242]Tell G., M. Di Piazza, M. M. Kamocka, and C. Vascotto. Combining RNAi and in vivo confocal microscopy analysis of the photoconvertible fluorescent protein Dendra2 to study a DNA repair protein. *Biotechniques*. 55:198-203, 2013.

[243]ter Haar G. Therapeutic applications of ultrasound. *Prog Biophys Mol Biol*. 93:111-29, 2007.

[244]Thomas C. E., A. Ehrhardt, and M. A. Kay. Progress and problems with the use of viral vectors for gene therapy. *Nat Rev Genet*. 4:346-58, 2003.

[245]Udvardi A., I. Kufferath, H. Grutsch, K. Zatloukal, and B. Volc-Platzer. Uptake of exogenous DNA via the skin. *J Mol Med (Berl)*. 77:744-50, 1999.

[246]van der Aa M. A., U. S. Huth, S. Y. Hafele, R. Schubert, R. S. Oosting, E. Mastrobattista, W. E. Hennink, R. Peschka-Suss, G. A. Koning, and D. J. Crommelin. Cellular uptake of cationic polymer-DNA complexes via caveolae plays a pivotal role in gene transfection in COS-7 cells. *Pharm Res*. 24:1590-8, 2007.

[247]Vaughan E. E. and D. A. Dean. Intracellular trafficking of plasmids during transfection is mediated by microtubules. *Mol Ther*. 13:422-8, 2006.

[248]Vytla D., R. E. Combs-Bachmann, A. M. Hussey, I. Hafez, and J. J. Chambers. Silent, fluorescent labeling of native neuronal receptors. *Org Biomol Chem*. 9:7151-61, 2011.

[249]Waehler R., S. J. Russell, and D. T. Curiel. Engineering targeted viral vectors for gene therapy. *Nat Rev Genet*. 8:573-87, 2007.

[250]Walton J. R., J. D. Murray, J. T. Marshall, and C. D. Nancarrow. Zygote viability in gene transfer experiments. *Biol Reprod*. 37:957-67, 1987.

[251]Wang L., L. Ott, K. Seshareddy, M. Weiss, and M. Detamore. Musculoskeletal tissue engineering with human umbilical cord mesenchymal stromal cells. *Regenerative medicine*. 6:95-109, 2011.

[252]Wang L., L. Ott, K. Seshareddy, M. L. Weiss, and M. S. Detamore. Musculoskeletal tissue engineering with human umbilical cord mesenchymal stromal cells. *Regen Med*. 6:95-109, 2011.

[253]Wang L., I. Tran, K. Seshareddy, M. L. Weiss, and M. S. Detamore. A comparison of human bone marrow-derived mesenchymal stem cells and human umbilical cord-derived mesenchymal stromal cells for cartilage tissue engineering. *Tissue Eng Part A*. 15:2259-66, 2009.

[254]Wang V. Y., B. A. Hassan, H. J. Bellen, and H. Y. Zoghbi. Drosophila atonal fully rescues the phenotype of Math1 null mice: new functions evolve in new cellular contexts. *Curr Biol*. 12:1611-6, 2002.

[255]Watanabe K., M. Ueno, D. Kamiya, A. Nishiyama, M. Matsumura, T. Wataya, J. B. Takahashi, S. Nishikawa, S. Nishikawa, K. Muguruma, and Y. Sasai. A ROCK inhibitor permits survival of dissociated human embryonic stem cells. *Nat Biotechnol*. 25:681-6, 2007.

[256]Weaver J. C. Electroporation: a general phenomenon for manipulating cells and tissues. *J Cell Biochem*. 51:426-35, 1993.

[257]Weaver J. C. and Y. A. Chizmadzhev. Theory of electroporation: a review. *Bioelectrochemistry and Bioenergetics*. 41:135-160, 1996.

[258]Wells J. M., L. H. Li, A. Sen, G. P. Jahreis, and S. W. Hui. Electroporation-enhanced gene delivery in mammary tumors. *Gene Ther*. 7:541-7, 2000.

[259]Wiethoff C. M. and C. R. Middaugh. Barriers to nonviral gene delivery. *J Pharm Sci*. 92:203-17, 2003.

[260]Williams S. K. and R. C. Wagner. Regulation of micropinocytosis in capillary endothelium by multivalent cations. *Microvasc Res*. 21:175-82, 1981.

[261]Wolf H., B. G. Barisas, K. J. Dietz, and T. Seidel. Kaede for detection of protein oligomerization. *Mol Plant*. 6:1453-62, 2013.

[262]Woods C., M. Montcouquiol, and M. W. Kelley. Math1 regulates development of the sensory epithelium in the mammalian cochlea. *Nat Neurosci*. 7:1310-8, 2004.

[263]Wu J. Shear stress in cells generated by ultrasound. *Prog Biophys Mol Biol*. 93:363-73, 2007.

[264]Wu M. and F. Yuan. Membrane binding of plasmid DNA and endocytic pathways are involved in electrotransfection of mammalian cells. *PloS one*. 6:e20923, 2011.

[265]Wu S., K. Koizumi, A. Macrae-Crerar, and K. L. Gallagher. Assessing the utility of photoswitchable fluorescent proteins for tracking intercellular protein movement in the Arabidopsis root. *PloS one*. 6:e27536, 2011.

[266]Xie T. D. and T. Y. Tsong. Study of mechanisms of electric field-induced DNA transfection. V. Effects of DNA topology on surface binding, cell uptake, expression, and integration into host chromosomes of DNA in the mammalian cell. *Biophys J*. 65:1684-9, 1993.

[267]Xu B., G. Song, Y. Ju, X. Li, Y. Song, and S. Watanabe. RhoA/ROCK, cytoskeletal dynamics, and focal adhesion kinase are required for mechanical stretch-induced tenogenic differentiation of human mesenchymal stem cells. *Journal of cellular physiology*. 227:2722-2729, 2012.

[268]Xu Y. and F. C. Szoka, Jr. Mechanism of DNA release from cationic liposome/DNA complexes used in cell transfection. *Biochemistry*. 35:5616-23, 1996.

[269]Yamamoto F., M. Furusawa, I. Furusawa, and M. Obinata. The 'pricking' method. A new efficient technique for mechanically introducing foreign DNA into the nuclei of culture cells. *Exp Cell Res*. 142:79-84, 1982.

[270]Yang C., K. Cheng, and W. Weng. Immobilization of RGD peptide on HA coating through a chemical bonding approach. *J Mater Sci Mater Med*. 2009.

[271]Yang J., N. Cong, Z. Han, Y. Huang, and F. Chi. Ectopic hair cell-like cell induction by Math1 mainly involves direct transdifferentiation in neonatal mammalian cochlea. *Neurosci Lett*. 549:7-11, 2013.

[272]Yang N. S., J. Burkholder, B. Roberts, B. Martinell, and D. McCabe. In vivo and in vitro gene transfer to mammalian somatic cells by particle bombardment. *Proc Natl Acad Sci U S A*. 87:9568-72, 1990.

[273]Yang S. Y., J. S. Sun, C. H. Liu, Y. H. Tsuang, L. T. Chen, C. Y. Hong, H. C. Yang, and H. E. Horng. Ex vivo magnetofection with magnetic nanoparticles: a novel platform for nonviral tissue engineering. *Artif Organs*. 32:195-204, 2008.

[274]Yao C. P., Z. X. Zhang, R. Rahmanzadeh, and G. Huettmann. Laser-based gene transfection and gene therapy. *IEEE Trans Nanobioscience*. 7:111-9, 2008.

[275]Yockell-Lelievre J., V. Riendeau, S. N. Gagnon, C. Garenc, and M. Audette. Efficient transfection of endothelial cells by a double-pulse electroporation method. *DNA Cell Biol*. 28:561-6, 2009.

[276]Yoon C. S. and J. H. Park. Ultrasound-mediated gene delivery. *Expert Opin Drug Deliv*. 7:321-30, 2010.

[277]Yoon H., D. J. Lee, M. H. Kim, and J. Bok. Identification of genes concordantly expressed with Atoh1 during inner ear development. *Anat Cell Biol*. 44:69-78, 2011.

[278]Zaharoff D. A., J. W. Henshaw, B. Mossop, and F. Yuan. Mechanistic analysis of electroporation-induced cellular uptake of macromolecules. *Exp Biol Med (Maywood)*. 233:94-105, 2008.

[279]Zefirov A. L., M. M. Abdrakhmanov, M. A. Mukhamedyarov, and P. N. Grigoryev. The role of extracellular calcium in exo- and endocytosis of synaptic vesicles at the frog motor nerve terminals. *Neuroscience*. 143:905-10, 2006.

[280]Zeira E., A. Manevitch, A. Khatchatouriants, O. Pappo, E. Hyam, M. Darash-Yahana, E. Tavor, A. Honigman, A. Lewis, and E. Galun. Femtosecond infrared laser-an efficient

and safe in vivo gene delivery system for prolonged expression. *Mol Ther*. 8:342-50, 2003.

[281]Zelenin A. V., V. A. Kolesnikov, O. A. Tarasenko, R. A. Shafei, I. A. Zelenina, V. V. Mikhailov, M. L. Semenova, D. V. Kovalenko, O. V. Artemyeva, T. E. Ivaschenko, O. V. Evgrafov, G. Dickson, and V. S. Baranovand. Bacterial beta-galactosidase and human dystrophin genes are expressed in mouse skeletal muscle fibers after ballistic transfection. *FEBS Lett*. 414:319-22, 1997.

[282]Zelphati O. and F. C. Szoka, Jr. Mechanism of oligonucleotide release from cationic liposomes. *Proc Natl Acad Sci U S A*. 93:11493-8, 1996.

[283]Zhang K., H. Zhang, H. Xiang, J. Liu, Y. Liu, X. Zhang, J. Wang, and Y. Tang. TGF-β1 induces the dissolution of tight junctions in human renal proximal tubular cells: Role of the RhoA/ROCK signaling pathway. *International journal of molecular medicine*. 2013.

[284]Zhang L., J. M. Valdez, B. Zhang, L. Wei, J. Chang, and L. Xin. ROCK inhibitor Y-27632 suppresses dissociation-induced apoptosis of murine prostate stem/progenitor cells and increases their cloning efficiency. *PloS one*. 6:e18271, 2011.

[285]Zhang X. and W. T. Godbey. Viral vectors for gene delivery in tissue engineering. *Adv Drug Deliv Rev*. 58:515-34, 2006.

[286]Zhou Y., J. Shi, J. Cui, and C. X. Deng. Effects of extracellular calcium on cell membrane resealing in sonoporation. *J Control Release*. 126:34-43, 2008.

[287]Zimmermann U. Electric field-mediated fusion and related electrical phenomena. *Biochim Biophys Acta*. 694:227-77, 1982.

APPENDIX A: Figures

CHAPTER 1: No figures
CHAPTER 2: Figures 2.1 - 2.6
CHAPTER 3: Figures 3.1 - 3.4
CHAPTER 4: Figures 4.1 - 4.8
CHAPTER 5: Figures 5.1 - 5.9
CHAPTER 6: Figure 6.1

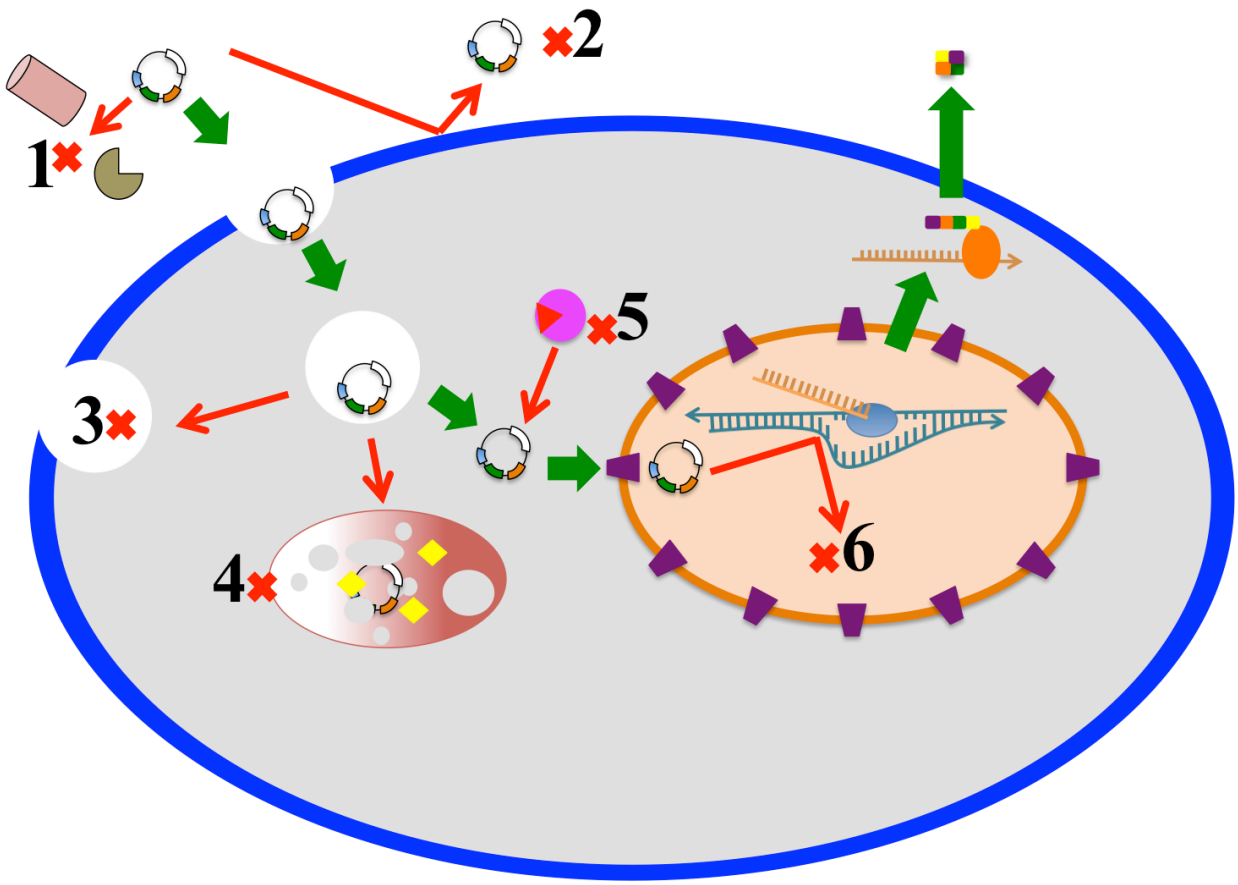

Figure 2.1: Gene delivery barriers.

DNA must overcome several barriers during the delivery process to successfully produce desired gene expression. The green arrows are the pathway DNA must follow to induce gene expression, while the red arrows indicate potential barriers and threats that prevent gene expression. 1) DNA must avoid extracellular nucleases and 2) DNA must associate with the cellular membrane in some form to gain access to the cell via penetration, electrostatic interactions, adsorption, or ligand mediated receptor binding. DNA that enters through endocytosis must escape the endosome before the endosome 3) is recycled back to the cell membrane or 4) the endosome and DNA are degraded in a lysosome. In the cytoplasmic compartment, DNA must traffic toward the nuclear envelope and 5) avoid degradation by intracellular nucleases. Finally, to produce gene expression, 6) DNA must cross the nuclear envelope by transport through a nuclear pore (non-dividing cells) or passively re-locate into the nucleus between the disassembly and reformation of the nuclear envelope during mitosis (dividing cells). Gene expression is produced when enough intact DNA is transcribed in the nucleus into mRNA, and then translated into an amino acid in the cytoplasm.

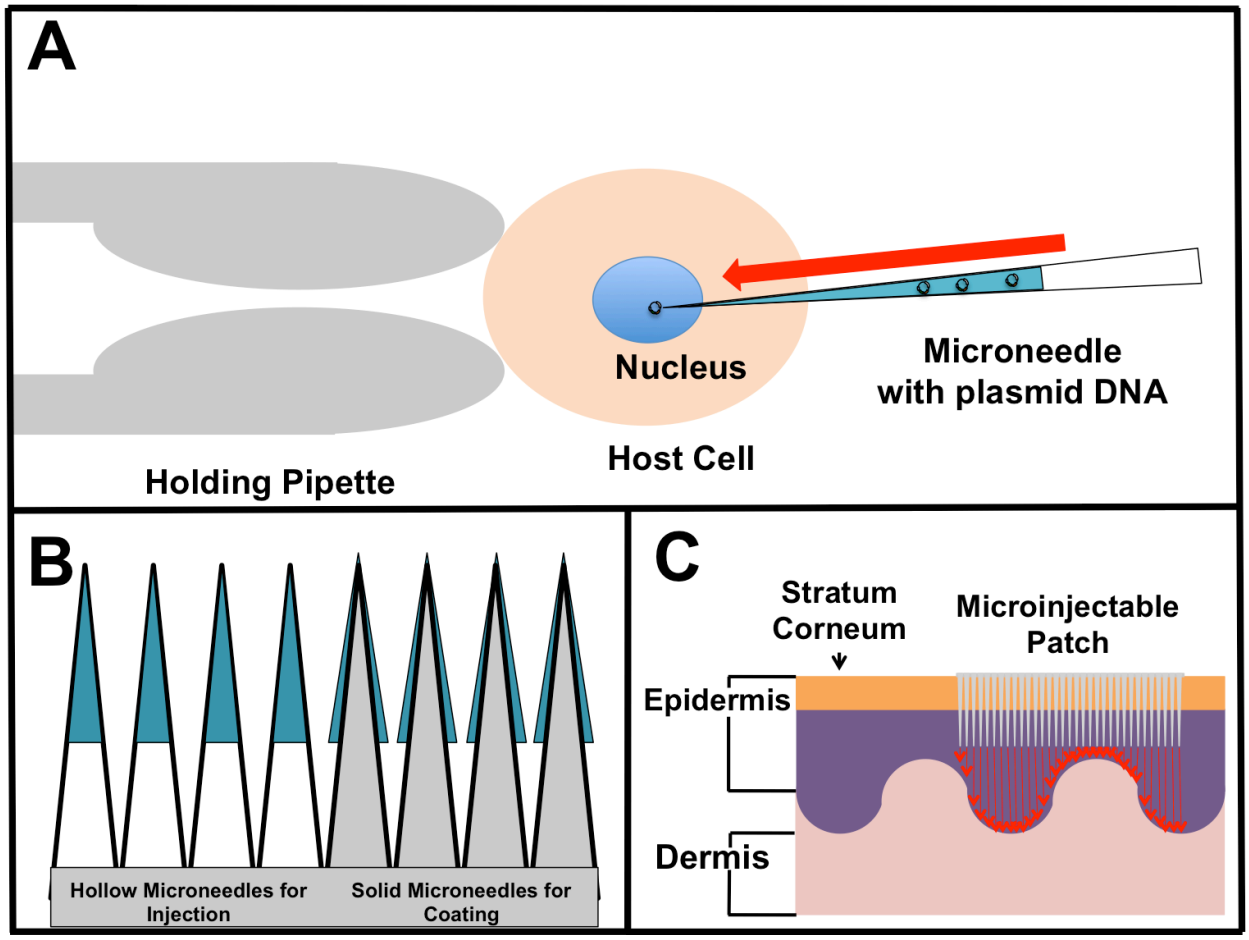

Figure 2.2: Microinjection.

Microinjection strategies utilize microneedles to deliver DNA directly to cell nuclei. A) In traditional microinjection, an individual cell is held in place by the tip of a pipette while a technician uses a microscope to pierce the cell membrane and nuclear envelope with a microneedle to deliver genetic material to the cell nucleus. B) Microneedles can be fabricated so that the shaft is hollow and able to carry a suspension of genetic material for injection, or microneedles can be fabricated so that the shaft is solid and the tip is dipped in a suspension of genetic material for application to tissues via coating or scratching. C) Microneedles can be arranged in arrays on patches that can be applied directly to the skin. The microneedle patches are capable of penetrating the stratum corneum and delivering drugs or genetic material to the epidermal tissues.

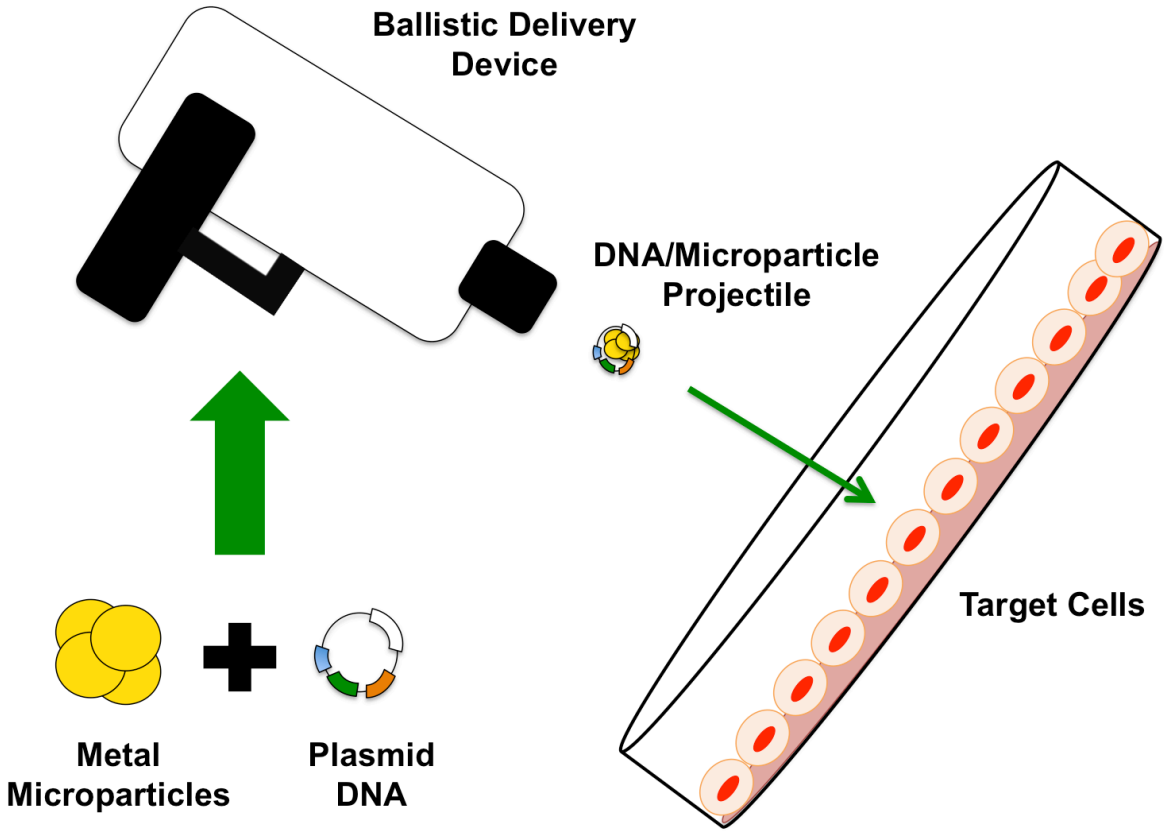

Figure 2.3: Ballistic gene delivery.

Plasmid DNA is mixed with gold or tungsten particles ranging in size from nanometers to micrometers. An electric or plasma discharge is used to propel the DNA/particle complexes into tissues or cell cultures.

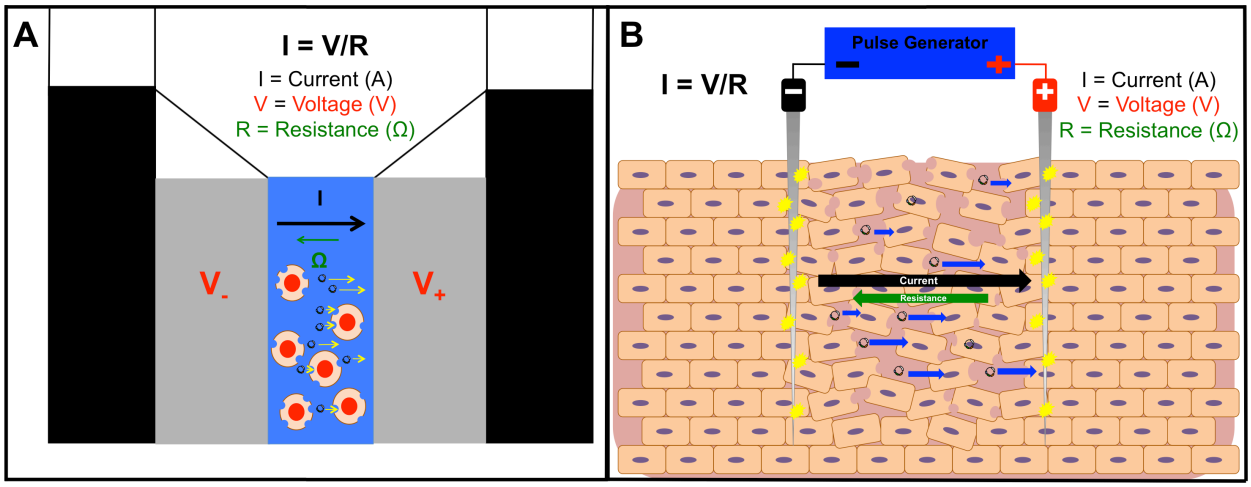

Figure 2.4: Electroporation.

Electroporation strategies apply a current across cells or tissues to make cell membranes more permeable to exogenous DNA. A) Traditional electroporators have a pulse generator and a pair of electrodes that can be applied directly to tissues or cells. A cuvette utilizes plate electrodes to apply a voltage potential across cells in suspension. Since resistance is constant, the current is proportional to the voltage potential. As voltage reaches a critical threshold, hydrophilic pores form in the cell membrane and make it permeable to plasmid DNA. The negatively charged DNA is mobile in the electrical field (toward the positive electrode) so DNA transport into permeabilized cells is greater than by diffusion alone. B) Needle electrodes have been used for *in vivo* applications where needles are inserted directly into primary tissues such as skin or skeletal muscle fibers after DNA has been injected. A current is applied across a very small area of tissue to facilitate the same process as in a cuvette.

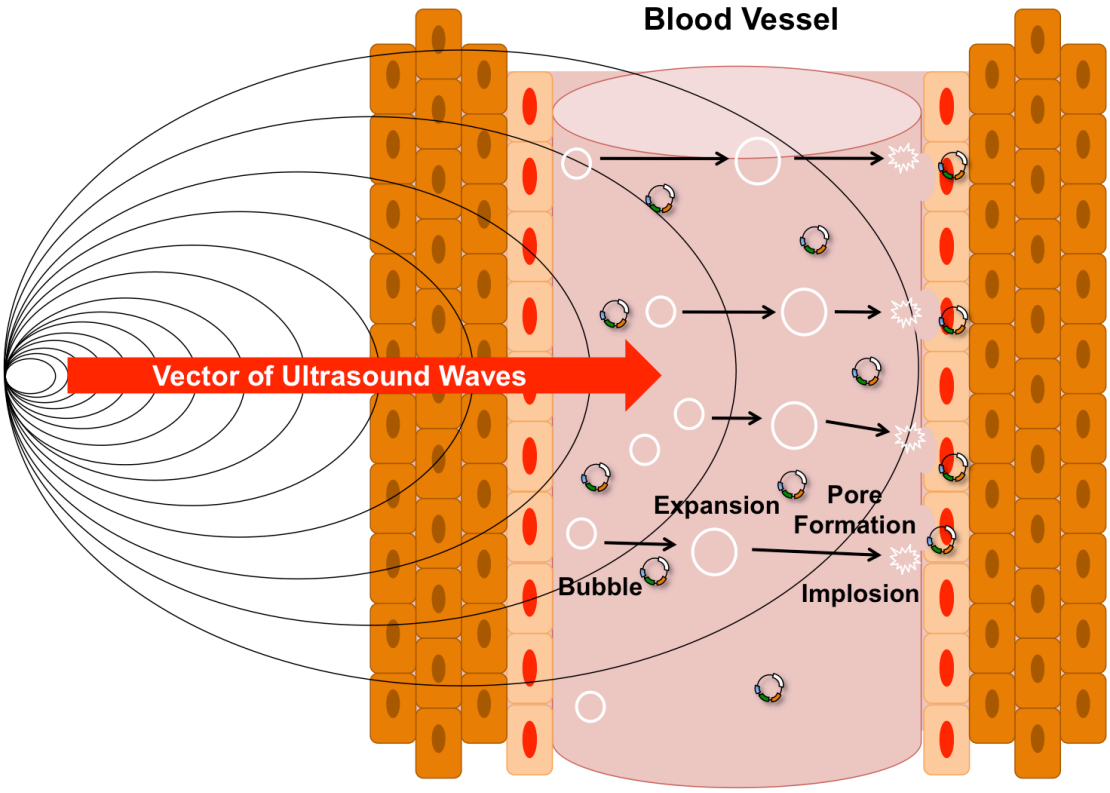

Figure 2.5: Sonoporation.

Ultrasonic frequencies are used to induce the cavitation of microbubbles for creating pores in cells contained in culture or tissue. The acoustic waves cause microbubbles to expand and then collapse. When the microbubbles collapse, a microshockwave is emitted that can rupture a cell membrane if the collapsing microbubble is in close proximity to the cell membrane. The ruptured cell membrane forms a pore, which allows cells to be temporarily more permeable to plasmid DNA.

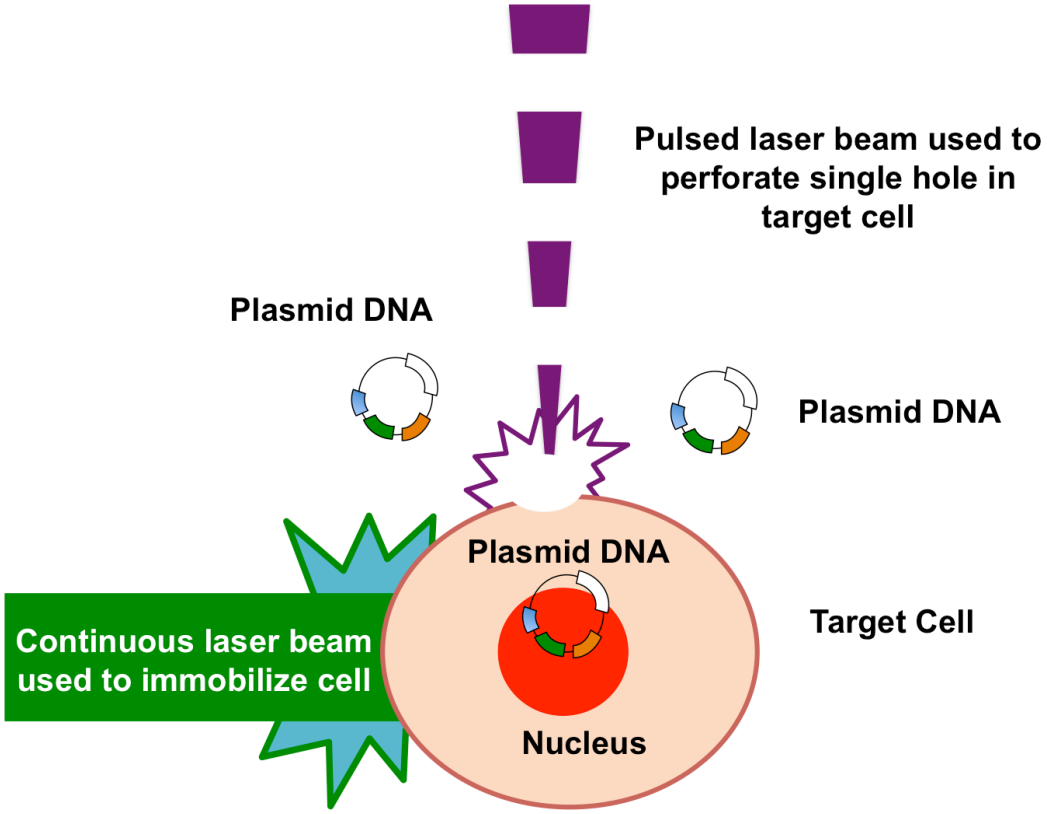

Figure 2.6: Laser induced pore formation.

Pulsed lasers have been shown to perforate cell membranes similar to microinjection strategies, but without the use of a needle. Investigators have shown a variety of laser beams of varying wavelengths are capable of making precise "holes" in cell membranes when beam energy, pulse frequency, and exposure duration are manipulated. Investigators can precisely target individual cells in culture or in tissue with aid of a microscope to target specific sites on cells for perforation to allow DNA to enter cells. A second laser with an uninterrupted beam can be used to immobilize individual cells in suspension while a pulsed laser is used to perforate cells.

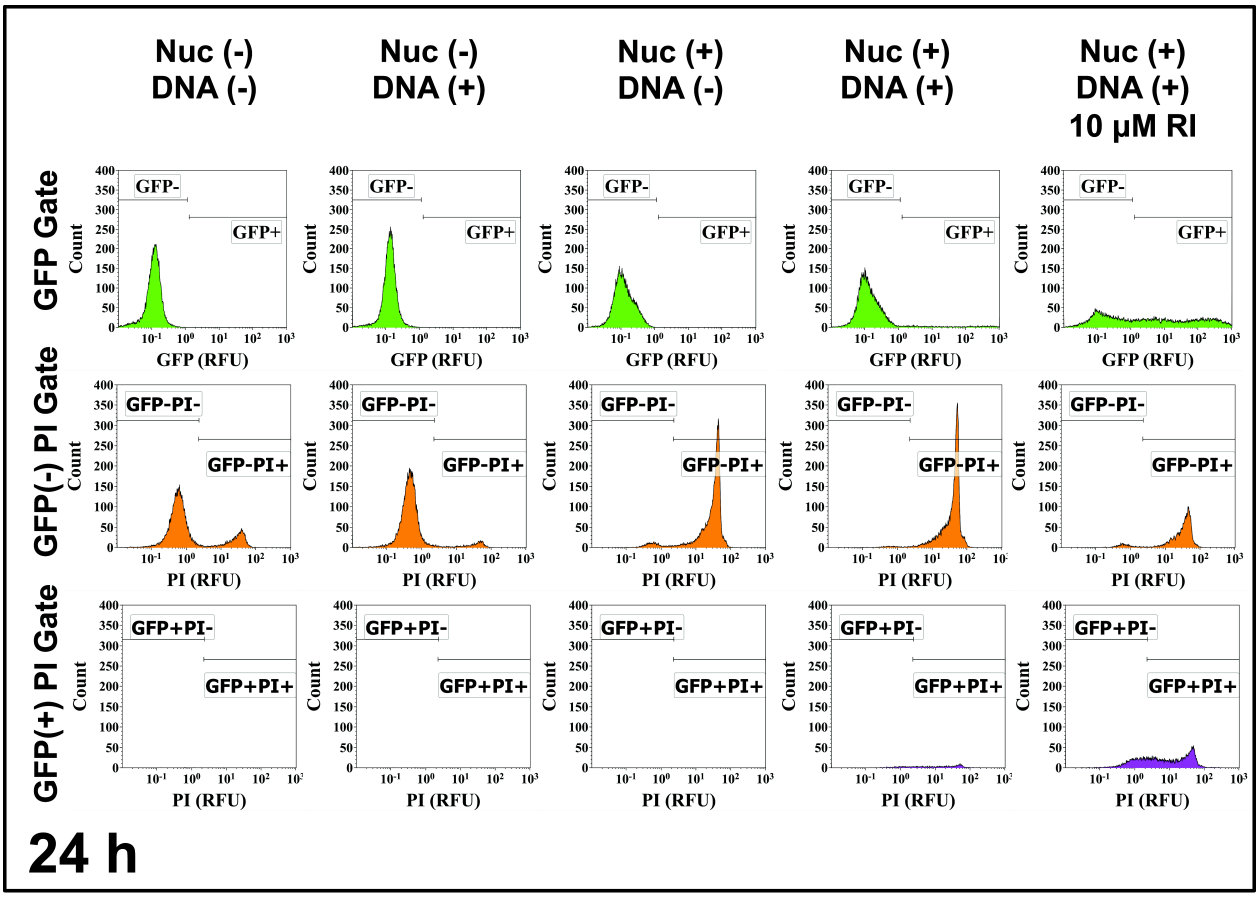

Figure 3.1: Flow cytometry gating parameters.

Flow cytometry gating parameters used to quantify cell numbers. The set of histograms displayed are an arbitrary selection of a single replicate for each treatment from one umbilical cord out of five tested. Nuc (+/-) (Nucleofection™) designates whether cells were Nucleofected™ or not. DNA (+/-) designates whether cells received 5 µg of pmaxGFP or not. RFU, Relative Fluorescent Units. RI, ROCK Inhibitor.

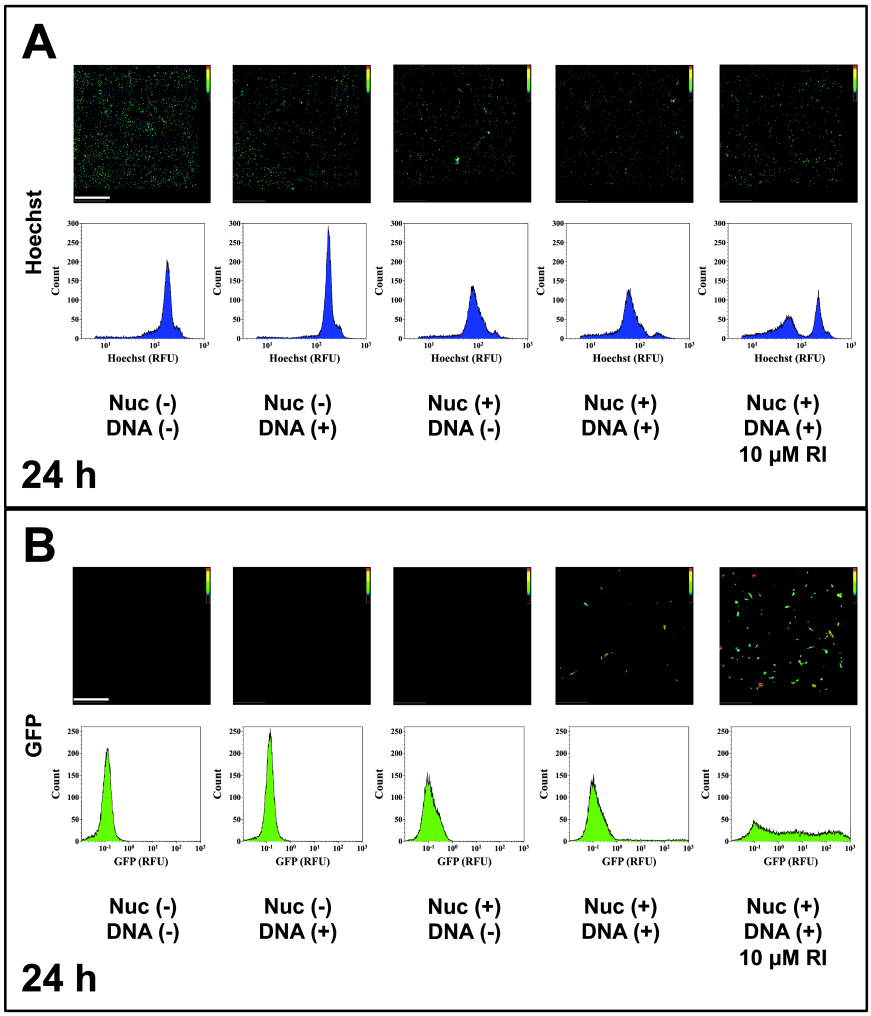

Figure 3.2: Cell density and GFP expression 24 h post-transfection.

A) Intensity maps of cell density with corresponding flow cytometry histograms of Hoechst signal distribution 24 h after transfection. B) Intensity maps of GFP expression with corresponding flow cytometry histograms of GFP expression 24 h after transfection. The set of images and corresponding histograms are an arbitrary selection from one cord out of five tested. Nuc (+/-) (Nucleofection™) designates whether cells were Nucleofected™ or not. DNA (+/-) designates whether cells received 5 µg of pmaxGFP or not. Scale bar, 500 µm. RFU, Relative Fluorescent Units. GFP, Green Fluorescent Protein. RI, ROCK Inhibitor.

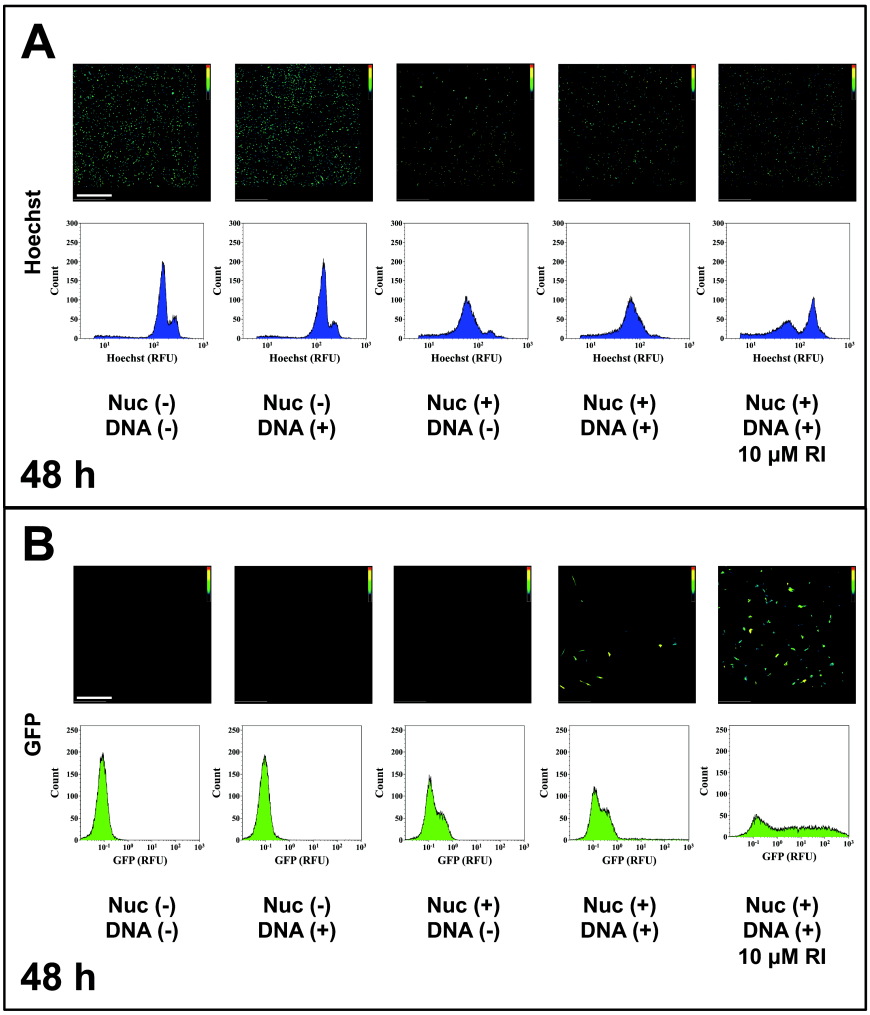

Figure 3.3: Cell density and GFP expression 48 h post-transfection.

A) Intensity maps of cell density with corresponding flow cytometry histograms of Hoechst signal distribution 48 h after transfection. B) Intensity maps of GFP expression with corresponding flow cytometry histograms of GFP expression 48 h after transfection. The set of images and corresponding histograms are an arbitrary selection from one cord out of five tested. Nuc (+/-) (Nucleofection™) designates whether cells were Nucleofected™ or not. DNA (+/-) designates whether cells received 5 µg of pmaxGFP or not. Scale bar, 500 µm. RFU, Relative Fluorescent Units. GFP, Green Fluorescent Protein. RI, ROCK Inhibitor.

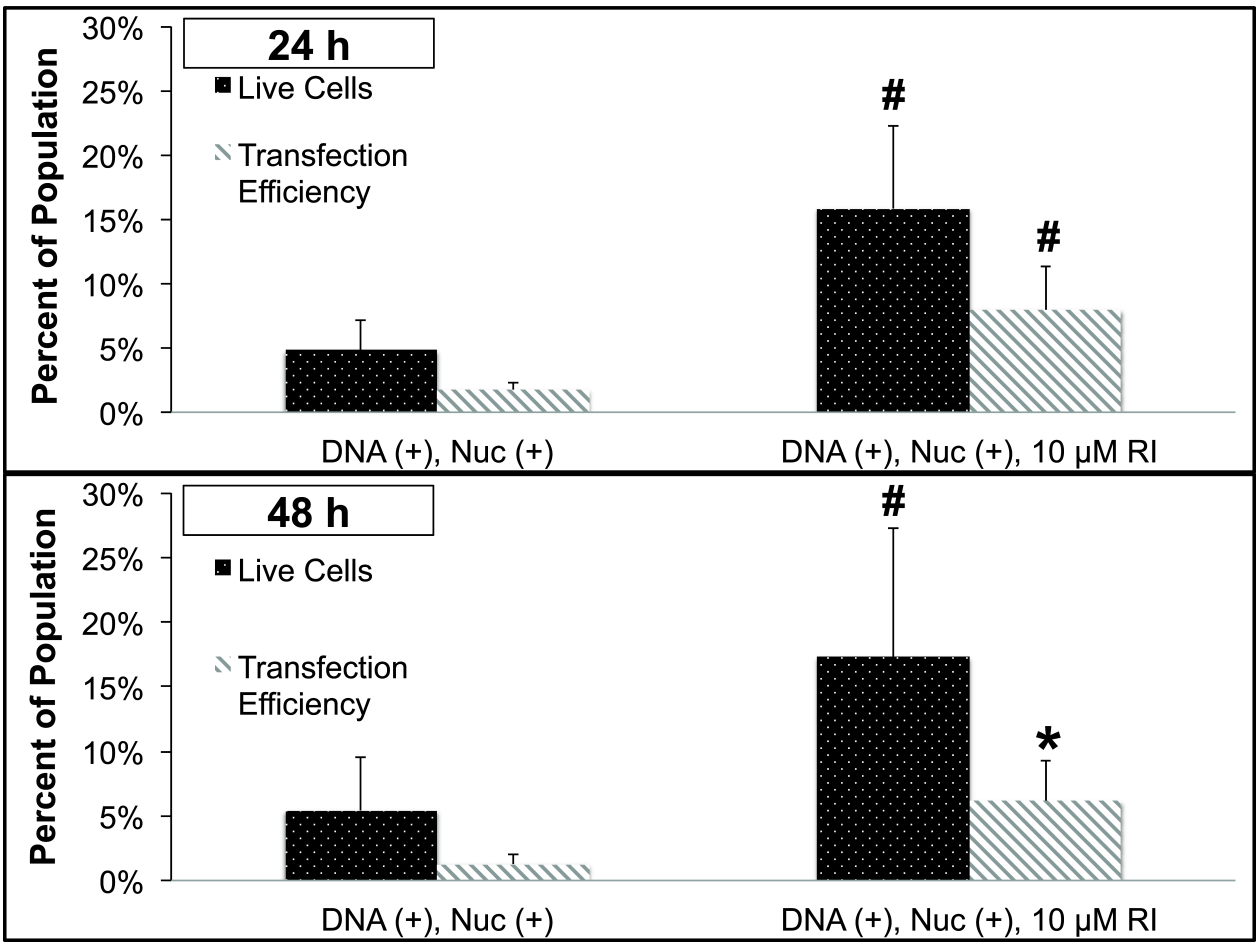

Figure 3.4: Cell viability and transfection efficiency.

Live/Dead and transfection efficiency collected via flow cytometry 24 h and 48 h after transfection. Groups that did not express GFP were not plotted in the bar chart. * = statistically significant difference ($p < 0.05$) from hWJCs that underwent Nucleofection™ without RI supplement. . # = statistically significant difference ($p \leq 0.01$) from hWJCs that underwent Nucleofection™ without RI supplement. The results are representative of cells collected from five different umbilical cords ($n = 5$), and are reported as statistical means. All experiments were repeated three times. Error bars represent standard deviations. Nuc (+/-) (Nucleofection™) designates whether cells were Nucleofected™ or not. DNA (+/-) designates whether cells received 5 µg of pmaxGFP or not. RI, ROCK Inhibitor.

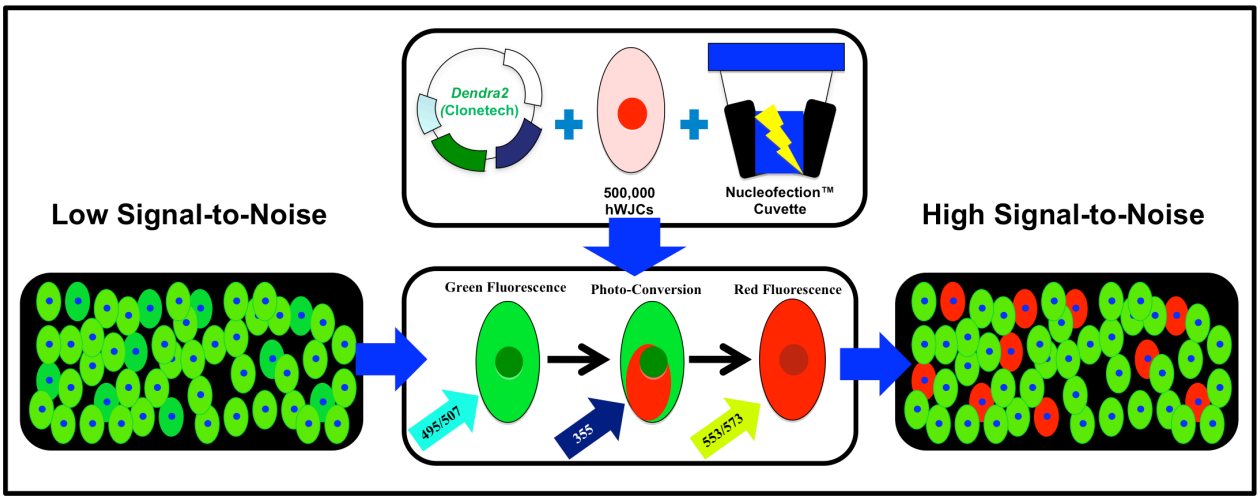

Figure 4.1: Schematic diagram of hWJC transfection and photo-conversion.

Photo-convertible reporter genes such as *Dendra2* enable cells that express extremely low levels of a reporter gene to be identified against background fluorescence by photo-converting green fluorescence to red fluorescence so that there is a very high signal-to-noise ratio. hWJCs were transfected via the electroporative method, Nucleofection™, with *pDendra2*. Cells were transfected at a density of $5x10^5$ cells per cuvette. After transfection, cells were imaged for green fluorescence, then converted to red fluorescence by exposure to UV light, and imaged for red fluorescence.

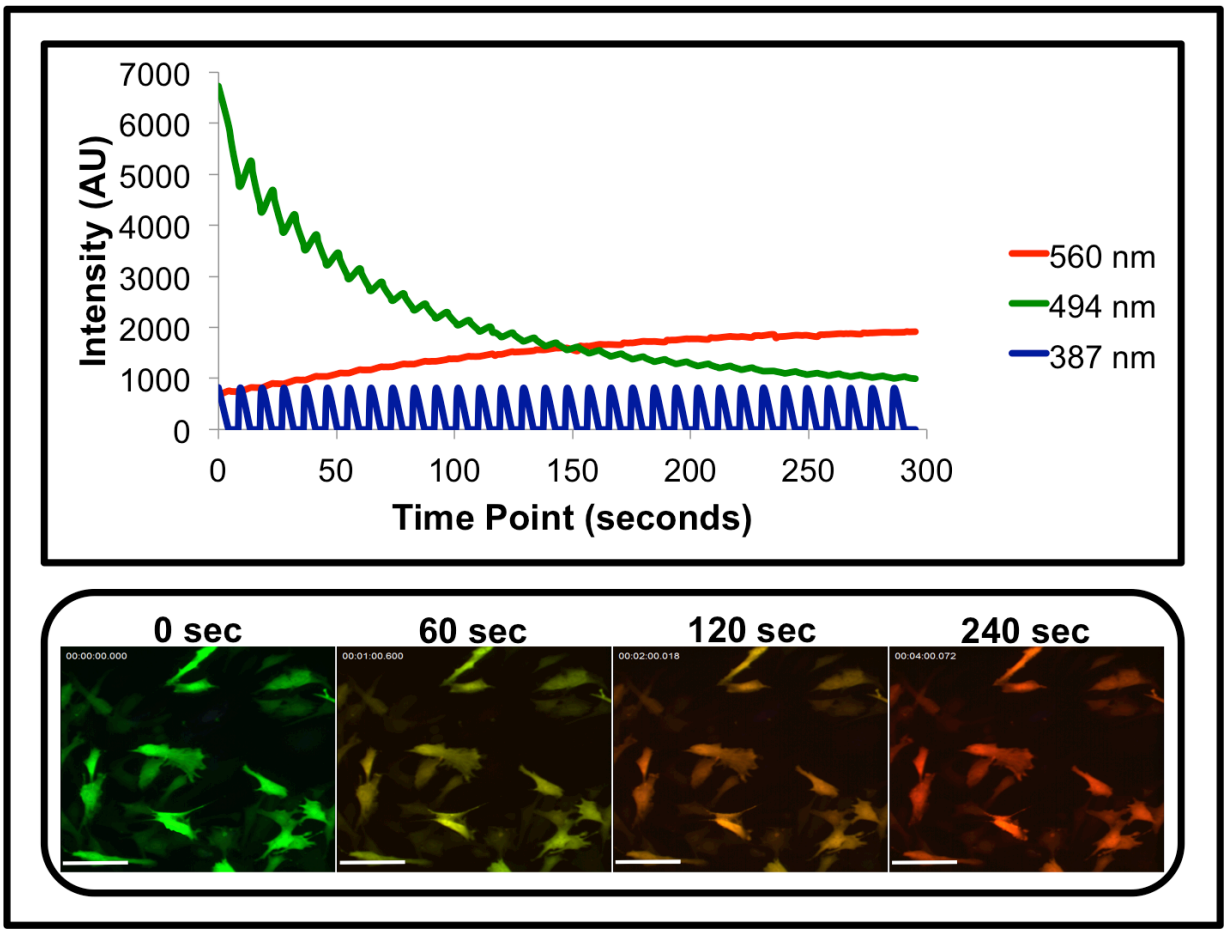

Figure 4. 2: Full photo-conversion of hWJCs.

Photo-conversion of hWJCs from green fluorescence to red fluorescence was very robust. hWJCs were gently exposed to UV light at 100 mW every 10 s at a frequency of 1 Hz for 300 s. Green fluorescence intensity and red fluorescence intensity were measured in real-time as hWJCs were photo-converted. There was a rapid decrease in green fluorescence intensity as red fluorescence intensity increased. The critical moment where red fluorescence eclipsed green fluorescence occurred at 125 ± 60 s. Please refer to Supplementary Figure 4.6 to view the full time-lapse video of a single recording of the photo-conversion that is representative of all attempts. The results displayed were fully consistent with nine attempts to photo-convert cells from three different umbilical cords. AU = Arbitrary Unit; Scale Bar = 100 μm.

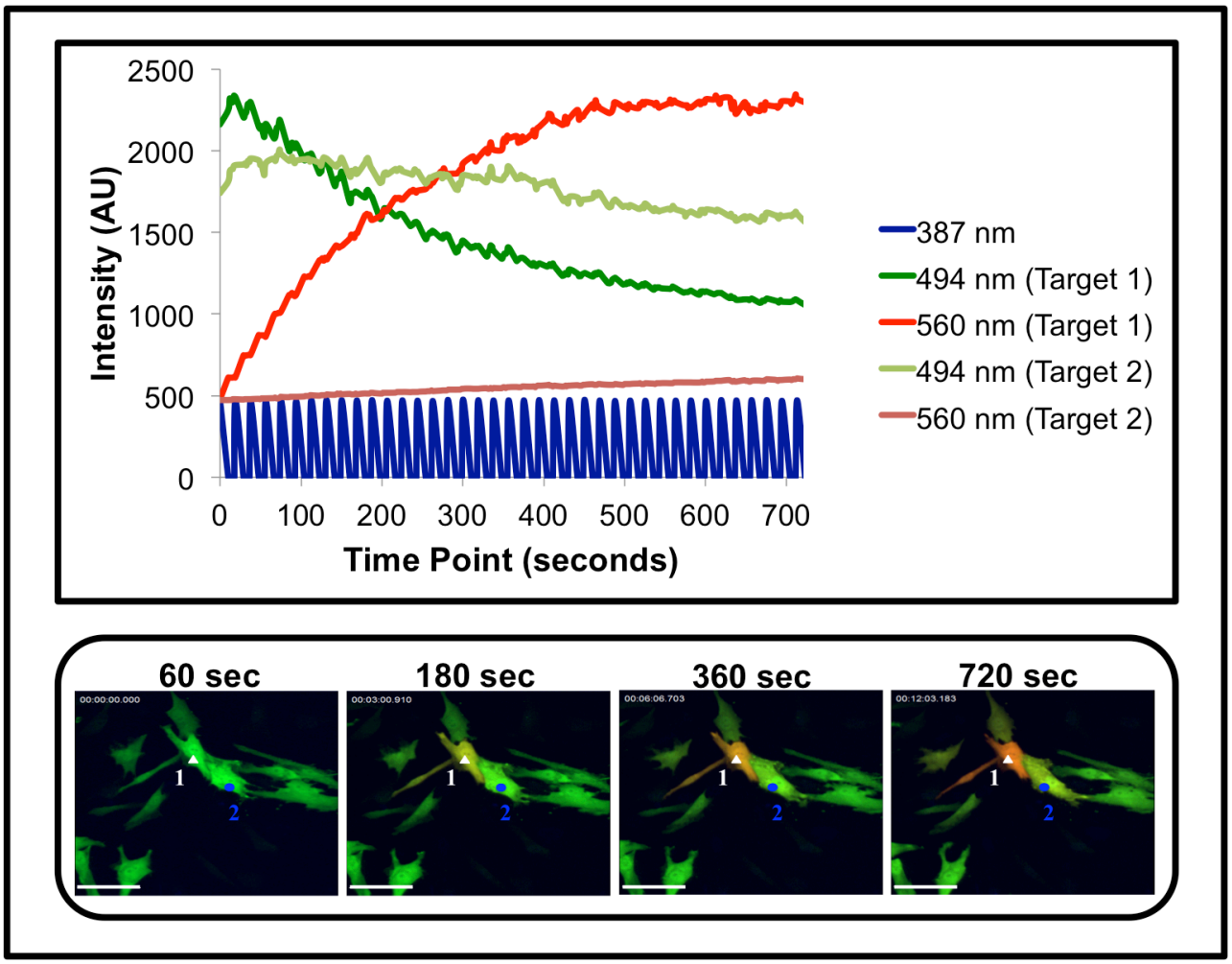

Figure 4.3: Isolated photo-conversion of a single hWJC.

The UV light beam was confined to a 15 – 20 μm diameter to restrict UV light exposure to a single hWJC. Changes in fluorescent intensity for both green and red fluorescence were measured in two adjacent cells over the course of 720 s. The cell designated "Target 1" is labeled with a white triangle and was exposed directly to the UV light beam, whereas the cell designated "Target 2" is labeled with a blue circle. Target 1 was exposed to UV light at 20 mW every 20 seconds at a frequency of 1 Hz. Over the course of 720 s, the green fluorescence rapidly decreased while the red fluorescence steadily increased in Target 1. Green fluorescence decreased slightly, and red fluorescence increased slightly in Target 2, but photo conversion did not occur demonstrating that it is possible to only photo-convert a single cell in a culture. Please refer to Supplementary Figure 4.7 to view the full time-lapse video a single recording representative of all attempts to demonstrate isolated photo-conversion. The results displayed were fully consistent with nine attempts to photo-convert individual cells from three different umbilical cords. AU = Arbitrary Unit; Scale Bar = 100 μm.

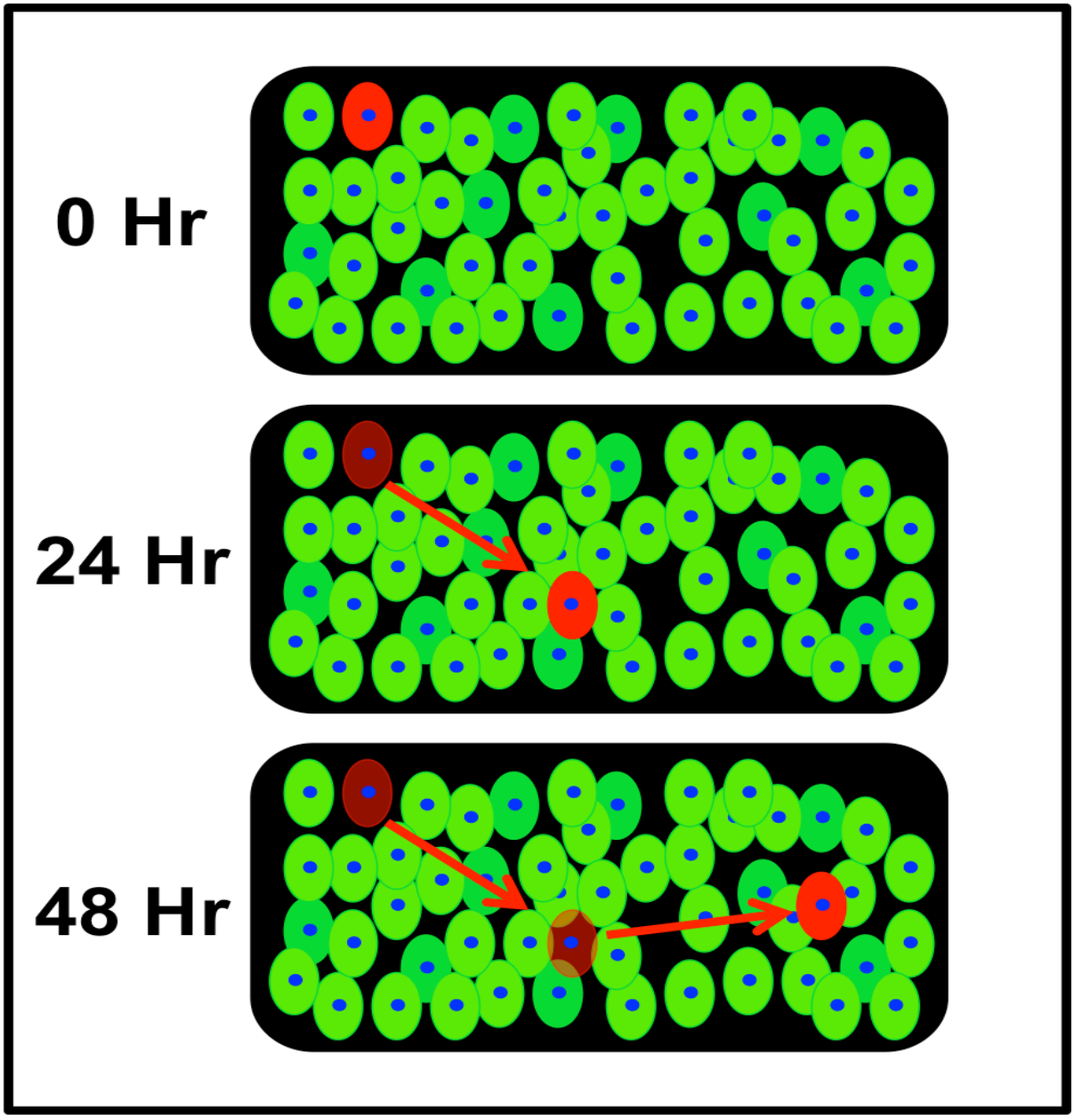

Figure 4.4: Schematic diagram of cell tracking in tissue culture.

The diagram illustrates how cell tracking could work in a tissue culture if a single transfected cell is photo-converted. The photo-converted cell would appear red against cells that are green, which would allow for precise tracking of cell movement and observation of morphological changes in tissue culture.

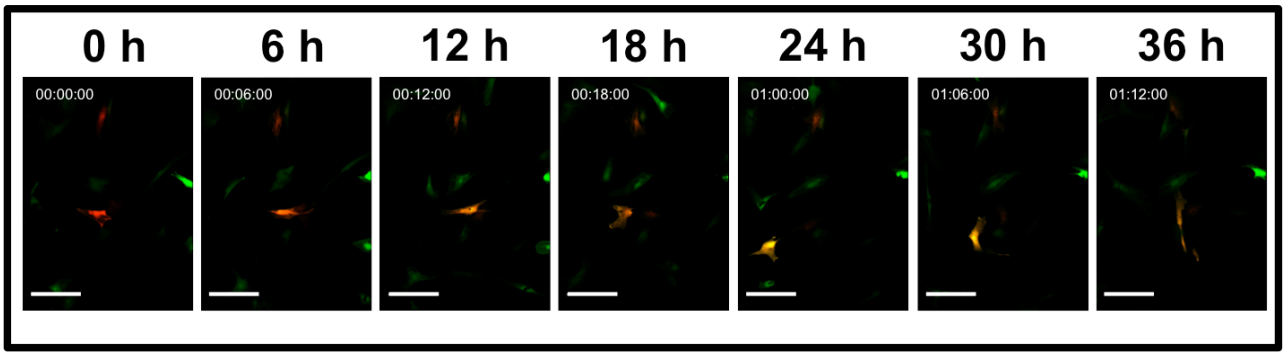

Figure 4.5: Cell tracking of a single photo-converted hWJCs over the course of 36 h.

One hWJC was photo-converted with UV light at an intensity of 100 mW for 10 s at a frequency of 1 Hz. The single cell was tracked for a total of 48 h. The panels show the movement and changes in the photo-converted cell every 6 h for 36 h. Please refer to Supplementary Figure 4.8 to view the full 48 h time-lapse video of the movement of the single photo-converted hWJC. The experiment was run twice, showing the same results both times. Scale Bar = 100 μm.

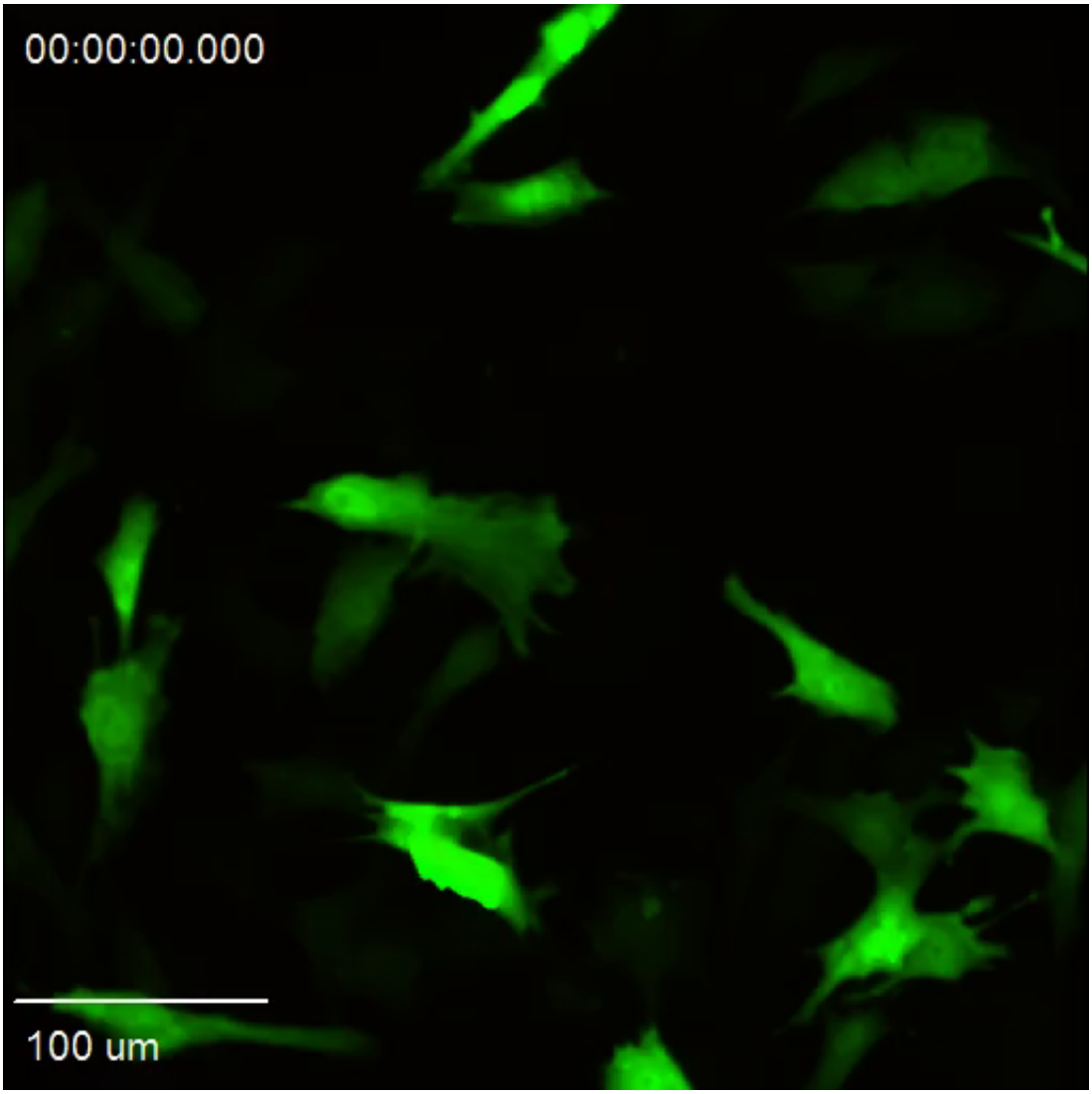

Supplemental Figure 4.6: Time-lapse video of full photo-conversion of hWJCs.

All hWJCs converted from green to red fluorescence with gentle exposure to UV light. Duration = 00:58. Scale Bar = 100 μm.

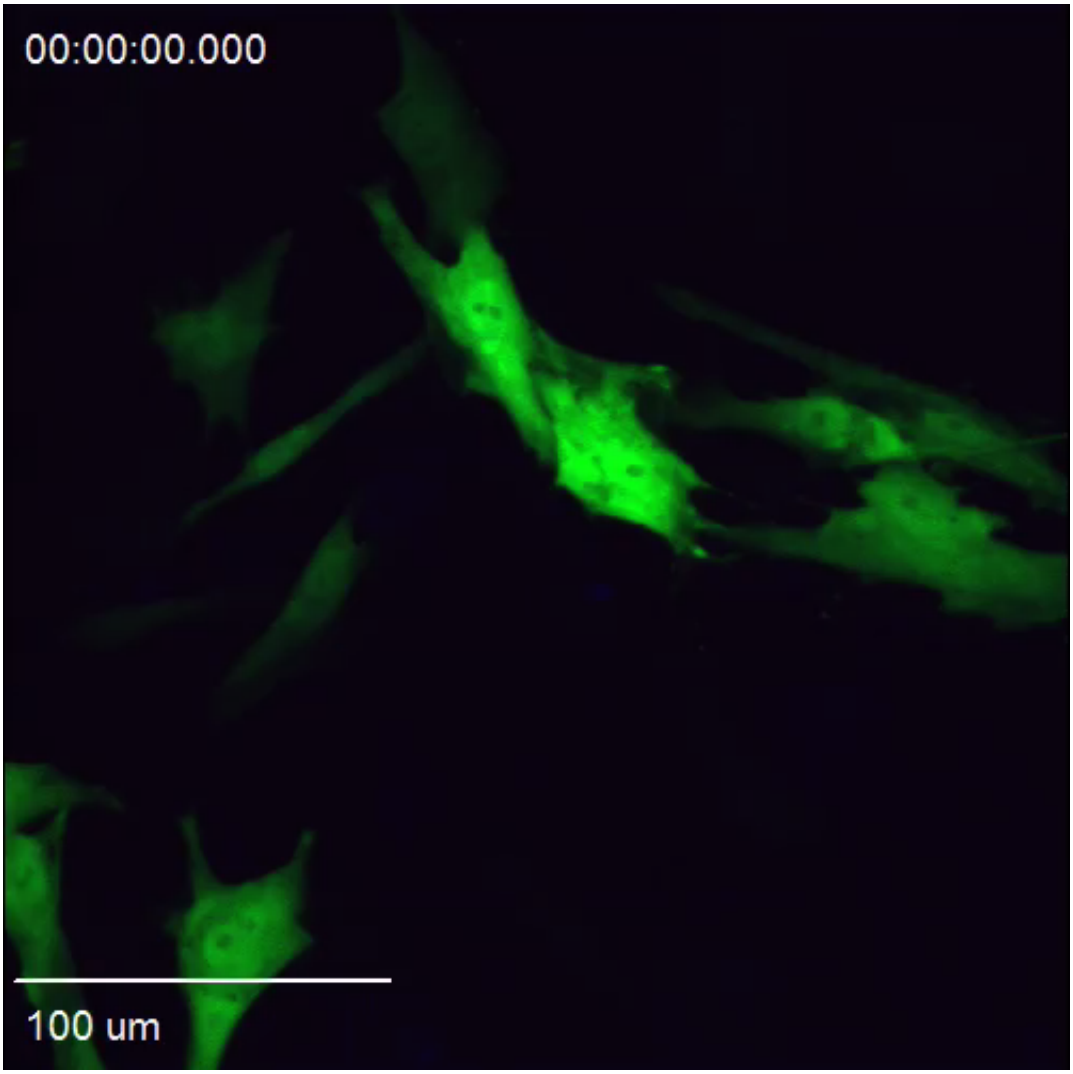

Supplemental Figure 4.7: Time-lapse video of isolated photo-conversion of hWJC.

A single hWJC was photo-converted from green to red fluorescence with targeted UV light exposure, while surrounding cells did not photo-convert. Duration = 01:41. Scale Bar = 100 μm.

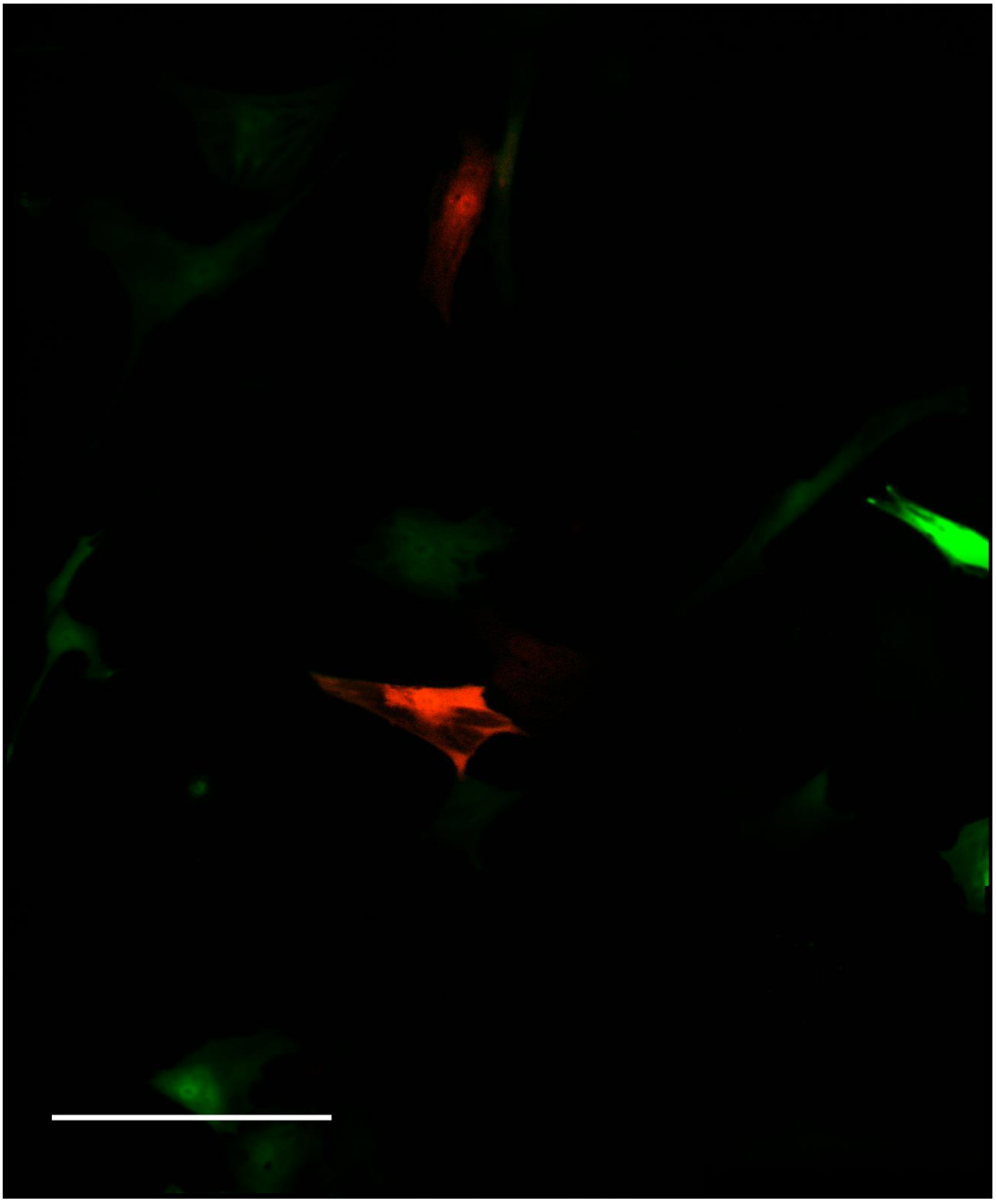

Supplemental Figure 4. 8: 48 h time-lapse video of the movement of the single photo-converted hWJC.

A single hWJC was photo-converted, and was tracked over the course of 48 h. No cells that came into contact with the photo-converted cell displayed any signs of photo-conversion. Duration = 00:30. Scale Bar = 100 μm.

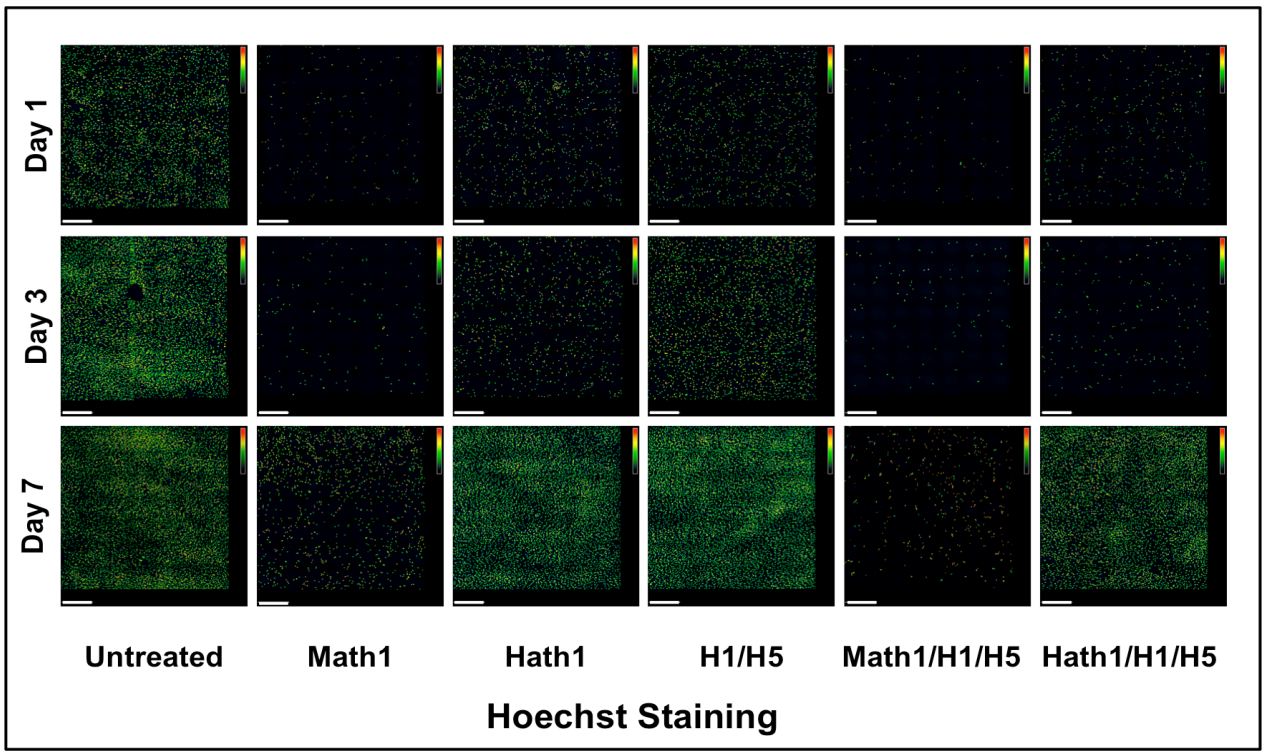

Figure 5.1: Cell density and proliferation.

Cells transfected with *hath1* or *hath1* and siRNA against *hes1* and *hes5* displayed more intact nuclei than *math1* at 1, 3, and 7 d after transfection. Cells co-transfected with math1 and siRNA against hes1 and *hes5* displayed few intact nuclei at 1, 3, and 7 d after transfection. Cells from each group were stained with Hoechst and imaged via an inverted epifluorescent microscope. Images are shown as intensity maps of fluorescence, where green fluorescence represents low fluorescence and red represents high fluorescence. Untreated control populations had the greatest cell density at each time point. Cells treated with *math1* had the lowest cell densities across all three time points, whereas cells treated with only siRNA against *hes1* and *hes5* had the greatest cell densities behind untreated control cells. Images are representative of cells from each treatment group across five umbilical cords (n = 5) at each time point. H1/H5 represents cells transfected with *hes1* and *hes5* siRNA. *Math1*/H1/H5 represents cells co-transfected with *math1* pDNA, *hes1* siRNA, and *hes5* siRNA *Hath1*/H1/H5 represents cells co-transfected with *hath1* pDNA, *hes1* siRNA, and *hes5* siRNA. Scale Bar = 500 μm.

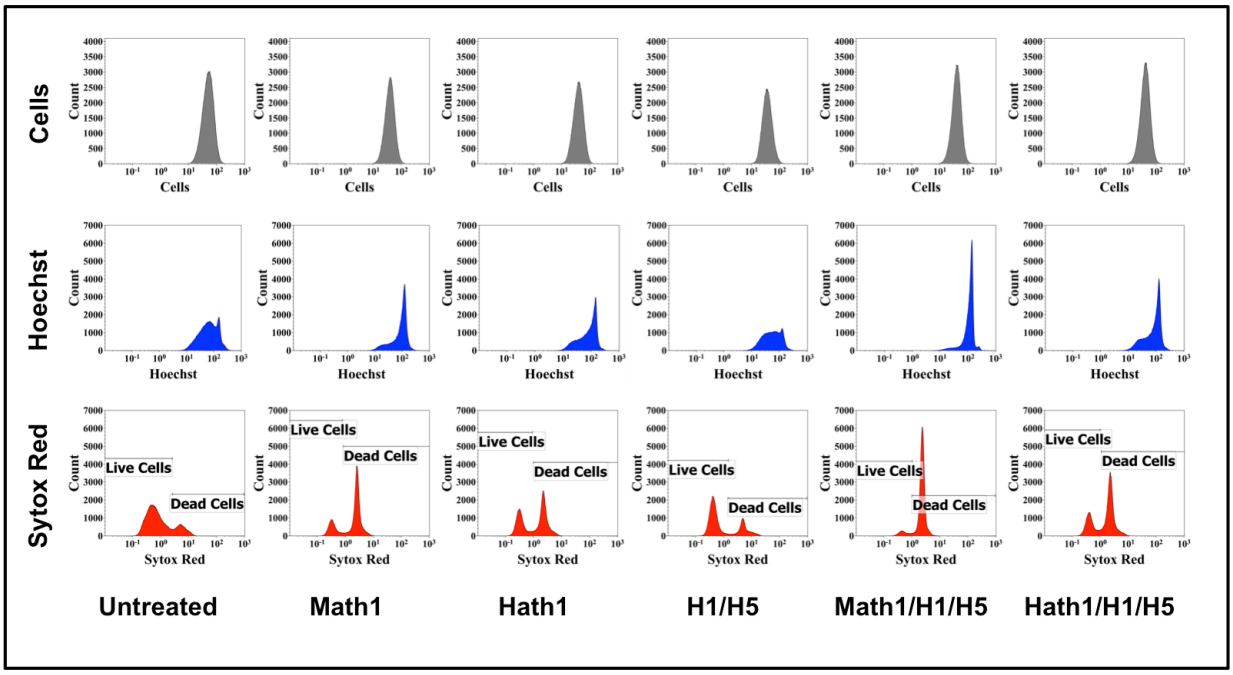

Figure 5.2: Live/Dead analysis of transfected hWJCs.

Transfection with *hath1* led to a greater cell viability than transfection with *math1*. A minimum of 20,000 events were analyzed via flow cytometry to determine the viability of treatments 1 d after transfection. The top row shows the distribution of cells. The middle row displays cells with an intact nucleus positively identified by Hoechst staining. The bottom row displays the distribution of cells identified as live or dead based on Sytox Red (Dead Cell Stain) staining. The histograms shown are an arbitrary selection from one umbilical cord out of five tested. H1/H5 represents cells transfected with *hes1* and *hes5* siRNA. *Math1*/H1/H5 represents cells co-transfected with *math1* pDNA, *hes1* siRNA, and *hes5* siRNA *Hath1*/H1/H5 represents cells co-transfected with *hath1* pDNA, *hes1* siRNA, and *hes5* siRNA.

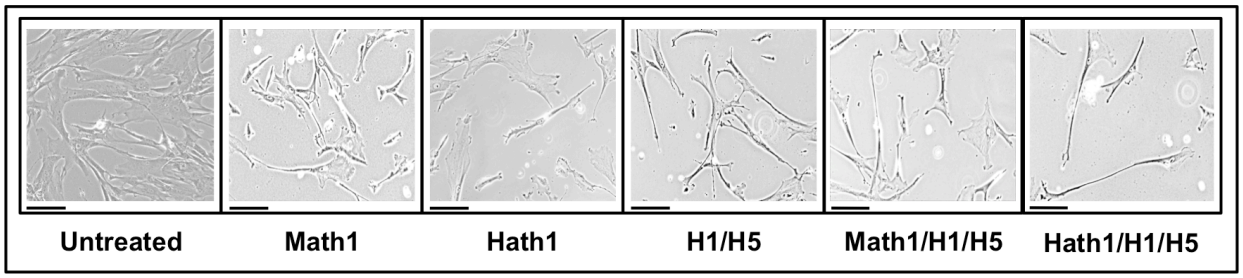

Figure 5.3: Phase contrast images of transfected hWJCs.

The images were taken at a 10X magnification 4 d after cells were transfected. Untreated control cells displayed fibroblastic phenotype, while cells treated with both *hath1* and siRNA against *hes1* and *hes5* displayed an elongated body and bipolar phenotype with projections at the terminal ends of the cell. The images shown are an arbitrary selection from one umbilical cord out of five tested. H1/H5 represents cells transfected with *hes1* and *hes5* siRNA. *Math1*/H1/H5 represents cells co-transfected with *math1* pDNA, *hes1* siRNA, and *hes5* siRNA *Hath1*/H1/H5 represents cells co-transfected with *hath1* pDNA, *hes1* siRNA, and *hes5* siRNA. Scale Bar = 50 μm.

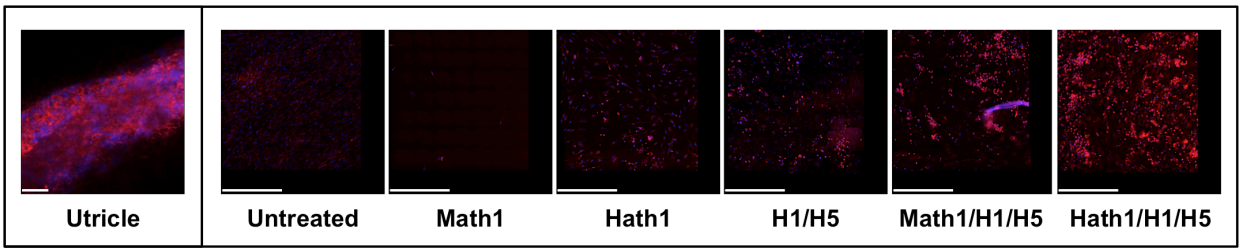

Figure 5.4: Transfected hWJCs stained with FM® 1-43.

Transfected cells were imaged with an epifluorescent microscope 7 d after transfection. Cells transfected with *hath1* and *Hath1*/H1/H5 displayed far superior infiltration of FM® 1-43 than cells transfected with *math1*. Images are composite image montages composed of 25 neighboring fields of view stitched together into a 5 x 5 image. FM® 1-43 (Red) intensely stained hWJCs transfected *Hath1*/H1/H5. The montage images shown are an arbitrary selection from one umbilical cord out of five tested. Cell nuclei are represented by DAPI staining (Blue). A single field of view from a C57BL mouse utricle is shown as a positive control for FM® 1-43 staining. H1/H5 represents cells transfected with *hes1* and *hes5* siRNA. *Math1*/H1/H5 represents cells co-transfected with *math1* pDNA, *hes1* siRNA, and *hes5* siRNA *Hath1*/H1/H5 represents cells co-transfected with *hath1* pDNA, *hes1* siRNA, and *hes5* siRNA. Utricle Scale Bar = 20 μm. Scale Bar = 500 μm.

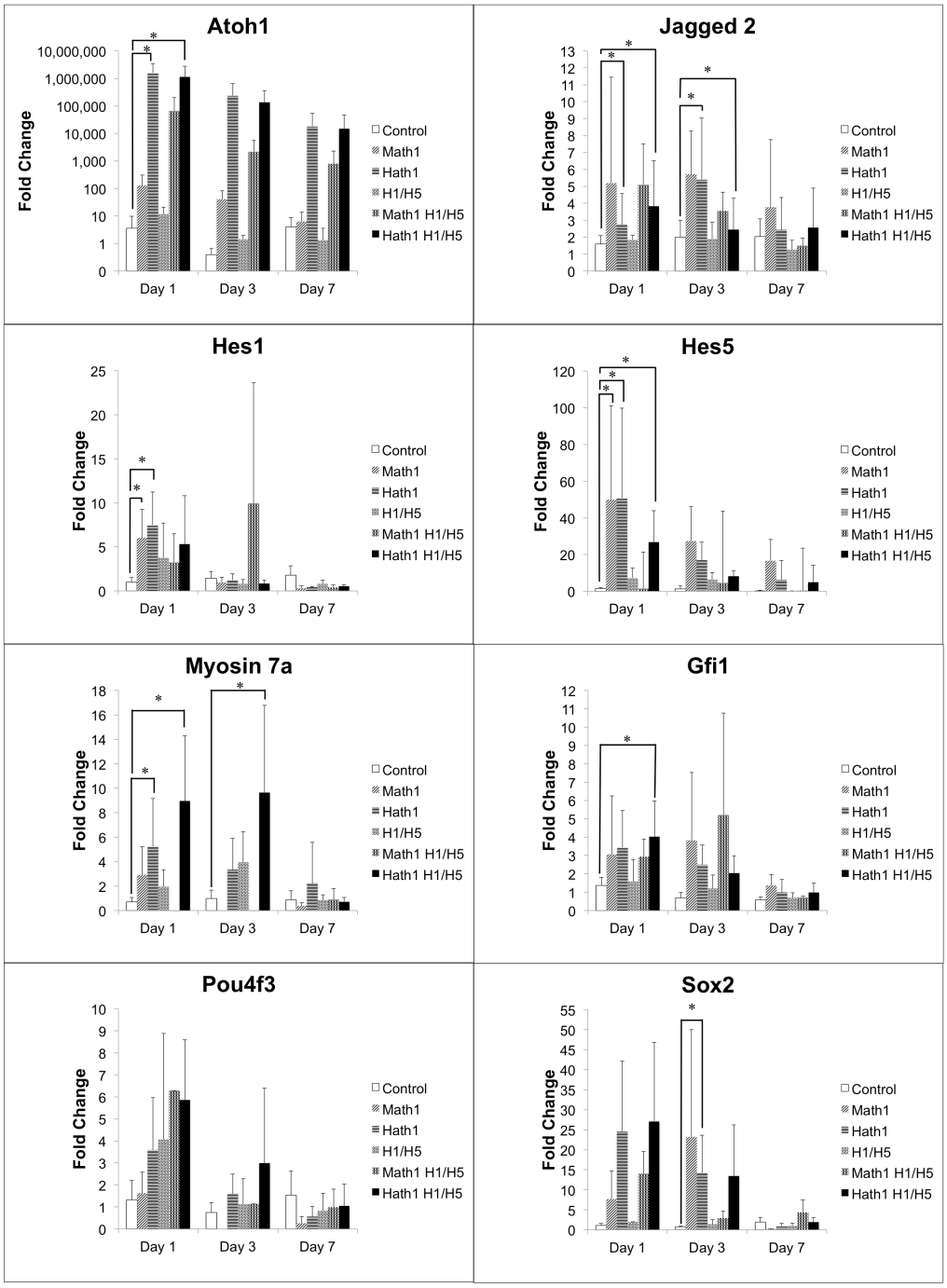

Corresponding Figure 5.5 Legend is on the following page.

Figure 5.5: Gene Expression of transfected hWJCs.

Hath1/H1/H5-transfected cells showed significant increases in gene expression across most genes compared to untreated control cells 1 d after transfection, whereas *math1*-transfected cells only showed significant increases in gene express in *jagged2*, *hes1*, and *hes5*. Treated hWJCs were assessed for gene expression using RT-qPCR at 1, 3, and 7 d after transfection. (*) Statistically significant difference from untreated hWJCs ($p < 0.05$). *Atoh1*, *hes1*, and *hes5* are genes pertaining to pDNA and siRNA used for different treatments. *Jagged2* is a *notch* ligand that initiates the *notch* pathway. *Myosin VIIa*, *gfi1*, *pou4f3*, and *sox2* are key hair cell markers. *Myosin VIIa* is a critical marker that was significantly expressed in hWJCs treated with *Hath1*/H1/H5 at 1 and 3 d after transfection. The results are representative of cells collected from five different umbilical cords ($n = 5$) and are reported as statistical means. All experiments were performed in triplicate. Error bars represent standard deviations. H1/H5 represents cells transfected with *hes1* and *hes5* siRNA. *Math1*/H1/H5 represents cells co-transfected with *math1* pDNA, *hes1* siRNA, and *hes5* siRNA *Hath1*/H1/H5 represents cells co-transfected with *hath1* pDNA, *hes1* siRNA, and *hes5* siRNA.

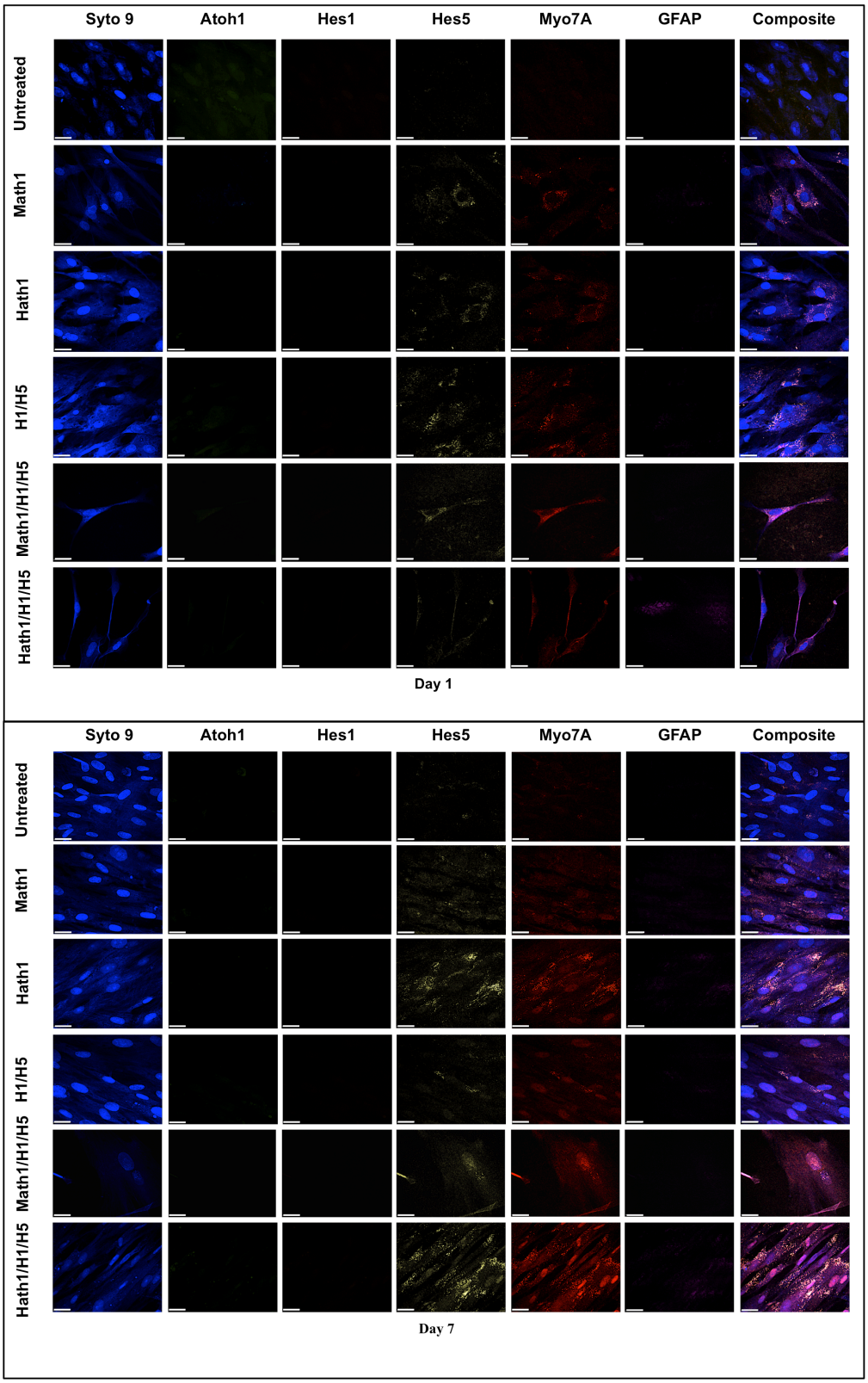

Corresponding Figure 5.6 Legend is on the following page.

Figure 5.6: Immunostaining of transfected hWJCs.

Hath1/H1/H5-transfected cells showed increased expression of *myosin VIIa* and *hes5* from 1 d to 7 d after transfection, whereas *math1*-transfected cells showed a decrease in *myosin VIIa* and *hes5* expression. Treated hWJCs were assessed for protein expression by immunostaining at 1 and 7 d after transfection. Primary antibodies were pre-conjugated to quantum dots. Cell nuclei are represented by Syto 9 staining (Blue). *Atoh1* (Green) and *hes1* (Orange) were not positively identified. *Hes5* (Yellow) and *myosin VIIa* (Red) were positively identified in all treated groups. Cells transfected with *Hath1*/H1/H5 displayed positive identification of *GFAP* (Pink) 1 d after transfection. H1/H5 represents cells transfected with *hes1* and *hes5* siRNA. *Math1*/H1/H5 represents cells co-transfected with *math1* pDNA, *hes1* siRNA, and *hes5* siRNA *Hath1*/H1/H5 represents cells co-transfected with *hath1* pDNA, *hes1* siRNA, and *hes5* siRNA. Scale Bar = 20 μm.

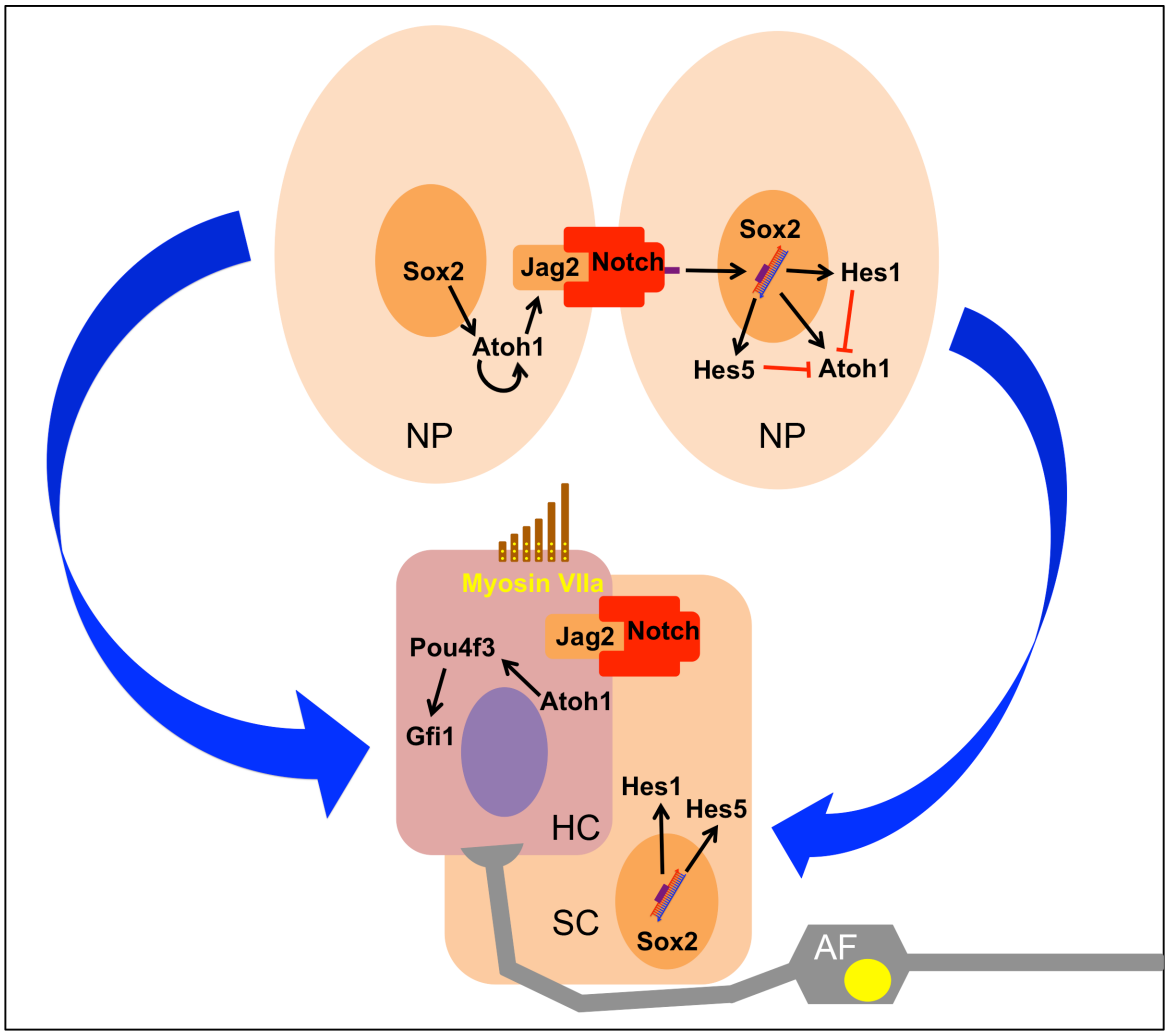

Supplemental Figure 5.7: Differentiation biochemical pathway behind development of hair cells and supporting cells.

The *notch* pathway is heavily involved in the differentiation of hair cells and supporting cells in the inner ear. *Sox2* initiates expression of *atoh1*. *Atoh1* expression enters a positive feedback loop and leads to the expression of the surface ligand, *jagged2* (JAG2). JAG2 binds to a transmembrane *notch* receptor, which initiates lateral inhibition through the cleavage of the *notch* intercellular domain (NICD). The NICD travels to the nucleus and initiates expression of *hes1* and *hes5*, which negatively regulate *atoh1*. Thus, the cell expressing *atoh1* differentiates into a hair cell, and initiates expression of *pou4f3*, followed by *gfi1*. *Pou4f3* and *gfi1* expression are required for hair cell maintenance and survival. *Myosin VIIa* is a motor protein involved in the maintenance of stereocilia that develop on the apical surface of hair cells. The expression of *hes1* and *hes5* in the adjacent cell allow for support cell differentiation. However, *sox2* is down regulated in support cells, but is still present to activate *atoh1* if needed to transdifferentiate the support cell into a hair cell. NP = Neuroprogenitor, HC = Hair Cell, SC = Support Cell, AF = Afferent Neuron.

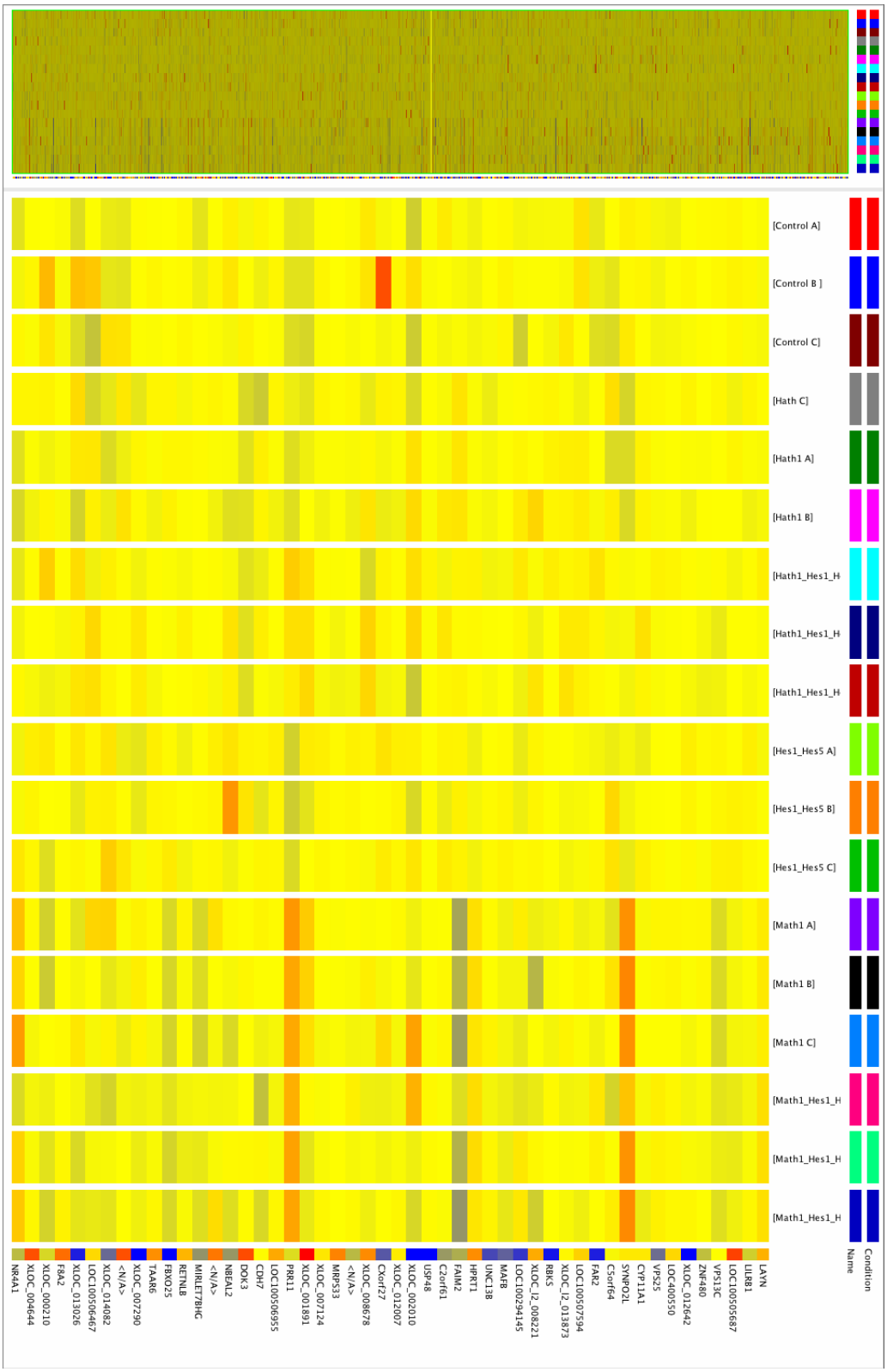

Corresponding Supplemental Figure 5.8 Legend is on the following page.

Supplemental Figure 5.8: Microarray heat map of gene expression across human genome.

Hath1-transfected cells significantly up-regulated/down-regulated half as many genes tested in the human genome as *math1*. Gene expression of all groups of treated hWJCs were assessed across the human genome. Three replicates from each treatment group were compared against the untreated control cells. The heat map ranges from Blue to Red. Blue represents a full 2-fold decrease in gene expression compared against the control. Yellow represents a net zero change in gene expression. Red represents a 2-fold increase in gene expression compared against the control. Fold changes are significant at ($p < 0.05$) as assessed via a one-way ANOVA. The heat map is representative of all treatment groups collected from one umbilical cord 7 d after transfection.

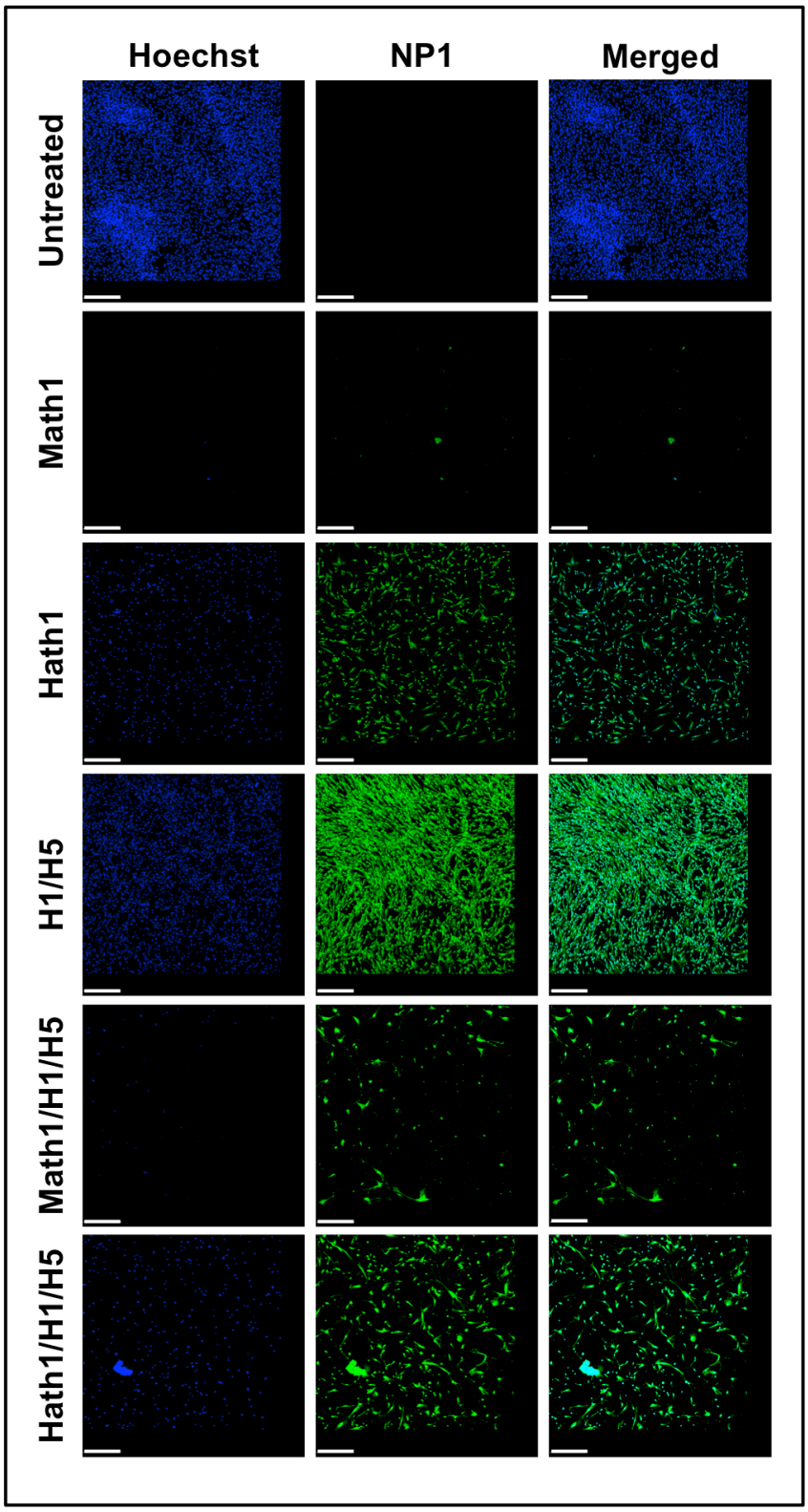

Corresponding Supplemental Figure 5.9 Legend is on the following page.

Supplemental Figure 5.9: AMPA receptor staining.

hWJCs transfected with *hath1*, siRNA against *hes1* and *hes5*, or a combination of both displayed strong staining for AMPA receptors found on live neurons. Untreated controls displayed no presentation of AMPA receptors. *Math1*-transfected cells and cells co-transfected with *math1* and siRNA against *hes1* and *hes5* showed very minor AMPA receptor staining. Nuclei are represented by Hoechst staining (Blue). NP1 (Green) is a fluorescent probe that binds to active AMPA receptors that have been forced open by exposure to glutamine. NP1 stands for Nano-probe 1. H1/H5 represents cells transfected with *hes1* and *hes5* siRNA. *Math1*/H1/H5 represents cells co-transfected with *math1* pDNA, *hes1* siRNA, and *hes5* siRNA *Hath1*/H1/H5 represents cells co-transfected with *hath1* pDNA, *hes1* siRNA, and *hes5* siRNA. Scale Bar = 500 μm.

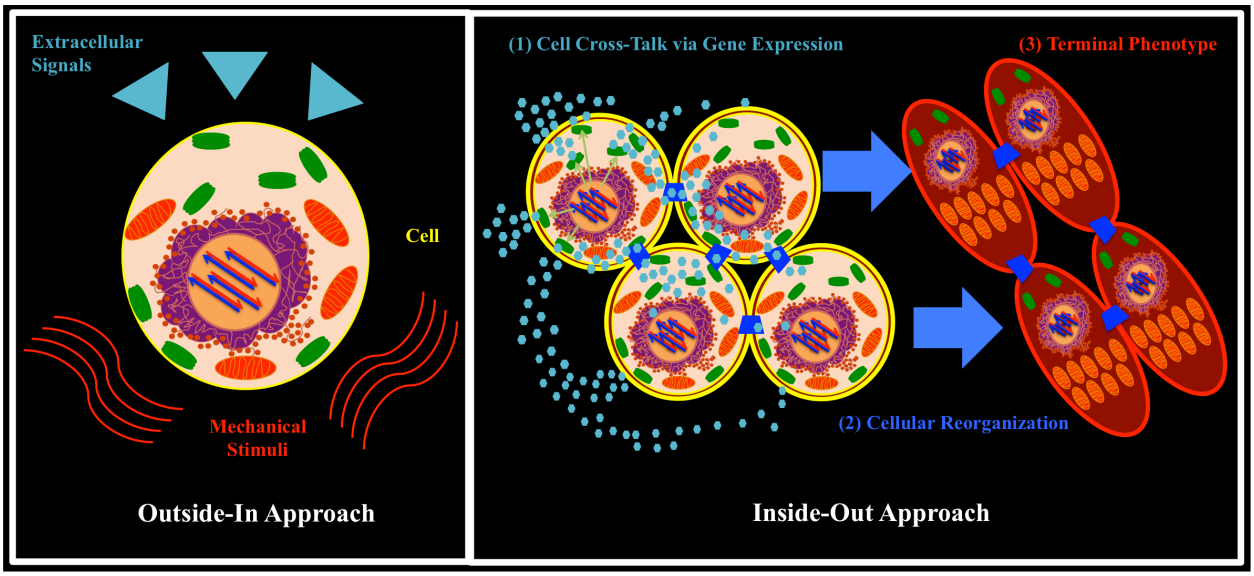

Figure 6.1: Outside-In and Inside-Out Approaches to Tissue Engineering.

Tissue engineering classically approaches problems through an outside-in approach where cells, extracellular signals (chemical and mechanical), and scaffolds are used in concert to solve regenerative medicine problems. Inside-out approaches used in gene therapy rely on changing the intracelluar gene expression and protein production to reorganize the cells. This is accomplished through intracellular cross-talk and can influences the modualtion and distribution of intracellular signals, which affect cellular differentiation and maintenance.

APPENDIX B: Tables

CHAPTER 1: No tables.
CHAPTER 2: Tables 2.1 – 2.5
CHAPTER 3: Table 3.1
CHAPTER 4: Table 4.1
CHAPTER 5: Table 5.1 – 5.2
CHAPTER 6: No tables.

Table 2.1: Transfection studies of stem cells, progenitor cells, and connective tissues using Nucleofection™

Reference	Cell type	Gene(s)	Nucleofector™ program	Cell density	Transfection efficiency	Max gene expression	Cell recovery	Cell viability	Additional notes
Aluigi, M. *et al.* 2006 [6]	hBMSC	*GFP, IL-12*	U-23	4-5x10^5 cells/100 µL	27.4 ± 2.9%	73.7 ± 2.9%	38.7 ± 2.9%	44.5 ± 3.9%	Mean *Il-12* protein production: 290.5 ± 97.6 pg/mL
Aslan, H. *et al.* 2006 [8]	hBMSC	*EGFP, hBMP2, hBMP9*	G-22	5x10^5 cells/100 µL	68.2 ± 4.1%.	N/A	53.6 ± 2.5%	Not Reported	2000-fold and 8000-fold increase in hBMP2 and hBMP9 detected, respectively through RT-qPCR 24 hours post-transfection.
Badakov, R. *et al.* 2006 [9]	ZEF	*GFP*	O-20	3x10^6 cells/100 µL	43%	N/A	30%	N/A	
Baksh, D. *et al.* 2007 [11]	HUCPVC	*DsRed*	U-23	5x10^5 cells/100 µL	>50%	>80%	~50%	N/A	
Balyasnikova, I. *et al.* 2010 [12]	hMSC	*scFv EGFRvIII*	U-23	5x10^5 cells/100 µL	~50%	20.3 ± 2.8%	N/A (Stable Expression Selection)	N/A (Stable Expression Selection)	
Cao, F. *et al.* 2010 [25]	hES	*GFP*	A-23	4-5x10^5 cells/100 µL	16.1 ±3.6%	12.10%	25 ± 9%	70% - 75%	
Cesnulevicius, K. *et al.* 2006 [27]	SDrMNP	*EGFP, DsRed*	A-033	2.08x10^4 cells/100 µL	47.6 ± 8.6%	47.6 ± 8.6% (*GFP*), 16.7 ± 10.25% (*DsRed*)	40%	N/A	

Table 2.1 (continued)

Reference	Cell type	Gene(s)	Nucleofector ™ program	Cell density	Transfection efficiency	Max gene expression	Cell recovery	Cell viability	Additional notes
Cui, M. *et al.* 2008 [36]	mPIVDC	*GDF-5*	U-24	$1x10^5$ cells/100 µL	N/A	N/A	N/A	N/A	*GDF-5* gene delivery via Nucleofection ™ produced a ~3.5 fold and ~1.5 fold increase in type II collagen and aggrecan expression, respectively.
Dhara, S. *et al.* 2009 [36]	hES	*EGFP*	B-16	$1x10^6$ cells/100 µL	20 - 25%	>15%	>5%	39%	
Dickens, S. *et al.* 2010 [43]	hKC	*GFP*	T-07	$5x10^5$ cells/100 µL	14.78 ± 1.75	N/A	Not Reported	Not Reported	
Dickens, S. *et al.* 2010 [43]	hFB	*GFP*	V-13	$5x10^5$ cells/100 µL	46.20 ± 1.22	N/A	Not Reported	Not Reported	
Dickens, S. *et al.* 2010 [43]	hEPC	*GFP*	M-03	$5x10^5$ cells/100 µL	10.90 ± 0.72	N/A	Not Reported	Not Reported	
Distler, J. *et al.* 2005 [44]	hPKC	*EGFP*	T-24	$2x10^5$ cells/µL	56 ± 9%	Not Reported	Not Reported	82.7 ± 7.0%	
Duffy, G. *et al.* 2010 [48]	hMSC	*GFP, Ephrin-B2*	U-23	$5x10^5$ cells/100 µL	46.90%	73% (*GFP*), 46.9% (*Ephrin-B2*)	66.3 ± 1.5%	N/A	
Geoffroy, C. *et al.* 2007 [57]	mNPC	*GFP, YFP, DsRed, Cre Recombinase*	A-33	$3\text{-}4x10^6$ cells/100 µL	31.5 ± 2.7% (YFP)	30.2 ± 3.6% (*GFP*), 92.5 ± 1.2% (*DsRed-Cre co transfection)*	Not Reported	>90%	

Table 2.1 (continued)

Reference	Cell type	Gene(s)	Nucleofector ™ program	Cell density	Transfection efficiency	Max gene expression	Cell recovery	Cell viability	Additional notes
Gonzalez, F. *et al.* 2008 [70]	mEF	*GFP, Oct4, Sox2, Klf4, c-Myc*	T-020	$2x10^6$ cells/100 µL	N/A	37% (GFP)	N/A	N/A	GFP was used as a reporter gene in a polycistronic plasmid expressing Oct4, Sox2, Klf4.
Gresch, O. *et al.* 2004 [75]	hB-CLL	*EGFP*	U-15	$3x10^7$ cells/100 µL	43.60%	N/A	Not Reported	Not Reported	
Gresch, O. *et al.* 2004 [75]	hCD34C	*EGFP*	U-08	1-$5x10^6$ cells/100 µL	70%	N/A	85%	64%	
Gresch, O. *et al.* 2004 [75]	rCM	*DsRed*	G-08	$2x10^6$ cells/100 µL	37.4 ±2.4%	N/A	Not Reported	~60%	
Gresch, O. *et al.* 2004 [75]	hCh	*EGFP*	U-24	0.$5x10^6$ cells/100 µL	62%	N/A	>70%	Not Reported	
Gresch, O. *et al.* 2004 [75]	NHDF-neo	*EGFP*	U-20	3-$4x10^5$ cells/100 µL	66.39 ± 11.10%	N/A	91.39 ± 4.71%	Not Reported	
Gresch, O. *et al.* 2004 [75]	HUVEC	*EGFP*	U-01	3-$5x10^5$ cells/100 µL	54.64 ± 8.95%	N/A	81.49 ±8.52%	Not Reported	
Gresch, O. *et al.* 2004 [75]	NHEM-neo	*H2Kk*	U-20	2-$4x10^5$ cells/100 µL	50.60 ± 21.83%	N/A	94.37 ± 3.79%	Not Reported	
Gresch, O. *et al.* 2004 [75]	HAoSMC	*H2Kk*	U-25	2-4.$5x10^5$ cells/ 100 µL	49.14 ± 15.38%	N/A	91.88 ± 4.77%	Not Reported	
Gresch, O. *et al.* 2004 [75]	NHDF-adult	*EGFP*	U-23	$5x10^5$ cells/100 µL	47.68 ± 17.01%	N/A	93.06 ± 1.10%	Not Reported	
Gresch, O. *et al.* 2004 [75]	hMSC	*EGFP*	U-23	$5x10^5$ cells/100 µL	59.79 ± 8.14%	N/A	72.73 ± 11.08%	Not Reported	

Table 2.1 (continued)

Reference	Cell type	Gene(s)	Nucleofector™ program	Cell density	Transfection efficiency	Max gene expression	Cell recovery	Cell viability	Additional notes
Gresch, O. *et al.* 2004 [75]	hKC-neo	*EGFP*	T-07	4-10x10^5 cells/100 µL	48.83 ±11.40%	N/A	63.64 ± 7.33%	Not Reported	
Gresch, O. *et al.* 2004 [75]	hKC	*EGFP*	U-24	7-8x10^5 cells/100 µL	54.69 ±11.57%	N/A	64.40 ± 12.82%	Not Reported	
Gresch, O. *et al.* 2004 [75]	NIH-3T3	*EGFP*	U-30	4-10x10^5 cells/100 µL	77.42 ± 12.36%	N/A	85.68 ± 3.79%	Not Reported	
Haag, J *et al.* 2009 [77]	hACh	*GFP*	ER-100	2x10^5 cells/µL	73.98%	N/A	80%	72%	
Haleem-Smith, H. et al. 2005 [80]	hMSC	*GFP*	U-23	2x10^6 cells/100 µL	50 - 80%	N/A	Not Reported	16 - 50%	
Hamm, A. *et al.* 2002 [81]	PHM	*GFP*	1A	2-5x10^5 cells/100 µL	44.4 ± 2.7%	N/A	N/A	54.3 ± 5.7%	
Hamm, A. *et al.* 2002 [81]	hPCh	*GFP*	1A	2-5x10^5 cells/100 µL	32.4 ÷ 7.8%	N/A	N/A	16.2 ± 12.3%	
Hamm, A. *et al.* 2002 [81]	hMSC	*GFP*	3A	2-5x10^5 cells/100 µL	45.3 ÷ 5.6%	N/A	N/A	16.5 ± 9.3%	
He, S. *et al.* 2006 [86]	ZEF	*GFP*	T-27	2x10^6 cells/100 µL	≥70%	N/A	Not Reported	Not Reported	
Hohenstein, K. *et al.* 2008 [91]	hES	*GFP*	A-23	2x10^6 cells/100 µL	76%	85%	N/A (Stable Expression Selection)	N/A (Stable Expression Selection)	
Jacobsen, F. *et al.* 2006 [97]	hPKC	*β-gal*	T-24	1x10^5 cells/100 µL	>5%	N/A	23%	N/A	
Jacobsen, F. *et al.* 2006 [97]	hFB	*β-gal*	U-23	5.2x10^4 cells/100 µL	>8%	N/A	37%	N/A	
Jacobsen, F. *et al.* 2006 [97]	HaCat	*β-gal*	U-20	5x10^4 cell/100µL	>0.5%	N/A	22%	N/A	
Kang, J. *et al.* 2009 [104]	L6rSMC	*GFP*	X-05	1x10^6 cells/100 µL	~60%	N/A	Not Reported	~90%	

Table 2.1 (continued)

Reference	Cell type	Gene(s)	Nucleofector™ program	Cell density	Transfection efficiency	Max gene expression	Cell recovery	Cell viability	Additional notes
Lakshimipathy, U. *et al.* 2004 [118]	mTBM	*EGFP*	U-08	3-4x10^7 cells/100 µL	17 + 14%	N/A	Not Reported	10%	
Lakshimipathy, U. *et al.* 2004 [118]	mBML-	*EGFP*	U-08	3-4x10^7 cells/100 µL	25 + 14%	N/A	Not Reported	Not Reported	
Lakshimipathy, U. *et al.* 2004 [118]	mMAPC	*EGFP*	A-23	2-5x10^5 cells/100 µL	25.4 ± 6.0%	N/A	Not Reported	Not Reported	
Lakshimipathy, U. *et al.* 2004 [118]	hMAPC	*EGFP*	A-23	2-5x10^5 cells/100 µL	11.84 ± 0.88%	N/A	Not Reported	Not Reported	
Lakshimipathy, U. *et al.* 2004 [118]	rMAPC	*EGFP*	A-23	2-5x10^5 cells/100 µL	34.5 ± 9.3%	N/A	Not Reported	Not Reported	
Lakshimipathy, U. *et al.* 2004 [118]	hES (H1)	*EGFP*	A-23	1-2x10^6 cells/100 µL	21.44%	22.33 ± 1.28%	Not Reported	Not Reported	
Lakshimipathy, U. *et al.* 2004 [118]	mES (R1)	*EGFP*	A-23	1x10^6 cells/100 µL	63.7 + 9.4%	N/A	N/A (Stable Expression Selection)	N/A (Stable Expression Selection)	
Levetzow, G. *et al.* 2006 [227]	hCD34C	GFP	U-08	2x10^5 cells/100 µL	79.8 ± 14.1%	N/A	52.9 ± 18.9%	Not Reported	
Lorenz, P. *et al.* 2004 [130]	mEF	*EGFP*	A-33	4x10^6 cells/100 µL	85 - 97%	N/A	32 - 45%	52 - 66%	
Maurisse, R. *et al.* 2010 [137]	P16	*EGFP*	U-20	1-2x10^6 cells/100 µL	90%	N/A	Not Reported	95%	
Maurisse, R. *et al.* 2010 [137]	PTE	*EGFP*	T-20	1-2x10^6 cells/100 µL	90%	N/A	Not Reported	95%	
Maurisse, R. *et al.* 2010 [137]	16HBE41o-	*EGFP*	O-17	1-2x10^6 cells/100 µL	65%	N/A	Not Reported	62%	

Table 2.1 (continued)

Reference	Cell type	Gene(s)	Nucleofector™ program	Cell density	Transfection efficiency	Max gene expression	Cell recovery	Cell viability	Additional notes
Maurisse, R. *et al.* 2010 [137]	CFBE41o-	*EGFP*	O-17	1-2x10^6 cells/100 µL	81%	N/A	Not Reported	50%	
Maurisse, R. *et al.* 2010 [137]	HTE	*EGFP*	T-20	1-2x10^6 cells/100 µL	47%	N/A	Not Reported	17%	
Maurisse, R. *et al.* 2010 [137]	HSPC	*EGFP*	U-08	1-2x10^6 cells/100 µL	55%	N/A	Not Reported	50%	
Maurisse, R. *et al.* 2010 [137]	HEK 293	*EGFP*	X-01	1-2x10^6 cells/100 µL	93%	N/A	Not Reported	72%	
Maurisse, R. *et al.* 2010 [137]	MESC	*EGFP*	A-24	1-2x10^6 cells/100 µL	62%	N/A	Not Reported	66%	
Moore, J. *et al.* 2010 [152]	hES	*GFP*	96-CB-150	2x10^5 cells/20 µL	74.2 ± 1.4%	N/A	73.5 ± 3.2%	Not Reported	
Motoyama, H. *et al.* 2009 [154]	mHep	*EGFP, DsRed, Pdx1, Ngn3*	T-028	7x10^5 cells/100 µL	52.2 ± 3.7%	60.4 ± 16.0 (co-expression Pdx1 & Ngn3)	~90%	~25%	
Nakayama, A. *et al.* 2007 [158]	pEF	*EGFP*	U-23	1x10^6 cells/100 µL	79 ± 0.8%	N/A	57.80%	Not Reported	
Quenneville, S. *et al.* 2004 [185]	MD1	*GFP, DysE*	P-22	5-7.5x10^5 cells/ 100 µL	~20%	N/A	Not Reported	30%	
Quenneville, S. *et al.* 2004 [185]	hPM	*GFP, DysE*	P-22	5-7.5x10^5 cells/ 100 µL	>50%	N/A	Not Reported	60%	
Ryan, J. *et al.* 2011 [191]	mEG	*GFP, SRY*	C001	1 gonad/100 µL	7.9 ± 2.2%	11%	Not Reported	91%	
Scheibe, F. *et al.* 2011 [201]	mMSC	*GFP, EPO*	A-30	1x10^6 cells/100 µL	60 ± 2% (GFP)	26 ± 5% (Co-expression EPO & GFP)	37 ± 1%	94 ± 1%	
Schiøtz, B. *et al.* 2011 [203]	TO	*GFP*	T-20	5x10^6 cells/100 µL	90.80%	Not Reported	Not Reported	72 - 100%	

Table 2.1 (continued)

Reference	Cell type	Gene(s)	Nucleofector ™ program	Cell density	Transfection efficiency	Max gene expression	Cell recovery	Cell viability	Additional notes
Sheyn, D. *et al.* 2008 [209]	pADSC	*GFP, rhBMP-6*	G-22	1-2x10^6 cells/100 µL	62.50%	4.78 ± 0.97 ng/ 10^6 cells	Not Reported	52.90%	
Zaragosi, L. *et al.* 2007 [249]	hMADS	*EGFP, LIF*	U-23	6x10^5 cells/100 µL	67.20%	76.1 ± 1.3% (EGFP), 397.34 - 586.88 ng/mL	13.6 ± 6.1%	Not Reported	
Zhang, Z. *et al.* 2011 [255]	rSF	*GFP, bFGF, VEGF*	U-30	1x10^6 cells/100 µL	~60%	>250 pg/mL (bFGF), 11 ng/ mL (VEGF)	Not Reported	95%	

Terms and Abbreviations: Transfection Efficiency, percent of positive expressing cells out of total viable cell population; Max Gene Expression, maximum number of positive cells recorded or maximum quantity of protein detected; Cell Recovery, percent of live cells 24 hours after transfection; Cell Viability, percent of live cells 48 hours or more after transfection; hBMSCs, human bone marrow stem cells; ZEF, zebrafish embryonic fibroblasts; hUCPVCs, human umbilical cord perivascular cells; hMSCs, human mesenchymal stem cells; hES, human embryonic stem cells; SDrMNPC, Sprague-Dawley rat mesencephalic neuronal progenitor cells; mPIVDC, mouse primary intervertebral disc cells; hKC, human keratinocytes; hFB, human fibroblasts; hEPC, human endothelial progenitor cells; hPKC, human primary keratinocytes; mNPC, mouse neural precursor cells; mEF, mouse embryonic fibroblasts; B-CLL, human B cell chronic lymphocytic leukemia; rCM, rat cardiomyocytes; hCh, human chondrocytes; NHDF-neo, normal neonatal human dermal fibroblasts; HUVEC, human umbilical vein endothelial cells; NHEM-neo, normal neonatal human epidermal melanocytes; HAoSMC, human aortic smooth muscle cells; NHDF-adult, normal human dermal fibroblasts; hKC-neo, neonatal human keratinocytes; hKC-adult, human keratinozyten; NIH-3T3, mouse embryonic fibroblasts; hACh, human articular chondrocytes; PHM, primary human melanocytes; HaCat, immortalized human keratinocytes; L6rSMC, L6 rat smooth muscle cells; mTBM, mouse total bone marrow; mBMI-, mouse bone marrow lineage negative cells; mMAPC, mouse multipotent adult progenitor cells; hMAPC, human multipotent adult progenitor cells; rMAPC, rat multipotent adult progenitor cells; mES, mouse embryonic stem cells; hCD34C, human CD34+ cells; P16, pig fetal fibroblasts; primary pig tracheal epithelial cells; 16HBE41o-, immortalized human bronchial epithelial cell line; HTE, primary human tracheal epithelial cells; HSPC, primary hematopoietic stem/progenitor cells; HEK-293, human embryonic kidney cells; MESC, transgenic mouse embryonic stem cells; mHep, mouse hepatocytes; pEF, porcine embryonic fibroblasts; MD1, mouse muscle-derived stem cells; hPM, human primary myoblasts; mEG, mouse embryonic gonads; mMSC, mouse mesenchymal stem cells; TO, Atlantic salmon head kidney cells; pADSC, porcine adipose derived stem cells; hMADS, human multipotent adipose tissue derived stem cells; rSF, rat skin fibroblasts; *GFP*, green fluorescent protein; *Il-12*, interleukin 12; *EGFP*, enhanced green fluorescent protein; *hBMP2*, human bone morphogenetic protein 2; *hBMP9*, human bone morphogenetic protein 9; *DsRed*, Discoma species Red; *scF EGFRvIII*, stem cell factor epidermal growth factor receptor vIII; *GDF-5*, growth/differentiation factor 5; *YFP*, yellow fluorescent protein; *Oct4*, octamer-binding transcription factor 4; *Sox2*, sex determining region Y-box 2; *Klf4*, krueppel-like factor 4; *c-Myc*, v-myc myelocytomatosis viral oncogene homolog; *β-gal*, beta galactosidase; *Pdx1*, pancreatic and duodenal homeobox 1; *Ngn3*, neurogenin 3; *DysE*, human dystrophin; *SRY*, sex determining region Y; *EPO*, erythropoietin; *LIF*, leukemia inhibitory factor; *bFGF*, basic fibroblast growth factor; *VEGF*, vascular endothelial growth factor.

Table 2.2: Transfection studies of blood cells and blood vessel tissues using Nucleofection™

Reference	Cell type	Gene(s)	Nucleofector™ program	Cell density	Transfection efficiency	Max gene expression	Cell recovery	Cell viability	Additional notes
Becheli, J. *et al.* 2009 [17]	hMVEC	*GFP*	T-016	$2.5x10^6$ cells/100 µL	Not Reported	67%	Not Reported	Not Reported	
Bowles, R. *et al.* 2010 [21]	hMDDC	*GFP*	FF-137, FF-138	$5x10^5$ cells/20 µL	50%	>50%	Not Reported	70%	
Gerdemann, U. *et al.* 2009 [58]	hDC	*GFP, Penton antigen, Hexon antigen, Large T antigen*	U-02	$0.5\text{-}1x10^6$ cells/20 µL	38 ± 11%	38 ± 11%	66%	29%	Genes coding *Penton*, *Hexon*, and *Large T* viral antigens were delivered via Nucleofection™ to DCs to induce development of multivirus reactive cytotoxic T lymphocytes.
Goffinet, C. *et al.* 2006 [65]	RL	*EGFP*	U-14	$1x10^7$ cells/100 µL	54 ± 3.0%	82%	N/A	4 - 35%	
Gresch, O. *et al.* 2004 [75]	HTC	*H2Kk*	U-15	$50x10^5$ cells/100 µL	47.5 ± 12.7%	N/A	80.5 ± 6.4%	Not Reported	
Gresch, O. *et al.* 2004 [75]	HBC	*H2Kk*	U-15	$50x10^5$ cells/100 µL	35.7 ±12.6%	N/A	80.5 ± 6.3%	Not Reported	
Hamm, A. *et al.* 2002 [81]	haSMC	*GFP*	1A	$2\text{-}5x10^5$ cells/100 µL	28.9 ± 2.9%	N/A	N/A	50.0 ± 11.1%	
He, C. *et al.* 2010 [84]	mPCD4TC	*GFP*	X001	$3x10^6$ cells/100 µL	57.7 ± 1.6%	N/A	69.0 ± 1.8%	17.0 ± 0.5%	
Isakari, Y. *et al.* 2007 [96]	MEG-01	*EGFP*	U-01	$1x10^6$ cells/100 µL	48 ± 6%	70 ± 7%	68 ± 2%	Not Reported	
Johnson, J. *et al.* 2006 [101]	HN	*β-gal*	T-27	$2x10^6$ cells/100 µL	0.4 – 1.0%	N/A	78.8 ± 2.5%	N/A	
Kang, J. *et al.* 2009 [104]	HUAEC	*GFP*	S-05	$1x10^6$ cells/100 µL	40 - 50%	N/A	Not Reported	70 - 80%	
Kang, J. *et al.* 2009 [104]	HUVEC	*GFP*	S-05	$1x10^6$ cells/100 µL	40 - 50%	N/A	Not Reported	70 - 80%	

Table 2.2 (continued)

Reference	Cell type	Gene(s)	Nucleofector™ program	Cell density	Transfection efficiency	Max gene expression	Cell recovery	Cell viability	Additional notes
Kang, J. *et al.* 2009 [104]	BEC	*GFP*	S-05	$1x10^6$ cells/100 µL	40 - 50%	N/A	Not Reported	70 - 80%	
Kang, J. *et al.* 2009 [104]	LEC	*GFP*	S-05	$1x10^6$ cells/100 µL	40 - 50%	N/A	Not Reported	>90%	
Lai, W. *et al.* 2003 [117]	mPCD4TC	*EGFP*	T-27	3-4$x10^6$ cells/100 µL	>20%	N/A	Not Reported	>75%	
Landi, A. *et al.* 2007 [120]	hiDC	*GFP*	X-1	$1x10^6$ cells/100 µL	~50%	>50%	>75%	>50	
Lenz, P. *et al.* (2003) [123]	hDC	*EGFP*	T-01	$2x10^7$ cells/100 µL	55%	N/A	80-90%	14%	
Maasho, K. *et al.* 2003 [132]	hNKC	*EGFP, EYFP*	O-17	5x106 cells/100 µL	40 - 70%	N/A	Not Reported	85 - 90%	
Maurisse, R. *et al.* 2010 [137]	LT1-1B1	*EGFP*	G16	1-2$x10^6$ cells/100 µL	75%	N/A	Not Reported	80%	
Maurisse, R. *et al.* 2010 [137]	SC-1	*EGFP*	G16	1-2$x10^6$ cells/100 µL	75%	N/A	Not Reported	80%	
Melhem, N. et al. 2008 [140]	imDC	*GFP*	U-02	$1x10^6$ cells/100 µL	10%	14%	24%	Not Reported	
Mendez, P. *et al.* 2011 [141]	PBL	*GFP*	FF-138	$6x10^5$ cells/100 µL	50.50%	N/A	15.33%	Not Reported	
Nagaraj, S. *et al.* 2004 [157]	HCIKC	*EGFP, IL-2*	U-14	$1x10^6$ cells/100 µL	43.0 ± 3.8%	478.5 pg/10^6 cells (IL-2)	83%	Not Reported	
Tervo, H. *et al.* 2008 [221]	RbTL	*EGFP*	U-14	$5x10^6$ cells/100 µL	44 ± 3%	N/A	Not Reported	47 ± 7%	

Terms and Abbreviations: Transfection Efficiency, percent of positive expressing cells out of total viable cell population; Max Gene Expression, maximum number of positive cells recorded or maximum quantity of protein detected; Cell Recovery, percent of live cells 24 hours after transfection; Cell Viability, percent of live cells 48 hours or more after transfection; hMVEC, human microvascular endothelial cells; hMDDC, human monocyte derived dendritic cells; hDC, human dendritic cells; RL, rat lymphocytes; HTC, human T-cells; HBC, human B cells; haSMC, human arterial smooth muscle cells; mPCD4TC, mouse primary CD4+ T-cells; MEG-01, human megakaryocytes; HN, human neutrophils; HUAECs, primary human umbilical arterial endothelial cells; HUVECs, human umbilical venous endothelial cells; BEC, primary human dermal blood vascular endothelial cells; LEC, primary human lymphatic endothelial cells; hiDC, human immature dendritic cells; hNKC, human natural killer cells; LT1-1B1, immortalized human lymphoblasts; SC-1, immortalized human lymphoblasts; imDC, immature monkey dendritic cell; PBL, peripheral blood lymphocytes; hCIKC, human cytokine-induced killer cells; RbTL, rabbit T lymphocytes; *GFP*, green fluorescent protein; *EGFP*, enhanced green fluorescent protein; *β-gal*, β-galactosidase; *EYFP*, enhanced yellow fluorescent protein; *IL-2*, interleukin 2.

Table 2.3: Transfection studies of cancer cells using Nucleofection™

Reference	Cell type	Gene(s)	Nucleofector™ program	Cell density	Transfection efficiency	Max gene expression	Cell recovery	Cell viability	Additional notes
Bockstaele, F. *et al.* 2008	HCLL	*EGFP*	U-13	1.5 - 4x10^6 cells/100 µL	21%	12 ±13%	Not Reported	Not Reported	
Bradburne, C. *et al.* 2009	A549	*GFP*	DS-150	2.75x10^5 cells/ 20 µL	*7.70%*	7.40%	17.60%	92.70%	
Ear, T. et al. 2008	PLB-985	*EGFP, Luciferase, IκB-α (S32/364) , PKCα*	Q-01, U-15	5x106 cells/100 µL	73 ± 4% (EGFP)	>70%	56 ± 4%	~20%	PLB-985 cells over expressed genes IκB-α (S32/36A) , PKCα when delivered via Nucleofection™ . IL-8 promoters coupled to a luciferase reporter gene transiently expressed when delivered via Nucleofection™ .
Gresch, O. *et al.* 2004	HeLa	*EGFP*	O-05	4-6.5x10^5 cells/ 100 µL	71.02 ± 2.80%	Not Reported	82.95 ± 6.35%	Not Reported	
Gresch, O. *et al.* 2005	K562	*EGFP*	T-16	10x10^5 cells/100 µL	88.62 ± 3.17%	Not Reported	88.36 ± 5.20%	Not Reported	
Gresch, O. *et al.* 2007	C6	*EGFP*	U-30	10-20x10^5 cells/ 100 µL	88.56 ± 8.88%	Not Reported	74.23 ± 13.13%	Not Reported	
Hagemann, C. *et al.* (2006)	U251	*GFP*	T-20	1x10^6 cells/100 µL	95.70%	N/A	Not Reported	93.10%	
Han, S. *et al.* 2007	HMC	*LacZ, GFP*	U-20, A-24	2x10^6 cells/100 µL	20 - 90%	N/A	N/A	<5 - 50%	

Table 2.3 (continued)

Reference	Cell type	Gene(s)	Nucleofector™ program	Cell density	Transfection efficiency	Max gene expression	Cell recovery	Cell viability	Additional notes
Johnson, B. *et al.* 2005	AGN2a	*CD80/86, CD54/137L*	T-20	1x10^6 cells/100 µL	Not Reported	96.2% (CD80/86), 88.9% (CD54/137L)	40 - 50%	Not Reported	
Kang, J. *et al.* 2009	TPC1	*GFP*	X-01	1x10^6 cells/100 µL	>50%	N/A	Not Reported	~80%	
Klagge, A. *et al.* 2010	FRTL-5	*GFP*	A-030	1x10^6 cells/100 µL	62.15 ± 0.77%	N/A	Not Reported	72.9 ± 0.7%	
Lakshimipathy, U. *et al.* 2004	Ntera2ECC	*EGFP*	A-23	1x10^6 cells/100 µL	95.09%	86.92 ± 11.56%	Not Reported	Not Reported	
Schakowski, F. *et al.* 2004	PHAMLC	*GFP*	S-04	1x10^6 cells/100 µL	71.5 ± 1.8%	60.3 ± 9.7%	94.6 ± 0.2%	Not Reported	
Schakowski, F. *et al.* 2004	K562	*GFP*	T-02	5x10^5 cells/100 µL	76.1 ± 2.3%	74.7 ± 8.0%	66.0 ± 14.9	Not Reported	
Schakowski, F. *et al.* 2004	HL60	*GFP*	T-01, S-11	5x10^5 cells/100 µL	33.4 ± 14.9% - 49.0 ± 9.7%	49.0 ± 9.7%	49.6 ± 21.5% - 63 ± 16%	Not Reported	
Schnoor, M. *et al.* 2009	THP-1	*GFP*	Y-001	2.5x10^6 cells/ 100 µL	>50%	Not Reported	Not Reported	>80%	
Seiffert, M. *et al.* 2007	B-CLL	*GFP*	U-15	1-3x10^6 cells/ 100 µL	50 - 70%	N/A	20 - 60%	Not Reported	

Terms and Abbreviations: Transfection Efficiency, percent of positive expressing cells out of total viable cell population; Max Gene Expression, maximum number of positive cells recorded or maximum quantity of protein detected; Cell Recovery, percent of live cells 24 hours after transfection; Cell Viability, percent of live cells 48 hours or more after transfection; HCLL, human chronic lymphocytic leukemia; A549, adenocarcinomic human alveolar basal epithelial cells; PLB-985, human peripheral blood leukemia acute myeloid; HeLa, cervical cancer cells from Henrietta Lacks; K562, immortalized myelogenous leukemia; C6, rat glial tumor; U251, human glioblastoma; HMC, human melanoma cells; AGN2a, mouse neuroblastoma; TPC1, human thyroid cancer cells; FRTL-5, rat thyroid cells; Ntera2ECC, human embryonic carcinoma cells; PHAMLC, primary human acute myeloid leukemia cells; HL60, human acute myeloid leukemia; THP-1, human acute monocytic leukemia cell line; B-CLL, B-cell chronic lymphocytic leukemia; *EGFP*, enhanced green fluorescent protein; *GFP*, green fluorescent protein; *IκB-α (S32/36a)*, nuclear factor of kappa light polypeptide gene enhancer in B-cells inhibitor alpha (dominant negative form); *PKCa*, protein kinase calcium; *CD80/86*, cluster of differentiation 80/86; *CD54/137L*, cluster of differentiation 54/137L.

Table 2.4: Transfection studies of neuronal cells using Nucleofection™

Reference	Cell type	Gene(s)	Nucleofector™ program	Cell density	Transfection efficiency	Max gene expression	Cell recovery	Cell viability	Additional notes
Gresch, O. *et al.* 2004 [75]	RN	*EGFP*	G-013	1.2-3.8x10^6 cells/ 100 µL	>60%	N/A	Not Reported	Not Reported	
Gresch, O. *et al.* 2006 [75]	PC-12	*EGFP*	U-29	20x10^5 cells/100 µL	41.50 ± 9.43%	N/A	89.32 ± 5.40%	Not Reported	
Muyderman, H. *et al.* 2010 [155]	RA	*GFP*	T-20	2x10^6 cells/100 µL	68 ± 8%	N/A	79 ± 6%	Not Reported	
Whitlon, D. *et al.* 2010 [234]	MCSC	*GFP*	T-30	1x10^6 cells/100 µL	45%	N/A	Not Reported	~50%	

Terms and Abbreviations: Transfection Efficiency, percent of positive expressing cells out of total viable cell population; Max Gene Expression, maximum number of positive cells recorded or maximum quantity of protein detected; Cell Recovery, percent of live cells 24 hours after transfection; Cell Viability, percent of live cells 48 hours or more after transfection; RT, rat neurons; PC-12, pheochromocytoma rat adrenal medulla cells; RA, rat astrocytes; MCSC, mouse cochlear Schwann cells; *EGFP*, enhanced green fluorescent protein; *GFP*, green fluorescent protein.

Table 2.5: RNA studies using Nucleofection™

Reference	Cell type	Gene(s) targeted by siRNA	RNA dose (format)	Nucleofector ™ program	Cell density per transfection	Max transfection Efficiency	Max gene knockdown	Cell recovery	Cell viability	Additional notes
Banzon, V. *et al.* 2011 [13]	CID-βYACBMC	*DNMT1*	1 µM	D-012	5x106 cells/ 100 µL	90.30%	80 - 90%	Not Reported	Not Reported	
Becheli, J. *et al.* 2009 [17]	HMVEC	*cIAP2*	200 nmol/L siRNA (12 well-plate)	T-016	2.5x106 cells/ 100 µL	Not Reported	50%	Not Reported	Not Reported	
Bowles, R. *et al.* 2010 [21]	HMDDC	*RIG-I*	0.25 µg siRNA (0.75 mL Matrix Tube)	FF-168	5x105 cells/20 µL	55%	75%	Not Reported	70%	
Bradburne, C. *et al.* 2009 [22]	A549	*RelA*	100 nM/250 nM/500 nM siRNA (96 well-plate)	DS-150	2.75x105 cells/ 20 µL	*7.70%*	70-95%	17.60%	92.70%	
Gandhirajan, R. *et al.* 2010 [56]	HBCLL	*Lef-1*	0.5 µM siRNA	U-013	8x106 cells/ 100 µL	Not Reported	Not Reported	Not Reported	Not Reported	Gene knockdown was measured indirectly through apoptosis.
Goffinet, C *et al.* 2006 [65]	RTL	*hCD4*	0.24 nmol siRNA	U-14	1x107 cells/ 100 µL	70 - 80%	~50%	Not Reported	Not Reported	
Gresch, O. *et al.* 2004 [75]	HL	*STAT6*	2 µM, 5 µM, 10 µM siRNA	V-024	1-5x106 cells/ 100 µL	~100%	60% (5 µM)	Not Reported	Not Reported	
Gresch, O. *et al.* 2004 [75]	RCN	*Si-kinase*	3 µg	G-13	1.2x106 cells/ 100 µL	Not Reported	>85%	Not Reported	Not Reported	
Haag, J *et al.* 2009 [77]	HAC	*GAPDH*	10-1000 nM	ER-100	2x105 cells/µL	Not Reported	>95%	Not Reported	Not Reported	
Hagemann, C. *et al.* (2006) [79]	U251	*A-Raf*	3 µg	T-20	1x106 cells/ 100 µL	Not Reported	96%	Not Reported	Not Reported	
Han, S. *et al.* 2007 [82]	HMC	*p53*	10 µg	T-20	2x106 cells/ 100 µL	Not Reported	80.60%	Not Reported	Not Reported	

Table 2.5 (continued)

Reference	Cell type	Gene(s) targeted by siRNA	RNA dose (format)	Nucleofector ™ program	Cell density per transfection	Max transfection Efficiency	Max gene knockdown	Cell recovery	Cell viability	Additional notes
Kang, J. *et al.* 2009 [104]	PHLEC	*Prox1, COUP-TFII*	20 pmol	S-05	1x106 cells/ 100 µL	90%	N/A	Not Reported	Not Reported	
Merkerova, M. *et al.* 2007 [144]	CMLPC	*PCNA, MMP8, MMP9, p38, JNK2, BCR/ ABL*	50 nmol	T-20	$5x10^6$ cells/ 100 µL	36-42%	65% (BCR/ ABL), 63%, (PCNA), ~70% (MMP8), ~64% (MMP9), ~70% (p38), ~75% (JNK2)	Not Reported	74.7 ± 32.9%	
Mo, D. *et al.* 2010 [151]	MDCK	Galectin-3	10 µg	T-23	$4x10^6$ cells/ 100 µL	~70%	~85%	N/A	N/A	
Moore, J. *et al.* 2010 [152]	hES	*GFP*	200, 300, 600 ng	96-CB-150	$2x10^5$ cells/20 µL	74.2 ± 1.4%	71.75%	73.5 ± 3.2%	Not Reported	
Schnoor, M. *et al.* 2009 [204]	THP-1	*TIP47*	1 µg	Y-001	$2.5x10^6$ cells/ 100 µL	100%	75%	20% - 60%	Not Reported	
Verreault, M. et al. 2009 [226]	U251MG	*ILK*	0.0625 - 2 µg	U-16	Not Reported	73%	93%	78%	>90%	

Terms and Abbreviations: Transfection Efficiency, percent of positive expressing cells out of total viable cell population; Max Gene Expression, maximum number of positive cells recorded or maximum quantity of protein detected; Cell Recovery, percent of live cells 24 hours after transfection; Cell Viability, percent of live cells 48 hours or more after transfection; CID-βYACBMC, chemical inducer of dimerization dependent mouse βYAC bone marrow cells; hMVEC, human microvascular endothelial cells; hMDDC, human monocyte derived dendritic cells; A549, adenocarcinomic human alveolar basal epithelial cells; hBCLL, human B cell chronic lymphocytic leukemia; RTL, rat T lymphocytes; HL, human lymphocytes; RCN, rat cortical neurons; HAC, human articular chondrocytes; U251, human glioblastoma cells; hMCs, human melanoma cells; PHLECs, primary human lymphatic endothelial cells; CMLPCs, CML primary cells; MDCK, Madin Darby canine kidney cells; hES, human embryonic cells; THP-1, human acute monocytic leukemia cells; U251MG, U251 glioblastoma; *DNMT1*, DNA (cytosine-5)-methyltransferase 1; *cIAP2*, cellular inhibitor of apoptosis; *RIG-1*, retinoid-induced gene 1; *Lef-1*, lymphoid enhancer-binding factor-1; *hCD4*, human cluster of differentiation 4; *STAT6*, signal transducer and activator of transcription 6; *GAPDH*, glyceraldehyde 3-phosphate dehydrogenase; *A-Raf*, v-raf murine sarcoma 3611 viral oncogene homolog; *p53*, tumor protein 53; *Prox1*, prospero homeobox 1; *COUP-TFII*, chicken ovalbumin upstream promoter transcription factor 2; *PCNA*, proliferating cell nuclear antigen; matrix metallopeptidase 8; *MMP9*, matrix metallopeptidase 9; *p38*, mitogen-activated protein kinase 14; *JNK2*, c-Jun N-terminal kinase; *BCR/ABL*, breakpoint cluster region/Abelson murine leukemia viral oncogene homolog 1; *GFP*, green fluorescent protein; *TIP47*, mannose-6-phosphate receptor binding protein 1; *ILK*, integrin-linked kinase.

Table 3.1: Gating Statistics

Gating Statistics						
Treatment	**Replicate**	**Cell Number From Gate**	**GFP (+)**		**GFP (-)**	
			Live	**Dead**	**Live**	**Dead**
Nuc(-) DNA(-)	**A**	18,811	0.0%	0.0%	91.2%	8.8%
	B	19,297	0.0%	0.0%	97.0%	3.0%
	C	19,571	0.0%	0.0%	96.9%	3.1%
	Mean	19,226 ± 384.9	0.0%	0.0%	95.0 ± 3.3%	5.0 ± 3.3%
Nuc(-) DNA(+)	**A**	18,805	0.0%	0.0%	11.9%	88.1%
	B	18,933	0.0%	0.0%	12.1%	97.9%
	C	18,989	0.0%	0.0%	10.1%	89.9%
	Mean	18,909 ± 94.3	0.0%	0.0%	11.4 ± 1.1%	92.0 ± 5.2%
Nuc(+) DNA(-)	**A**	19,753	0.0%	0.0%	93.3%	6.7%
	B	19,756	0.0%	0.0%	96.9%	3.2%
	C	19,738	0.0%	0.0%	97.0%	3.0%
	Mean	19,749 ± 9.6	0.0%	0.0%	95.7 ± 2.1%	4.3 ± 2.1%
Nuc(+) DNA(+)	**A**	19,323	0.2%	5.0%	1.9%	92.9%
	B	19,178	1.4%	4.7%	1.4%	92.6%
	C	19,161	1.2%	3.8%	1.4%	93.6%
	Mean	19,221 ± 89.0	0.93 ± 0.64%	4.5 ± 0.62%	1.6 ± 0.32%	93.0 ± 0.53%
Nuc(+) DNA(+) 10 µM RI	**A**	19,033	16.5%	36.3%	3.8%	43.4%
	B	19,298	25.8%	29.8%	7.9%	36.5%
	C	18,876	8.2%	29.6%	2.6%	59.6%
	Mean	19,069 ± 213.3	16.8 ± 8.8%	31.9 ± 3.8%	4.8 ± 2.8%	46.5 ± 11.8%

Nuc (+/-) (Nucleofection™) designates whether cells were Nucleofected™ or not. DNA (+/-) designates whether cells received 5 µg of pmaxGFP or not. RI, ROCK Inhibitor.

Table 4.1: Cell Characterization of Stem Cell Markers at Passage 2

Umbilical Cord	Sample	Events	Gated Cells	CD34 (-)	CD45 (-)	CD73 (+)	CD90 (+)	CD105 (+)	STRO-1 (+)
A	1	20,000	19,555	97.70%	75.13%	16.68%	90.52%	19.71%	6.67%
	2	20,000	455	97.58%	67.47%	18.90%	88.57%	19.12%	4.40%
	3	20,000	6,870	97.15%	60.45%	20.87%	99.14%	19.33%	5.97%
	Mean		8,960 ± 9720	97.48 ± 0.29%	67.7 ± 7.3%	18.8 ± 2.1	92.7 ± 5.6	19.39 ± 0.30%	5.7 ± 1.2%
B	1	20,000	19,717	94.86%	70.76%	15.24%	98.29%	33.89%	10.90%
	2	20,000	19,783	95.69%	88.34%	10.21%	99.29%	30.13%	9.63%
	3	20,000	19,783	95.17%	89.00%	9.15%	99.82%	36.56%	10.83%
	Mean		19,761 ± 38	95.24 ± 0.42%	83 ± 10%	11.5 ± 3.4%	99.13 ± 0.78%	33.5 ± 3.2%	10.45 ± 0.71%
C	1	20,000	19,815	98.88%	87.61%	10.10%	98.79%	10.10%	2.29%
	2	20,000	19,853	98.76%	94.66%	6.65%	99.80%	11.78%	2.60%
	3	20,000	19,871	99.11%	96.40%	7.08%	99.74%	13.91%	2.37%
	Mean		19,846 ± 29%	98.92 ± 0.18%	92.9 ± 4.7%	7.9 ± 1.9%	99.44 ± 0.57%	11.9 ± 1.9%	2.42 ± 0.16%

Table 5.1: TaqMan Primers used for RT-qPCR

Gene Name	Gene Abbreviation	Species	Dye	Entrez Gene ID	Life Technologies ID
atoh1	ATOH1	Human	Fam	474	Hs00944192_s1
gapdh	GAPDH	Human	Fam	2597	Hs02758991_g1
gfi1	GFI1	Human	Fam	2672	Hs00382207_m1
hes1	HES1	Human	Fam	3280	Hs00172878_m1
hes5	HES5	Human	Fam	388585	Hs01387463_g1
jagged2	JAG1	Human	Fam	182	Hs01070032_m1
myosin VIIa	MYO7A	Human	Fam	4647	Hs00934542_m1
POU class 4 homeobox 3	POU4F3	Human	Fam	5459	Hs00231275_m1
Sox2	SOX2	Human	Fam	6657	Hs01053049_s1

Supplemental Table 5.2: Cell Characterization

Passage Number	Day	Group	CD34 (-)	CD45 (-)	CD73 (+)	CD90 (+)	CD105 (+)	STRO-1 (+)
P2-5	10	Untreated	99.58 ± 0.34%	86.87 ± 14.12%	4.03 ± 2.71%	91.96 ± 5.58%	1.21 ± 1.40%	0.31 ± 0.29%
		Math1	96.23 ± 7.61%	83.94 ± 13.96%	10.31 ± 10.12%	76.86 ± 39.97%	2.25 ± 3.12%	4.12 ± 6.42%
		Hath1	98.75 ± 2.04%	82.76 ± 18.54%	4.90 ± 3.44%	93.06 ± 8.53%	0.50 ± 0.70%	0.46 ± 0.90%
		H1/H5	99.74 ± 0.49%	89.37 ± 14.19%	2.26 ± 1.69%	93.89 ± 6.41%	0.06 ± 0.07%	0.03 ± 0.02%
		Math1/H1/H5	99.42 ± 1.22%	79.92 ± 22.53%	3.96 ± 4.44%	80.88 ± 34.34%	0.10 ± 0.14%	0.13 ± 0.17%
		Hath1/H1/H5	97.80 ± 4.79%	86.39 ± 10.33%	8.52 ± 14.95%	93.61 ± 7.10%	0.10 ± 0.07%	0.09 ± 0.16%